Theoretical Study on Mechanism of Ethylene and Butadiene Polymerization Catalyzed by Cationic Gadolinium Metallocene

Rika Fukushima

Contents

Chapter 1

General Introduction

1.1. Introduction

Since the discovery of natural rubber (NR), synthetic rubber was born in the 20th century, and today rubber is one of the essential materials for our lives. Global consumption of newly produced rubber is 29.72 million tons (2021, according to IRSG),[1] while that in Japan is 1,594,000 tons (2018), of which synthetic rubber accounts for 55.7%.[2] According to synthetic rubber shipments by product type in 2018, styrene butadiene rubber (SBR) accounted for 40% of the total, butadiene rubber (BR) for 21%, and isoprene rubber (IR) for 5%; these three types of diene rubber are called commodity rubber and account for about 66% of global synthetic rubber shipments. Most of these are applied to tires, tubes, and various other automotive components.[2]

Among synthetic rubbers, BR has the largest production and consumption volume as a general-purpose rubber, second only to SBR. BR is noted for its high resistance to abrasion, low hysterisis, and resistance to cracking. BR is an addition polymer of the conjugated dienemonomer 1,3-butadiene, and depending on the bonding mode of the monomer, three types of geometric isomers, *cis*-1,4 bond, *trans*-1,4 bond, and *vinyl*-1,2 bond, are formed in the main chain (Figure 1). In general, BR is classified according to their microstructure and divided into high *cis*-BRs (*cis* content > 90%) and low *cis*-BRs (*cis* content around 35%). Unlike NR, high-cis BR does not crystallize at room temperature even when highly elongated, but it has excellent abrasion

resistance, high resilience, and low-temperature properties. In particular, wear resistance is better than other rubbers as wear conditions become more severe. [2][3]

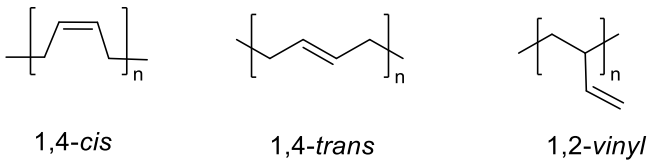

Figure 1. Microstructures of Polybutadiene.

While generally Ziegler catalysts are used in polymerization reactions, there are two types of Ziegler catalysts used in the industrial synthesis of high *cis*-BRs: transition metal systems of Ti, Co, and Ni, and rare earth metal systems of Nd. These catalysts affect the microstructure of BR and increase the cis content in the following order: 90–93% by Ti-based, 96–98% by Co- and Ni-based, and 97–99% by Nd-based. [3(b)] This slight difference in *cis* content has significant effects on physical properties such as tensile strength, hysteresis loss, and wear resistance, with higher cis content giving superior properties. In addition to microstructure, the central metal species used in the catalyst also affects the molecular weight distribution (MWD) and branching. These industrialized high *cis*-BRs have relatively broad MWDs ($M_w/M_n > 2$). However, in order to improve wear resistance, resilience, and low hysteresis, it is desirable to have narrow MWDs. Therefore, the research on synthesis of BR with high *cis*-selectivity and narrow MWDs at or above industrially desirable room temperatures have been arduously pursued.[3(d)–5]

In 1999, Kaita, Hou, Wakatsuki et al. reported a samarocene/cocatalyst system which achieved for the first time both high 1,4-*cis* selectivity and living (well-controlled molecular weight) polymerization in high yields.[6(a)] Especially effective was $Cp^*_2Sm[(\mu\text{-Me})AlMe_2(\mu\text{-}$

Me)]$_2$SmCp*$_2$ (Cp* = η^5-pentamethylcyclopentadienyl) in combination with two additional cocatalysts, Al(^{i}Bu)$_3$ and [Ph$_3$C][B(C$_6$F$_5$)$_4$], which produced BR with a 1,4-*cis* selectivity of 99.0% and M_w/M_n = 1.20–1.23 at –20 8 ℃.[6(b)] Furthermore, Kaita et al. reported the [Cp*$_2$Gd][B(C$_6$F$_5$)$_4$] complex[7]. This Gd-based complex with a small amount of Al(^{i}Bu)$_3$ gives BR with 1,4-*cis* selectivity of 97.5% and M_w/M_n = 1.73 at 50 °C. Further decreasing the polymerization temperature, BR with highly controlled stereoregularity are obtained (1,4-*cis* selectivity of 99.6 % and M_w/M_n = 1.41 at –20 °C, and 1,4-*cis* selectivity > 99.9% and M_w/M_n = 1.45 at –78 °C). It has also been found that this catalyst system can synthesize not only high *cis*-BR but also high *cis*-IR, [7(c)] and can also polymerize ethylene as a heterogeneous monomer. [8]

This Gd catalyst system is characterized simply as "highly active" and "highly selective" homogeneous "single-site" catalysts. For example, it is possible to synthesize high *cis*-BR using this Gd catalyst system instead of the industrialized Nd catalysts mentioned above, in which the amount of Gd catalyst used is less than 1/5 of that of the Nd catalysts.

In addition, homogeneous catalysts allow the design of reaction fields around the central metal by chemical modification of the ligands. This has the advantage that polymerization can be precisely controlled and that computational chemistry can efficiently analyze the mechanism and predict reactions based on that analysis (see "Active species of homogeneous Ziegler-Natta catalysts" in section 1.2.1.). Therefore, in order to create the next generation of synthetic rubbers, we are searching for new coordination polymerization catalysts, focusing on Gd catalyst systems, with the help of computational chemistry.[9]

Computational chemistry has made great progress in recent years, expanding its use to understand reaction mechanisms, to construct catalyst design guidelines, and to provide explanatory and objective variables for materials informatics, and is becoming indispensable even

for research groups that mainly conduct experiments. I am also aiming to establish catalyst design guidelines based on the polymerization mechanism by utilizing computational chemistry. For this purpose, it is most important to understand the polymerization mechanism. However, the polymerization mechanism of this catalytic system had not been clarified because the structure isolated and identified as the active species of this catalytic system does not have the initial Gd-alkyl bond, which is necessary for the conventional polymerization mechanism. Therefore, in this thesis, a theoretical analysis of the polymerization mechanism of this catalyst system was performed by electronic state calculations using computational chemistry.

Chemistry is the science that investigates the properties and changes of matter, and until now, experimental methods have been the main means of development in this field. In recent years, however, the approach of "computational chemistry," which uses computers to investigate the properties of material and reaction mechanism, has become an extremely practical approach, and has developed to the stage where it is considered a third means of research besides experiment and theory. Computational chemistry includes quantum mechanics (QM) method, molecular mechanics (MM) method, and molecular dynamics (MD) method. QM are methods to analyze the structure and properties of atoms and molecules by electronic state calculations.[10]

In the early 20th century, it was shown that the physical phenomena of atoms and molecules are governed by their electronic states, and quantum mechanics was systematized as a principle to describe them. Then, with the invention of computers, methods were developed to approximately solve the Schrödinger equation, which is the fundamental equation of quantum chemistry. Two basic approaches for approximate solution of the Schrödinger equation are known: the ab initio molecular orbital method based on the Hartree-Fock (HF) method and Density Functional Theory (DFT). The HF method is an approximation that treats the behavior of other electrons as a mean

field by averaging the interaction energies between electrons (mean field approximation) and does not include experimental parameters. While the total energy can be calculated 99.5% by the HF method, electron correlations are not taken into account. An error of 1% in energy calculation is important for quantitative discussions with experimental results. To account for electron correlation, the excited state electron configurations are mixed with the ground state electron configuration, and the Møller-Plesset method (MP method), the Configuration Interaction (CI) method, and the Coupled Cluster (CC) method are known as such methods. In particular, the CCSD(T) method is often used as the "gold standard" reference method for comparison of energies and other parameters that are difficult to measure experimentally. While methods that consider electron correlations to a higher order are more accurate, they are also computationally expensive due to the increase in the number of basis sets, which dramatically increases the computation time. On the other hand, DFT is based on the Hohenberg-Kohn theorem that "the Hamiltonian operator of the non-degenerate ground state of a molecule is uniquely determined by the functional of the ground state electron density. In DFT, the Kohn-Sham (KS) orbitals are used to calculate the electron interaction potential, which is a functional of the electron density, and the lowest energy and the corresponding KS orbital are obtained according to the variational principle. This method has been widely used in chemistry since the 1990s and is now the main theory used in more than 80% of quantum chemical calculations.[10(d)]

In this thesis, DFT calculations were used to analyze the mechanism of cationic Gd metallocene catalyzed polymerization.

1.2. Coordination polymerization.[11,12]

In coordination polymerization, the coordinating unsaturated transition metal complex is the active species. Typical coordination polymerization catalysts are Ziegler-Natta catalysts, which consist of a combination of transition metal compounds and alkyl, aryl, or hydride compounds of main group metal, and allow stereospecific polymerization of olefins and conjugated dienes to proceed.

Heterogeneous Ziegler-Natta catalysts have been the mainstream in polyethylene and polypropylene production since their discovery by Ziegler, Natta et al. in the 1950s.[13] However, in the late 1970s, Kaminsky et al. discovered that homogeneous Ziegler-Natta catalysts consisting of group IV metallocene compounds activated with methylaluminoxane (MAO) were highly active in the polymerization of olefins.[14] Furthermore, it was found that the copolymerization reactivity and stereospecificity of the homogeneous Ziegler-Natta catalysts can be controlled by the molecular design of the metallocene ligands, which stimulated researches on homogeneous catalysts with transition metal complexes as active species precursors. These catalytic systems are called "single-site" catalysts because they are most characterized by the homogeneity of the polymerization active species. In contrast, conventional heterogeneous Ziegler-Natta catalysts are called multi-site catalysts. In the following, I first describe the polymerization active species and elementary reactions of Ziegler-Natta catalysts in the polymerization of ethylene, the simplest monomer among olefins. Next, I mention the polymerization active species of homogeneous Ziegler-Natta catalysts, which have been remarkably developed in recent years. Then, conjugated diene is explained in the same way, using butadiene polymerization as an example.

1.2.1. Elementary reactions of ethylene polymerization.

Initiation and Propagation Reaction

Polymerization of olefins by coordination polymerization catalysts is basically initiated by the coordination-insertion of the olefin into the active species, the coordinately unsaturated transition metal alkyl or transition metal hydride. Olefin coordination to the transition metal involves electron donation from the bonding π orbital of the olefin to the empty d orbital of the transition metal and back donation from the transition metal d orbital to the antibonding π* orbital of the olefin, as shown in Figure 2 (Dewar–Chatt–Duncanson model).[12,15] The insertion reaction proceeds by insertion of a coordinating olefin into the transition metal-alkyl bond, and the polymer molecular chain grows by repeated coordination-insertion of the olefin (Figures 3).

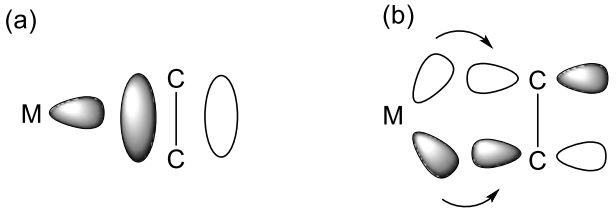

Figure 2. π-coordination of ethylene to transition metals (Dewar–Chatt–Duncanson model).[12,15]

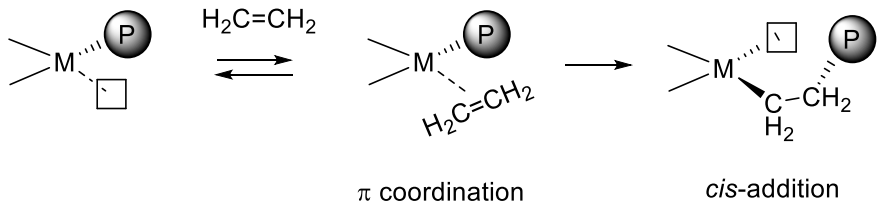

Figure 3. Coordination-insertion reaction of ethylene.

Chain Transfer Reactions.

Chain transfer is a polymerization reaction that transfers the activity of a growing polymer chain to another molecule. The main chain transfer reactions in olefin polymerization are the transfer of β-hydrogen from the growing chain to the coordinating monomer or active center metal to form a C=C bond ((a) and (b) in Figure 4) and the exchange of alkyl groups between main group metal–alkyl compound used as an alkylating agent and the growing chain (Figure 4 (c)). Hydrogen is used industrially as a chain transfer agent (Figure 4 (d)), but in every case, the metal (M) –alkyl or –hydrid bond is regenerated and the propagation reaction continues.

(a) β-hydrogen transfer to monomer.

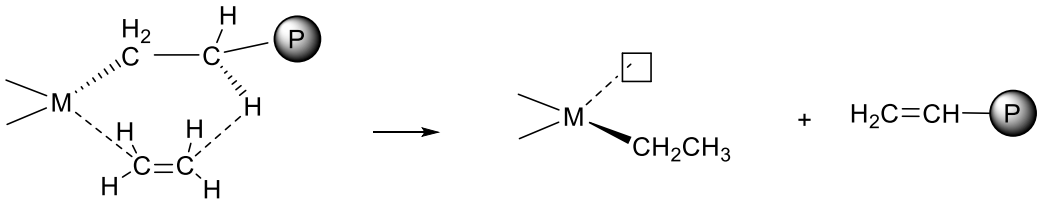

(b) β-hydrogen transfer to central metal.

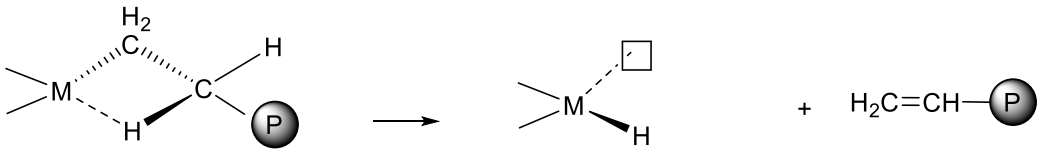

(c) Alkyl group exchange with main group metal alkyl compound.

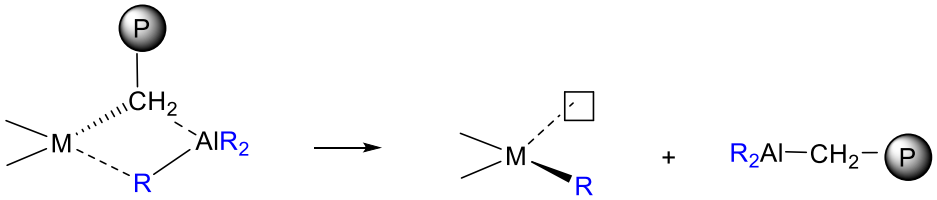

(d) σ-bond metathesis with added hydrogen

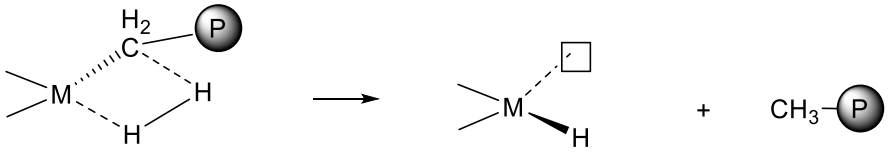

Figure 4. Chain transfer reactions in olefin polymerization.

Coordinative Chain-Transfer Polymerization (CCTP).[16]

There is a reaction mechanism called CCTP that combines transition metal-based catalyst for polymer chain growth (Figure 3) and alkyl exchange (Figure 4 (c)) between CTA (usually in the form of main group metal alkyl) and the growing chain. Commonly, zinc, aluminum, or magnesium alkyls are used as CTAs. In this case, the growing polymer chain can transfer via transalkylation from the catalyst (active species) to the CTA, which is normally considered a dormant species in the polymerization process. Thus, CCTP is a process involving a dynamic equilibrium between propagating and dormant species (Scheme 1b). In contrast to classical living polymerization, in which a single molecule of catalyst grows a single polymer chain (Scheme 1a), chain transfer from catalyst to CTA can grow several polymer chains per molecule of catalyst (Scheme 1b). This transition must be fast and reversible in propagation contrast rate, and chain termination pathways such as β-H elimination must not occur or be negligible if they do occur. When the chain transfer efficiency is high, i.e., most alkyl groups are involved in transmetalation, the polymer appears to be growing on the main group metal alkyl.

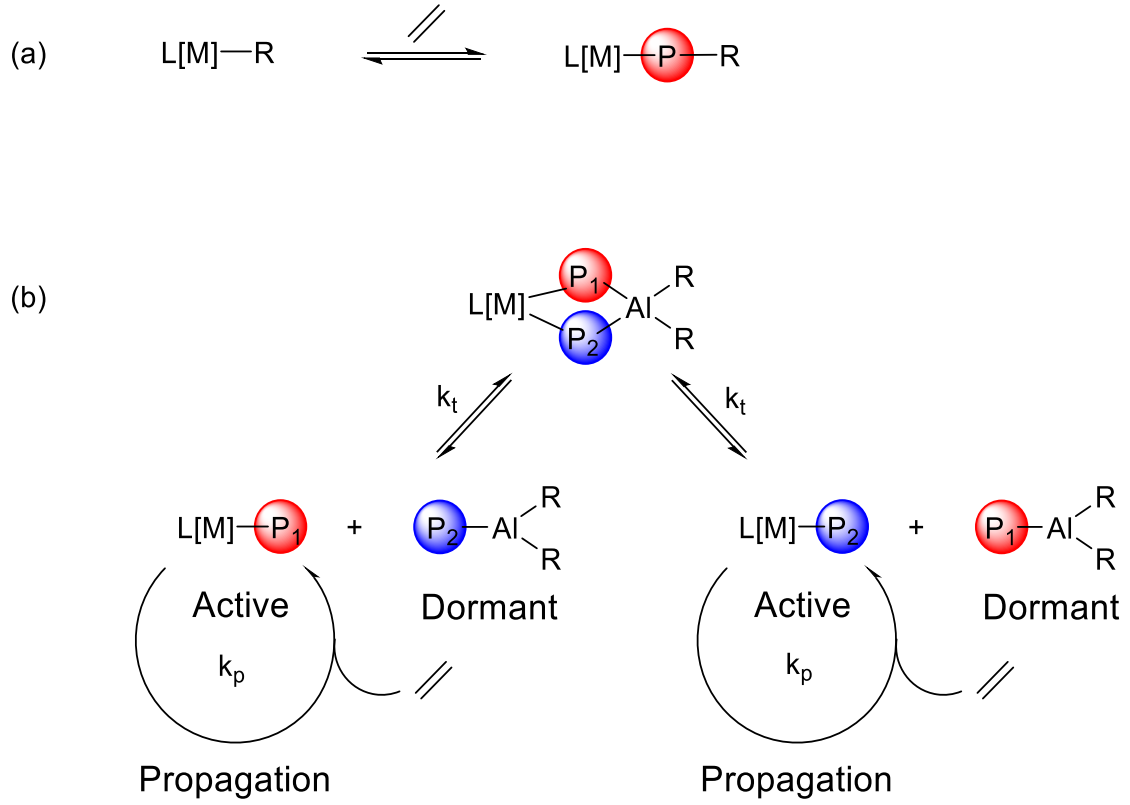

Scheme 1. Classical Coordinative polymerization (a) and Coordinative chain transfer polymerization (CCTP) using AlR_3 as the chain transfer agent (CTA) (b).

Active species of homogeneous Ziegler-Natta catalysts.

Group 4 metallocene catalyst (Kaminsky catalyst).[14][17] Ziegler-Natta catalysts are very useful in industry, but because the reaction system is heterogeneous, the "near-solid surface (slurry surface)" conditions in which the active species exist are various, and they are so-called multi-site catalysts, in which there are multiple active species. Since each active species has a different reactivity, a huge amount of experimental man-hours have been required to optimize the molecular weight, molecular weight distribution, polymer composition, and steric structure of the generated polymers. This was greatly changed by the homogeneous (soluble) polymerization catalysts using group 4 metallocene complexes reported by Kaminsky et al. in 1976. Kaminsky used metallocene

alkyl complexes of group 4 transition metals (Ti, Zr, and Hf). This complex does not show polymerization activity by itself, but by adding methylaluminoxane (MAO) or trityltetraoxypentafluorophenylborate ($[Ph_3C][B(C_6F_5)_4]$) as an activator, a coordinately unsaturated tetravalent alkyl cation species (**5a**) is formed. It has been shown that propagation occurs in the coordination-insertion cycle by the insertion of ethylene into the M–alkyl bond after the coordination of ethylene to the empty coordination site (□ portion) of this active species (**5a** in Figure. 5). This catalytic system is called Kaminsky catalyst. A notable feature of this system is that polymerization proceeds only by activation of a single complex molecule with a definable structure, so-called single-site catalyst. As a result, the reaction system is simplified and "catalyst design" becomes possible. In general, the catalytic performance of metallocene catalysts is highly dependent on the type of central metal, co-catalysts, and ligand structure. In the activator, it is desirable that the interaction between the counter anion (Lewis base) and the coordinately unsaturated cation species be weak and that the counter anion be stable against electrophilic reactions of the cation species in order for the cation complex formed to be highly active and remain active. From this viewpoint, $[Ph_3C][B(C_6F_5)_4]$, $[HNR_3][B(C_6F_5)_4]$, and $B(C_6F_5)_3$ with pentafluorophenyl (C_6F_5) groups are used as activators, and have achieved polymerization activity comparable to that of the MAO systems. As mentioned above, since the active species are ion pairs, the polymerization activity is greatly affected by the solvent. These catalyst systems exhibit very high catalytic activity and narrow molecular weight distribution of polymers, and the stereo-regularity of α-olefins can be controlled by modifying the Cp ligands, making it easy to control the properties of polymers. These characteristics have led to an increasing number of industrial applications in place of heterogeneous Ziegler-Natta catalysts. Many advanced forms of Kaminsky

catalysts have also been studied, including the constrained geometry catalyst (CGC), which bridges two Cp rings, half metallocene catalysts, and systems without Cp rings.

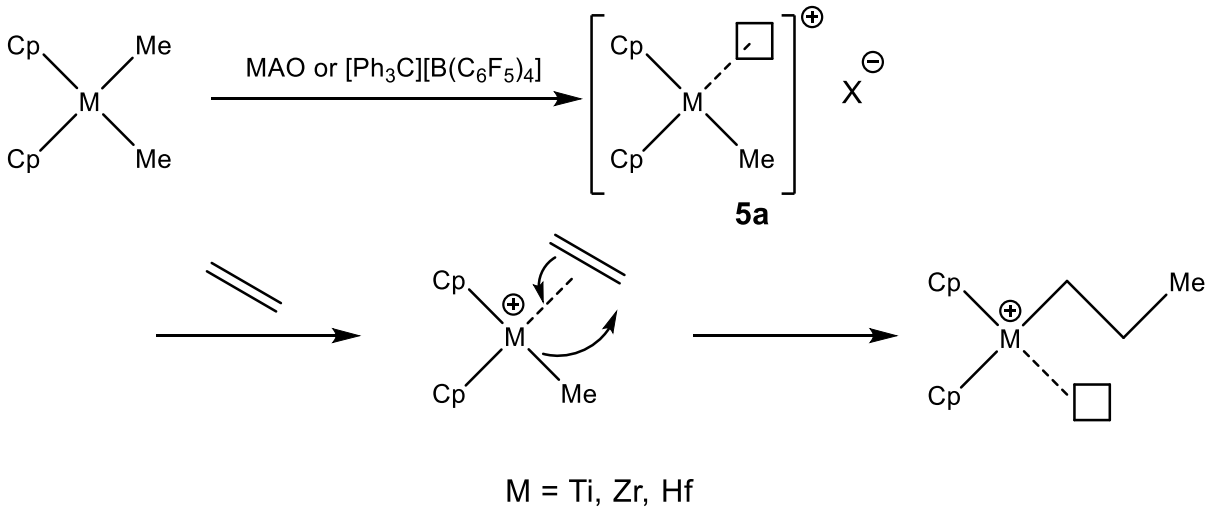

Figure 5. Reaction Mechanism of Kaminsky Catalyst.

Group 3 metallocene catalyst (rare earth metal complex).[18] Around the same time as the Kaminsky catalysts, research on polymerization reactions using rare earth metal (group 3) complexes also began to be conducted. Ballard et al. first used rare earth metallocene–alkyl complexes for the polymerization of ethylene, and since then, Watson, Marks, and others have been actively studying the polymerization of ethylene with metallocene–alkyl complexes. The ligand modification of metallocene and the application of ligands other than Cp are similar to those of Kaminsky catalysts. The most important feature of these group 3 metallocene catalysts is that the polymerization active species (**6a** in Figure 6) of group 3 metallocene catalysts and the active species (**5a** in Figure 5) of group 4 metallocene catalysts are isoelectronic, and they develop polymerization activity without the use of activators such as MAOs.

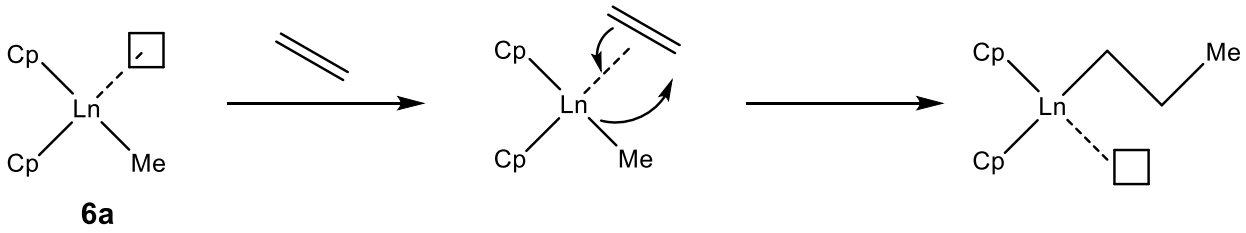

Figure 6. Reaction mechanism of rare earth metal complexes

1.2.2. Elementary reactions of butadiene polymerization.

Since the discovery in 1954 that Ziegler-Natta catalysts give polyisoprene with a 1,4-*cis* structure,[19] many coordination polymerization catalysts for dienes have been investigated and highly stereospecific catalyst systems have been developed. As mentioned in section 1.1, one of the most important industrial issues in the polymerization of dienes is the regulation of the structure (stereospecificity, molecular weight, MWDs, etc.) of the resulting polymers. For example, in the case of butadiene polymerization, there are three types of geometric structural isomers as shown in Figure 1. Among these isomers, polybutadiene with high 1,4-*cis* content is useful as a BR with high performance properties such as high elasticity and wear resistance.

Several mechanisms have been proposed for the stereospecific polymerization of conjugated dienes by coordination polymerization catalysts.[20] The coordination polymerization mechanism of conjugated diene monomers is basically the same as that of ethylene (see section 1.2.1), consisting of two steps: coordination to the active site of the monomer and insertion into the transition metal (M)–C or M–H bond. However, the case of conjugated dienes differs from ethylene polymerization in the points that the coordination form of the diene to the metal is diverse, the ends of the growing chain form transition metal (M)–π-allyl type bonds, and coordination to the metal of C=C bonds (mostly penultimate monomer unit) in the polymer chain can occur. As shown in Figure 7, there are a four possible coordination modes of 1,3-butadiene to the metal,

depending on the combination of the number of occupied coordination sites (η^2 and η^4) and the stereo configuration of the butadiene (s-*cis* and s-*trans*). If only one coordination site of the metal is available, it will be η^2-coordinated. In η^2-coordination, the s-*trans* structure is considered to be more stable than the s-*cis* structure.[12] Insertion of an s-*cis*-η^4-coordinated diene into an M–C bond kinetically forms an anti-π-allyl end, whereas insertion of a s-*trans*-η^4-coordinated diene and a s-*trans*-η^2-coordinated diene forms a syn-π-allyl end. There are two modes of bonding between the allyl group at the end of this growing chain and the central metal: η^1-σ and η^3-π. The η^3-π is more stable than η^1-σ because the charge is delocalized in the π-allyl structure (Figure 8). The reaction sites of the allyl group are C2 and C4. Adding at C2 to the next monomer gives 1,2-unit, and adding at C4 gives 1,4-unit. There are two isomers of the π-allyl species, anti and syn. anti and syn π-allyl species are interconvertible via the σ-allyl species, and the *syn* is thermodynamically more stable than the *anti*. Therefore, there are two important factors in the cis-trans stereoselectivity in the 1,4-polymerization of butadiene: the stability of the anti and syn forms of the π-allyl complexes and the coordination mode of the butadiene to the central metal.

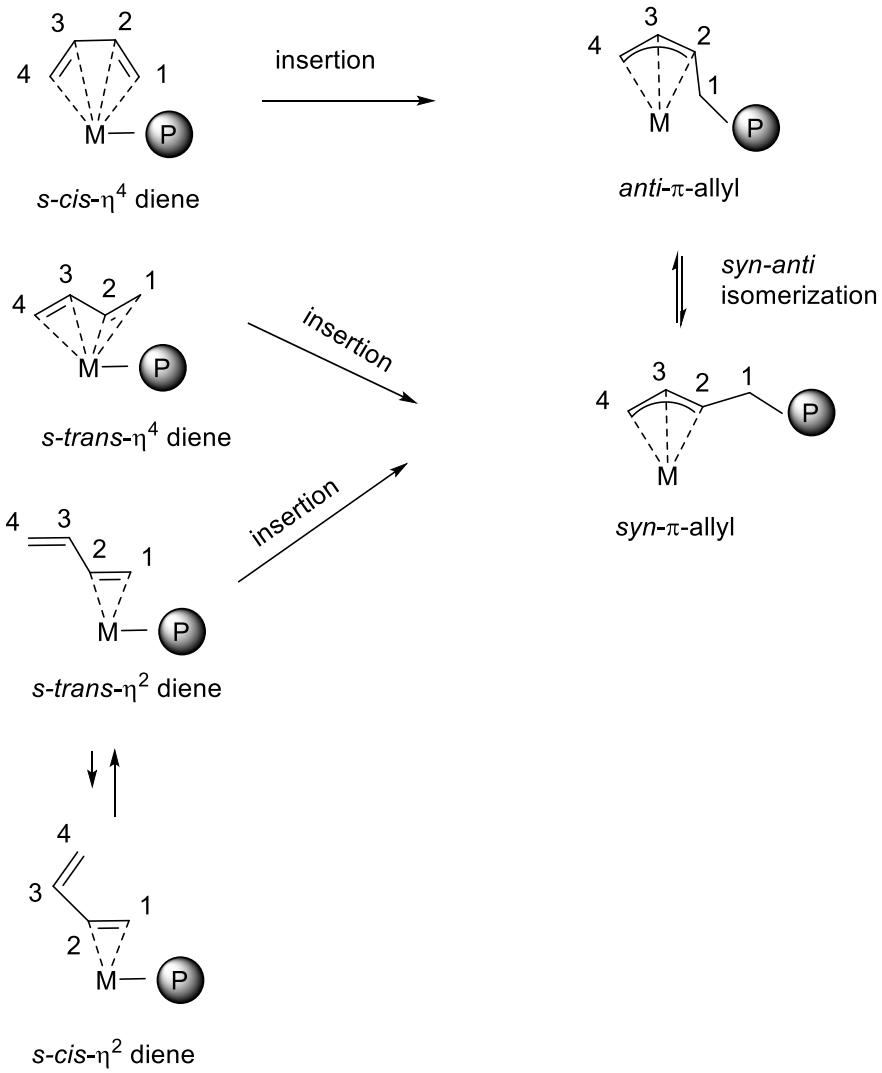

Figure 7. Coordination-insertion reaction of 1,3-butadiene monomer to the central metal.

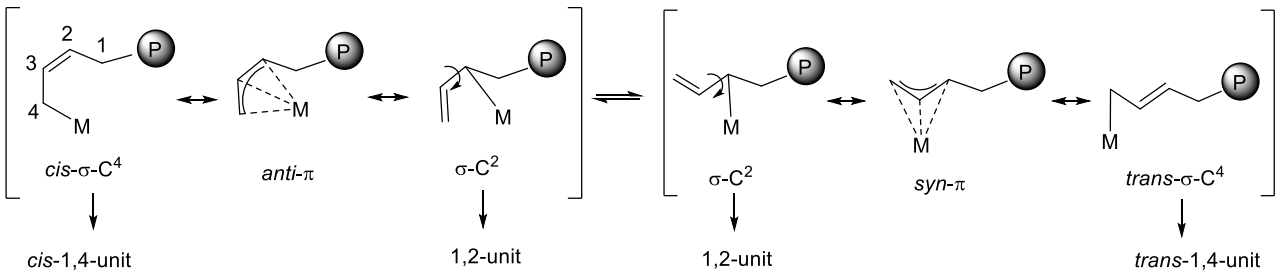

Figure 8. π–σ conversion of terminal allyl groups.

1.2.3. Application of Computational Chemistry to Polymerization Mechanism Analysis.

The homogeneous Ziegler-Natta catalysts are so-called "single-site" catalysts. The advantage of "single-site" catalysts is that the reaction mechanism can be easily studied because of the single active species in the polymerization. Computational studies have been widely and successfully conducted to elucidate the mechanism of olefins polymerization catalyzed by group 4 and late transition metal complexes. These theoretical results have effectively promoted the design and development of homogeneous transition metal catalyst. However, most studies have focused on the polymerization of mono-olefins, and there are still few examples of polymerization studies of dienes. Furthermore, computational studies on the rare-earth-metal-catalyzed polymerization of dienes are extremely limited,[21] and most studies on butadiene polymerization are based on the π-allyl insertion mechanism proposed by Taube et al.[22]. In recent years, there have been an increasing number of reported examples of studies using DFT to analyze the polymerization mechanism in rare-earth metallocene-catalyzed diene polymerization and copolymerization of olefin dienes and other compounds,[23,24] Furthermore, there have been reports of studies using these computational models to investigate the effects of central metals, ligands, and solvents, and it is expected that these studies will be utilized in catalyst design.[25] There are also reports of dissociation state studies with catalysts using molecular dynamics simulation to investigate the effect of counter anions on catalytic activity.[26] However, the force fields developed for MD are only for very common elements and are not currently available for elements such as transition metal elements. Therefore, in order to run MD simulations, it is necessary to first develop a force field. In developing a force field, it is common to set up the force field so that it reproduces the results of quantum chemical calculations, so the study of the polymerization mechanism using the QM method is indispensable.

As described above, analysis of the polymerization mechanism by the QM method is one of the most important issues that will serve as the basis for both subsequent utilization in the establishment of catalyst design guidelines and further applied computational research.

1.3. Computational chemistry[10],[27]

1.3.1. Density Functional Theory (DFT)

The Schrödinger equation cannot be solved exactly except for hydrogen-like atoms in two-body systems. Most approximate solutions of the equations for many-electron systems are based on solving the equations for one-electron systems without interaction and then taking into account electron correlations. One such approximation is the HF method or Kohn-Sham DFT method. In DFT, the Kohon-Sham (KS) orbitals are used to calculate the electron interaction potential, which is a functional of the electron density, and the lowest energy and the corresponding KS orbital are obtained according to the variational principle. The validity of such a procedure is guaranteed by the Hohenberg-Kohn theorem. Following this theorem, the total energy E can be formulated as the sum of the nuclear-electron interaction energy ($E\mathrm{ne}[\rho]$), the kinetic energy of the no-interaction system ($T\mathrm{s}[\rho]$), the classical Coulomb interaction energy between the electrons ($J[\rho]$), and the exchange-correlation energy between the electrons ($E\mathrm{xc}[\rho]$).

$$E = E\mathrm{ne}[\rho] + T\mathrm{s}[\rho] + J[\rho] + E\mathrm{xc}[\rho]$$

Within the terms of this formula, the approximation of $E\mathrm{xc}[\rho]$ is a key issue, and many $E\mathrm{xc}[\rho]$ have been developed. $E\mathrm{xc}[\rho]$ developed to date include Local Density Approximation (LDA), which is expressed only in terms of electron density ρ, Generalized Gradient Approximations (GGA), which incorporate the gradient of the electron density ρ, the Hybrid functional methods that mix a constant fraction of the exact Hartree-Fock exchange integral into the exchange functional, the meta-GGA functional, and semi-empirical functional. In LDA, the

inhomogeneous electron distribution of the molecule is divided into micro portions and the homogeneous electron gas equation is used for these portions. $E\mathrm{xc}[\rho]$ of the inhomogeneous electron distribution is obtained by adding the contributions of these micro portions over the entire space. Therefore, LDA can be applied to systems in which the electron distribution varies moderately, but becomes difficult to apply in systems that deviate significantly from homogeneity. For this reason, GGA was considered. However, GGA incorporating an electron density gradient is not sufficient for the discussion of chemical reactions in isolated systems because the activation energy is underestimated and the HOMO-LUMO gap is underestimated due to an overestimation of the delocalization of electronic states.[27] Therefore, it has been used the hybrid functional method, which mixes the exact Hartree-Fock exchange integral with the exchange functional. For example, the B3LYP method, which combines Becke's three parameter exchange functional (Hartree-Fock exchange energy fraction is 20%)[28] and the Lee-Yang-Parr correlation functional, is often utilized. An alternative method to solve the problems of GGA is the meta-GGA functional, which is a functional that uses the kinetic energy density to improve the approximation of GGA. Semi-empirical functionals have also been developed to estimate physical properties with high accuracy using many semi-empirical parameters. The semi-empirical parameters are optimized using experimental databases of atomization energies and reaction activation energies. In particular, series such as M06 developed by Truhlar's group at the University of Minnesota are often utilized,[29] and the M06 functional has 38 parameters.

In addition, the following correction method is used to account for physical effects that are not included in the exchange-correlation functional above. In principle, exchange interactions between long-range electrons are not taken into account since the general exchange functional is computed as an integral over the one-electron coordinate. Therefore, Long-range Correction (LC)

method or the Coulomb Attenuating Method (CAM)–B3LYP are used [30–31]. This long-range correction improves van der Waals force, electronic excitation spectra, optical response properties, and orbital energies. There is also van der Waals force as an electron correlation that is not considered in most correlation functionals. The van der Waals force is the general term for the interaction between dipoles, which can be classified into three categories: orientation force, induction force, and dispersion force. All of their potentials vary inversely proportional to r^6 (r : intermolecular distance), and the dispersion force is usually the largest of the three. Especially for nonpolar molecules, only the dispersion force acts.[32] Only the dispersion force is a van der Waals force that cannot be accounted for by the Kohn-Sham method using the correlation functional.[10(d)] Various dispersion force correction methods have been proposed in recent years, and the DFT-D3 method, which includes $1/r^6$ and $1/r^8$ terms, has recently been often used.[33] The C-H/ π and π-π interactions can be improved if the dispersion force correction is taken into account.

1.3.2. Basis set

Since almost all current DFT methods are Kohn-Sham density functional methods that use molecular orbitals, called Kohn-Sham orbitals, to calculate electron density, in both HF and DFT methods, the energy equation is obtained for molecular orbitals, and the molecular orbitals are optimized to minimize the energy.

The molecular orbitals of polyatomic molecules are generally approximated by the Linear Combination of Atomic Orbital (LCAO) approximation, which is a superposition of atomic orbitals expanded for the atoms composing the molecule. Slater-type orbital (STO) and Gauss-type orbital (GTO) are usually used as basis sets for these atomic orbitals. The solution for hydrogen-type atoms is represented by the STO, which can express asymptotic behavior near the

nucleus that is valid for exact wave functions and gradual decay that works for long-range super exchange interaction. Therefore, STO is more appropriate as a basis function for atoms and molecules than GTO, but STO is not often used because of the difficulty of molecular integration for polyatomic molecules. Contracted GTO (CGTO), which is a linear combination of GTO, is the mainstream in non-empirical molecular orbital methods because it is easy to perform molecular integrations. The simplest LCAO approximation assigns one CGTO to each atomic orbital. This is called the minimal basis set. For example, in H_2O, 5 STOs of 1s, 2s, 2px, 2py, 2pz are used for O atoms and 1s STO for each H atom. When STOs are represented by *N* GTOs, they are called STO-*N*G. Usually, STO-3G with N=3 was often used. The minimal basis set is useful, at least for investigating the stable electron configuration of molecules that do not contain transition metals, but it is not quantitative enough because it can hardly represent orbital stretching.

A treatment that goes one step further from the minimal basis set is providing flexibility for changes in orbital broadening by using two types of CGTOs with different broadening for the occupied orbitals. Examples are the double zeta (DZ) basis set of Huzinaga-Dunning [34] and the 3-21G and 6-31G basis set developed by Pople et al.[35] The Huzinaga-Dunning basis sets specified in D95 are full double-zeta basis set, where double-zeta (DZ) means that two CGTOs are assigned to one atomic orbital, and full means all orbitals including the core. On the other hand, the basis function of Pople et al. is a split valence basis set, which means that multiple basis functions are assigned to only the valence basis set. To improve the accuracy of calculations, the basis functions of valence electrons are often doubled or tripled (e.g., 6-311G), but such methods cannot change the fundamental shape of the orbitals. Therefore, basis sets were considered in

which p-type functions are added to the H atoms, d-type functions to the atoms from Li to F, and f-type functions to the transition elements. These basis sets are called polarized basis sets.[10(c)]

While the above basis sets consider all electrons including core electrons, there is methods that do not explicitly consider core electrons but instead treat them as providing effective potentials for valence electrons, since most chemical properties are governed by valence electrons. This is called the effective core potential (ECP) method. When this method is used for atoms in period 3 and beyond, calculation time is significantly reduced. In addition, since the effects of relativity can be incorporated into the ECP (RECP : relativistic ECP method), it is particularly useful for calculations of molecules containing heavy atoms.[10(c)]

1.3.3. Solvation effect

So far it has dealt with isolated molecules, but many chemical reactions occur with molecules in solution. Therefore, it is an important problem to determine the properties of solutes when they are surrounded by solvent molecules. For dilute solutions where there is no interaction between solutes, the wave function of the solute molecule is obtained by the following equation.

$$\left(\hat{H}_M + \hat{V}_{\text{int}}\right)\Psi_s = E\Psi_s$$

where $\hat{H}_M$ is the Hamiltonian of the isolated molecule and $\hat{V}_{\text{int}}$ is the potential for interaction between the solute and solvent. In the above equation, there are three ways to find $\hat{V}_{\text{int}}$. The first is to replace the solvent molecules around the solute molecule with a continuous dielectric. Calculations using this method are relatively simple and have been incorporated into calculation programs such as Gaussian. The second method is to estimate $\hat{V}_{\text{int}}$ by simulating the arrangement of solvent molecules surrounding the solute molecules using MD or Monte Carlo (MC) methods.

The third method is a statistical mechanics treatment in liquid theory instead of simulating the arrangement of solvent molecules.[10(b)]

Now, in the first continuous dielectric method, the solvent is replaced by a continuous medium with dielectric constant ε, and the solute molecules are placed in the cavities created in the medium (Figure 9). Figure 9-(a) is the simplest model, the dipole-in-a-cavity model, in which a solute molecule with an electric dipole is placed in a spherical vacancy of radius a_0. Figure 9-(b) is the polarizable-continuum model (PCM), in which each atom in a solute molecule is replaced by a sphere and the vacancy is defined by the aggregation of these atoms. Figure 9-(c) is the isodensity polarizable continuum model (IPCM), which defines vacancies in the same electron density plane of solute molecules.

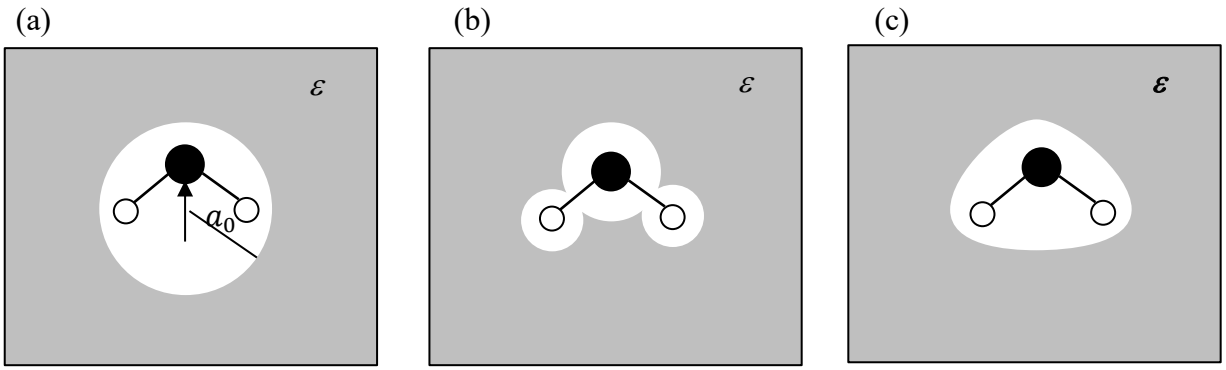

Figure 9. Continuous dielectric model of solution. (a) Dipole-in-a-cavity model. (b) Polarizable-continuum model (PCM). (c) Isodensity polarizable continuum model (IPCM).

1.4. Thesis Outline

In the present thesis, to discuss mechanism of ethylene and butadiene polymerization catalyzed by $[Cp^*_2Gd][B(C_6F_5)_4]/Al(^iBu)_3$ system, I divide this thesis into four chapters.

In Chapter 2, I investigate the ethylene polymerization mechanism using DFT calculations. The polymerization of this catalytic system cannot be explained by the conventional polymerization mechanism discussed in section 1.2, because there is no Gd–alkyl bond in the polymerization active species isolated in the past experiments.[7(a)] Therefore, I started by elucidating the polymerization mechanism by using ethylene, the simplest monomer. First, using DFT calculations, I identified the active species produced from this catalytic system and further estimated the possibility of transformation of the active species with metal–C or metal–H bond. Next, I investigated the possibility of dissociation of the counter anion in the coordination step of the monomer. I then calculated the energy profile of the monomer insertion reaction, in which an ethylene monomer coordinated by a cationic Gd metallocene is inserted into the Al-C bond of $Al(^iBu)_3$. Based on this polymerization mechanism, it is expected that the cationic Gd metallocene plays some important role in the ethylene polymerization reaction. Therefore, I will discuss the role of cationic Gd metallocene by comparing the activation energy of monomer insertion with and without cationic Gd metallocene and by analyzing the orbitals.

In Chapter 3, on the basis of the findings in Chapter 2, I extend the mechanism of ethylene polymerization by this catalytic system to butadiene polymerization and report computational study on the specific 1,4-*cis* polymerization of butadiene with this catalytic system. First, I calculate the energy profile of the coordination-insertion reaction of the butadiene monomer in the initiation reaction. Then, isomerization reactions in the insertion product of the initiation reaction are investigated. Next, in the propagation step, it is reasonably assumed that butadiene

polymerization proceeds via an intermediate with butadiene sandwiched by Gd and Al. For chain propagation, the reaction of each of the four insertion product isomers with a second s-*trans*-butadiene monomer is investigated. As their reaction pathways, reactions via four-center transition states and reactions via eight-membered ring transition states are assumed. These energy profiles are compared and the pathway with the lowest energy barrier is found. I discuss the stereoselectivity of the pathway with the lowest energy barrier and discuss its consistency with experimental results. On the basis of the polymerization mechanism, it is expected that cationic Gd metallocene plays some important role in the butadiene polymerization reaction as well. Therefore, same as in the case of ethylene polymerization, I compare the activation energy and conducted orbital analysis for the butadiene monomer insertion reaction with and without cationic Gd metallocene, and discuss the role of cationic Gd metallocene in the butadiene polymerization.

In Chapter 4, the general conclusion of this thesis is provided, including future perspectives.

References

[1] Memo: 2021nen sekai no shingomu shohiryo (IRSG shirabe), 2,972 man ton de 10.6% zou. *Gomu houchi shinbun.* April 20, **2022**, from https://gomuhouchi.com/materials/42424/ (in Japanese)

[2] *Gomunenkan*, **2022**, *61th ed.* p.176. (in Japanese)

[3] (a) *Nippon gomu kyokaishi* (*Journal of the Society of Rubber Science and Technology, Japan),* **2019,** *92*, 45. (in Japanese) (b) T. Sone, *Nippon gomu kyokaishi* (*J. Soc. Rubb. Sci. Tec., Japan),* **2015,** *88*, 178. (in Japanese) (c) K. Yamaguchi, *Nippon gomu kyokaishi* (*J. Soc. Rubb. Sci. Tec., Japan),* **2009,** *82*, 12. (in Japanese) (d) T. Tadaki, *Nippon gomu kyokaishi (J. Soc. Rubb. Sci. Tec., Japan),* **2005,** *78*, 42. (in Japanese)

[4] K. Endo, Y. Yamanaka, *Macromol. Rapid Commun.* **1999**, *20*, 312.

[5] A. Miyazawa, T. Kase, K. Soga, *Macromolecules.* **2000**, *33*, 2796.

[6] (a) S. Kaita, Z. Hou, Y. Wakatsuki, *Macromolecules* **1999**, *32*, 9078. (b) S. Kaita, Z. Hou, Y. Wakatsuki, *Macromolecules* **2001**, *34*, 1539.

[7] (a) S. Kaita, Z. Hou, M. Nishiura, Y. Doi, J. Kurazumi, A. C. Horiuchi, Y. Wakatsuki, *Macromol. Rapid Commun.* **2003**, *24*, 179. (b) S. Kaita, M. Yamanaka, A. C. Horiuchi, Y. Wakatsuki, *Macromolecules* **2006**, *39*, 1359. (c) S. Kaita, Y. Doi, K. Kaneko, A. C. Horiuchi, Y. Wakatsuki, *Macromolecules* **2004**, *37*, 5860.

[8] R. Fukushima, O. Tardif, S. Kaita, Y. Wakatsuki, N. Koga, *Chem. Asian J.* **2021**, *16*, 1403.

[9] S. Kaita, *Nippon gomu kyokaishi* (*J. Soc. Rubb. Sci. Tec., Japan),* **2022,** *95*, 241. (in Japanese)

[10] (a) S. Mori, *Bull. Jpn. Soc. Coord. Chem.* **2018**, 72, 15. (in Japanese) (b) *Keisankagaku Jikken kagaku kouza. 5th ed. Vol. 12*, (Eds.: The Chemical Society of Japan), Maruzen, **2004**, pp. 1–169. (in Japanese) (c) Y. Harada, *Ryoshikagaku gakan*, Shokabo, **2007**, pp. 1–306. (in

Japanese) (d) T. Tsuneda in *Mitsudohankansuuhou no kiso*, (Eds.: Kodansha scientific), Kodansha, **2012**, pp. 1–171. (in Japanese)

[11] T. Shiono, Y. Nakayama, S. Sai in *Kobunshi no gosei*, *ge*, (Eds.: T. Endo, Kodansha Scientific), Kodansya, **2010**, pp. 745–889 (in Japanese).

[12] A. Yamamoto in *Yuki kinzoku kagaku*, Shokabo. **2009**, pp.262-263 and pp.295-298 (in Japanese).

[13] (a) K. Ziegler, H. Gellert, K. Zosel, W. Lehmkuhl, W. Pfohl, *Angew. Chem.* **1955**, *67*, 424. (b) G. Natta, *Angew. Chem.* **1956**, *68*, 393. (c) G. Wilke, *Angew. Chem. Int. Ed*. **2003**, *42*, 5000.

[14] A. Andersen, H. G. Cordes, J. Herwig, W. Kaminsky, A. Merk, R. Mottweiler, J. Pein, H. Sinn, H. Vollmer, *Angew.Chem., Int. Ed. Engl.*, **1976**, *15*, 630

[15] (a) M. J. S. Dewar, *Bull. Soc. Chim. Fr.***1951** *18*, C71. (b) J. Chatt, L. A. Duncanson, *J. Chem. Soc.* **1953**, 2939.

[16] (a) A. Valente, A. Mortreux, M. Visseaux, P. Zinck, *Chem. Rev.* **2013**, 113, 3836. (b) D. J. Walsh, M.G. Hyatt, S. A. Miller, D. Guironnet *ACS Catalysis* **2019**, *9*, 11153.

[17] (a) R.F. Jordan, C. S. Bajgur, R. Willett, B. Scott, *J. Am. Chem. Soc.* **1986**, *108*, 7410. (b) P. G. Gassman, M. R. Callstrom, *J. Am. Chem. Soc.* **1987**, *109*, 7875. (c) C. Sishta, R. M. Hathorn, T. J. Marks, *J. Am. Chem. Soc.* **1992**, *114*, 1112. (d) Z. Hou, Y. Wakatsuki, *Coordination Chemistry Reviews*, **2002**, *231*, 1.

[18] (a) P. L. Watson , G. W. Parshall, *Acc. Chem. Res.* **1985**, *18*, 51. (b) D. G. H. Ballard, N. Coutic, J. Holton, J. McMeeking, R. Pearce, *J. Chem. Soc. Chem. Commun.* **1978**, 994. (c) G. Jaske, H. Lauke, H. Mauermann, P. N. Sweptson, H. Schumann, T. J. Marks, *J. Am. Chem. Soc.* **1985**, *107*, 8091.

[19] J. S. E. Horne, J. P. Kiehl, J. J. Shipman, V. L. Folt, C. F. Gibbs, E. A. Willson, E.B. Newton, M.A. Reinhart, *Ind. Eng. Chem.* **1956**, *48*, 784.

[20] (a) L. Porri, A. Giarrusso, G. Ricci, *Prog. Polym. Sci.* **1991**, *16*, 405. (b) S. K.-H. Thiele, D. R. Wilson, *J. Macromol. Sci. Part C: Polym. Rev.* **2003**, *4*, 581. (c) J. Huang, Z. Liu, D. Cui, X. Liu, *ChemCatChem.* **2018**, *10*, 42. (d) J. Furukawa, *Pure Appl. Chem.* **1975**, *42*, 495. (e) E. Kobayashi, S. Kaita, S. Aoshima, J. Furukawa, *J. Polym. Sci. Part A: Polymer Chemistry*, **1995**, *33*, 2175. (f) S. Tobisch, H. Bögel, R. Taube, *Organometallics* **1996**, *15*, 3563. (g) S. Tobisch, *Acc. Chem. Res.* **2002**, *35*, 96

[21] (a) L. Perrin, F. Bonnet, M. Visseaux, L. Maron, *Chem. Commun.* **2010**, *46*, 2965. (b) L. Perrin, F. Bonnet, T. Chenal, M. Visseaux, L. Maron, *Chem.—Eur. J.* **2010**, *16*, 11376. (c) X. Li, M. Nishiura, L. Hu, K. Mori, Z. Hou, *J. Am. Chem. Soc.* **2009**, *131*, 13870. (d) L. Zhang, T. Suzuki, Y. Luo, M. Nishiura, Z. Hou, *Angew. Chem., Int. Ed.* **2007**, *46*, 1909. (e) X. Li, M. Nishiura, L. Hu, K. Mori, Z. Hou, *J. Am. Chem. Soc.* **2009**, *131*, 13870. (f) L. Zhang, Y. Luo, Z. Hou, *J. Am. Chem. Soc.* **2005**, *127*, 14562. (g) Y. Luo, Z. Hou, *Organometallics* **2006**, *25*, 6162. (h) X. Kang, Y. Song, Y. Luo, G. Li, Z. Hou, J. Qu, *Macromolecules* **2012**, *45*, 640.

[22] R. Taube, J. Gehrke, R. Radeglia, *J. Organomet. Chem.* **1985**, *291*, 101.

[23] (a) X. Kang, Y. Luo, G. Zhou, X. Wang, X. Yu, Z. Hou, J. Qu, *Macromolecules* **2014**, *47*, 4596. (b) Y. Luo, Y. Luo, J. Qu, Z. Hou, *Organometallics* **2011**, *30*, 2908

[24] (a) H. Nsiri, I. Belaid, P. Larini, J. Thuilliez, C. Boisson, L. Perrin, *ACS Catal.* **2016**, *6*, 1028. (b) R. Ribeiro, R. Ruivo, H. Nsiri, S. Norsic, F. D'Agosto, L. Perrin, C. Boisson, *ACS Catal.* **2016**, *6*, 851. (c) L. Verrieux, J. Thuilliez, F. Jean-Baptiste-dit-Dominique, C. Boisson, M. Poradowski, L. Perrin, *ACS Catal.* **2020**, *10*, 12359.

[25] (a) F. Lin, X. Wang, Y. Pan, M. Wang, B. Liu, Y. Luo, D. Cui, *ACS Catal.* **2016**, *6*, 176. (b) X. Wang, F. Lin, J. Qu, Z. Hou, Y. Luo, *Organometallics* **2016**, *35*, 3205. (c) X. Wang, G. Zhou, B. Liu, Y. Luo, *Organometallics* **2018**, *37*, 882.

[26] (a) S. Yang, T. Ziegler, *Organometallics* **2006**, *25*, 887. (b) C. N. Rowley, T. K. Woo, *Organometallics* **2011**, *30*, 2071. (c) K. Matsumoto, K. S. Sandhya, M. Takayanagi, N. Koga, M. Nagaoka, *Organometallics* **2016**, *35*, 4099. (d) K. Matsumoto, M. Takayanagi, S. K. Sankaran, N. Koga, M. Nagaoka, *Organometallics* **2018**, *37*, 343. (e) N. Misawa, Y. Suzuki, S. Saha, N. Koga, M. Nagaoka, *Organometallics* **2021**, *40*, 48. (f) N. Misawa, Y. Suzuki, K. Matsumoto, S. Saha, N. Koga, M. Nagaoka, *J. Phys. Chem. B* **2021**, *125*, 1453.

[27] (a) A. J. Cohen. P. Mori-Sánchez, W. Yang, *Science*, **2008**, *321*, 792. (b) A. J. Cohen. P. Mori-Sánchez, W. Yang, *Chem. Rev.* **2012**, *112*, 289.

[28] A. D. Becke, *J. Chem. Phys.* **1993**, *98*, 5648.

[29] (a) Y. Zhao, D. G. Truhlar, *Acc. Chem. Res.* **2008**, *41*, 157. (b) Y. Zhao, D. G. Truhlar, *Theor. Chem. Acc.* **2008**, *120*, 215.

[30] H. Iikura, T. Tsuneda, T. Yanai, K. Hirao, *J. Chem. Phys.* **2001**, *115*, 3540.

[31] T. Yanai, D. P. Tew, N. C. Handy, *Chem. Phys. Lett.* **2004**, 393, 51.

[32] S. Tomoda in *Kiso Ryoshikagaku*, Tokyo daigaku shuppankai, **2007**, pp. 217–251. (in Japanese)

[33] S. Grimme, J. Antony, S. Ehrlich, H. Krieg, *J. Chem. Phys.* **2010**, 132, 154104.

[34] T. H. Dunning Jr., P. J. Hay, in *Modern Theoretical Chemistry*, Vol. 3 (Eds.: H. F. Schaefer III), Plenum, New York, **1977**, pp. 1−28.

[35] (a) R. Ditchfield, J. A. Pople, *J. Chem. Phys.* **1971**, 54, 724. (b) W. J. Hehre, R. Ditchfield, J. A. Pople, *J. Chem. Phys.***1972**, 56, 2257. (c) J. S. Binkley, J. A. Pople, W. J. Hehre, *J. Am. Chem. Soc.***1980**, 102, 939.

Chapter 2

Polymerization via Insertion of Ethylene into Al−C bond under Mild Conditions: Mechanistic Studies on the Promotion Exerted by a Catalytic Amount of Cationic Gadolinium Metallocene.

2.1. Introduction

Polymerization of olefins and dienes by homogeneous group 3 metals has attracted considerable attention in the past few decades due to their specific reactivity.[1,2] It has been reported that $Cp^*_2Sm[(\mu\text{-Me})AlMe_2(\mu\text{-Me})]_2SmCp^*_2$ ($Cp^* = \eta^5$-pentamethylcyclopentadienyl) first isolated by Evans et al.[3] acts as an efficient catalyst for the 1,4-polymerization of butadiene when mixed with $[Ph_3C][B(C_6F_5)_4]$ and excess trialkyl aluminum.[4] In 2003, Kaita et al. synthesized some lanthanide metal analogues with the composition $Cp^*_2Ln(\mu\text{-Me})_2AlMe_2$ (**1**, Ln= Gd, Nd, Pr), and isolated the powders in moderate to good yields from the reaction with $[Ph_3C][B(C_6F_5)_4]$.[5] In the case of Ln = Nd and Pr, the powders could be crystallized and were structurally characterized as a dimeric metallocene cation bridged by the Ln---F interaction (**2b** and **2c**, Scheme 1).

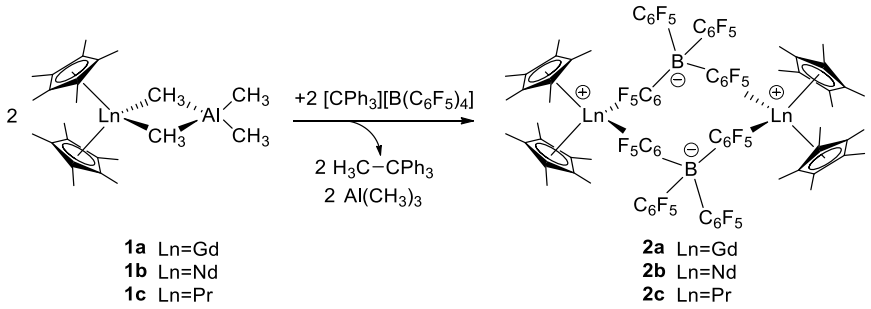

Scheme 1. Synthesis of $\{[Cp^*_2Ln][B(C_6F_5)_4]\}_2$ (Ln = Gd, Nd, Pr).

Addition of an excess amount of trialkyl aluminum to **2a** or **2b** led to excellent catalysis activity for butadiene polymerization. In particular, Gd complex **2a** showed extremely high catalytic activity and provided perfectly 1,4-*cis* regulated polybutadiene. Assuming **2a** has the structure similar to those of **2b** and **2c**, the conventional polymerization mechanism (e.g. coordinative chain-transfer polymerization (CCTP)) cannot explain this polymerization since **2a** itself has no Gd–alkyl bond. We became interested in the mechanism of butadiene polymerization catalyzed by the mixture of **2a** and trialkyl aluminum.

Herein, in order to elucidate the mechanism of this polymerization, we conducted experimental and computational studies [6] of the polymerization of the simplest monomer, ethylene, in place of butadiene. As shown in Table 1, the experiments showed that, when combined with an excess amount of Al(^{i}Bu)$_3$, **1a**/borate or **2a** efficiently produces polyethylene at 80 ℃ under 0.8 MPa pressure of ethylene. After quenching, the resulting polyethylene has an ethyl group at one end and an isobutyl group at the other terminal end.[6] Such polymerization behavior is observed in the CCTP. However, CCTP cannot account for the polymerization activity of the current catalyst system, since this reaction system has no initial Gd-alkyl bond.

Table 1. Ethylene polymerization results by using complexes **1a** and **2a** with various Al/Ln molar ratio.[a]

entry	Ln	Borate/[Ln] (equiv)	[Al]/[Ln] (equiv)	yield (g)	M_n[b]	M_w/M_n[b]
1	**1a**	—	0	11.0	15.3	19.70
2	**1a**	—	10	0.6	3.2	1.46
3	**1a**	—	59	0	—	—
4	**1a**	1.1	10	16.6	42.9	1.98
5	**1a**	1.1	59	23.3	16.8	1.48
6	**1a**	1.1	132	13.1	5.2	1.47
7	**2a**	—	0	0	—	—
8	**2a**	—	10	15.2	47.4	1.95
9	**2a**	—	59	21.2	16.6	1.40
10	**2a**	—	132	10.6	4.7	1.46

[a] General conditions: Neutral lanthanide complexes (**1a**): 20.4 μmol; Cationic Gd complex **2a**: 10.2 μmol; Borate: $[Ph_3C][B(C_6F_5)_4]$; [Al]: $Al(^iBu)_3$; 210 mL of toluene, ethylene pressure: 0.8 MPa, 30 min, 80 °C. [b] Determined by HT GPC, in units of kg/mol.

Two mechanisms have been well documented in the literature for the homogeneous polymerization mediated by catalysts composed of a main group metal alkyl and a d- or f-block metal complex. One is the classical coordination polymerization in which the main group metal alkyl works as an alkylating agent of the transition metal complex and the polymer chain grows simply via insertion of coordinated alkenes into thus formed transition metal alkyl bond.[2a] The other mechanism is developed more recently and called coordinative chain transfer polymerization (CCTP, Scheme 2).[2b] The CCTP catalyst systems in general are composed of a transition metal-alkyl (or lanthanide metal-alkyl) catalyst and an excess amount of main group metal alkyl compound (AlR_3, ZnR_2, MgR_2 etc.). It has been established that for the CCTP to take place, the

polymer chain on the transition metal center is able to quickly and reversibly transfer to the main group metal which is considered as a dormant species in the propagation step.

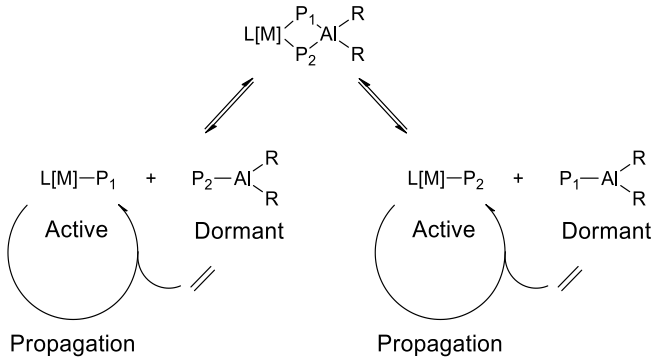

Scheme 2. Coordinative chain transfer polymerization (CCTP) using AlR_3 as the chain transfer agent (R, P_1, and P_2 denote alkyl or polymeryl).

The reversible alkyl exchange process between transition metal (or lanthanide metal) and main group metal moieties takes place most likely via a bis(μ_2-alkyl) bimetallic species.[7] Indeed, $[(Ind)_2Zr(\mu\text{-}Me)_2AlMe_2][B(C_6F_5)_4]$ was kinetically investigated as the precursor for the CCTP of ethylene.[8] It is noteworthy that the ideal CCTP condition is often not easy to realize; the rate of exchange of the polymer chain between the transition metal and main group metal must be of the order 100 times the rate of the olefin insertion into the transition metal carbon bond,[9] otherwise β-H elimination becomes relevant, typically leading to a broadening of the polymer distribution (PDI). Furthermore, to maintain CCTP condition, care must be taken to keep low solution viscosity for alleviating diffusion effect[10] which becomes more difficult at the later stage of the polymerization when polymer tends to precipitate.[11] Since long chain alkyl aluminum can be produced by this *trans*-alkylation reaction in CCTP, it looks as though the monomer has inserted

into the Al–C bond. It should be emphasized, however, that the real propagation step is the insertion of alkene into the transition metal–C(σ) bond (propagation step as shown in Scheme 2).

A straightforward method for obtaining long chain alkyl aluminum is the reaction of $Al(C_2H_5)_3$ with ethylene at elevated temperature (~120 °C) and high pressure (10–14 MPa). This is known as Ziegler "aufbau" reaction and provides the commercial route to unbranched primary alcohols (Alfol process) by repeated direct insertion of ethylene into the Al–C bond.[12] While the aufbau reaction usually gives only oligomeric products, there have been interests in the formation of high molecular weight polymer by the reaction of ethylene with some aluminum complexes followed by hydrolysis. Sen et al. claimed that in situ formed neutral complex $[(C_2H_5)(C_6F_5)_2Al]_x$ catalyzes polymerization of ethylene at 800 psi (5.5 MPa).[13] Jordan et al. reported polymerization of ethylene under milder conditions (60 °C, 0.2 MPa of ethylene) by cationic methyl aluminum complexes with amidinate ligand.[14] Theoretical investigations have suggested that a cationic dinuclear aluminum species could be a true active species.[15,16] These studies have implied that the direct propagation of ethylene on alkyl aluminum may be realized even under mild conditions if appropriate surroundings is arranged at the aluminum center.

In this chapter, I report computational study on the polymerization of ethylene catalyzed by **2a**/Al(^{i}Bu)$_3$ system and propose hitherto an unknown mechanism that is different from those of above mentioned CCTP or aufbau type reactions. The role of a catalytic amount of the lanthanide species in the novel mechanism is of particular interest.

2.2. Computational details

All calculations were performed with the Gaussian 09 program.[17] The density functional theory (DFT) method with M06 hybrid meta functional[18] was utilized for geometry optimization and

frequency calculations. Since 4f orbitals are much smaller than 6s and 5d orbitals, it is generally accepted that 4f orbitals are not responsible for the chemical bonds of lanthanide metal complexes. Therefore, the Gd atom was treated by the Stuttgart-Dresden quasi-relativistic large core effective core potential (ECP) and the associated basis sets.[19] D95V(d,p)[20] was used for the C and H atoms of Cp^* and ^{i}Bu groups and ethylene molecule and the 6-31G(d,p) basis set[21] was used for Al atom to which D95V(d,p) is not available. To save computational time, CEP-31G basis set[22] was used to B, C and F atoms of $[B(C_6F_5)_4]^-$, where the 1s electrons of those atoms were replaced by the ECPs. Transition state structures were checked by frequency calculations to prove that they were saddle points of order 1 and equilibrium structures were checked to have no imaginary frequency. Furthermore, the transition state structure was relaxed initially with the intrinsic reaction coordinate (IRC) calculations and then with geometry optimization calculations, to confirm that it does indeed connect the corresponding local minimum structures. The solvation effects were considered in geometry optimization calculations with SMD method.[23] Toluene (ε=2.37) was employed as a solvent in the SMD method. The reported energies include a zero-point energy correction (ZPE) but no thermal corrections to evaluate Gibbs free energy. The entropic effects calculated with textbook equations for ideal-gas molecules mainly come from the relative translation and rotation of the components. In solution, however, they are quenched, because components are individually solvated.[24] Therefore, I compare ΔE with ZPE correction, in which the solvation free energy has been taken care of by the PCM calculation with the SMD method. The validity of the discussion with Δ(E+ZPE) was confirmed by comparing Δ(E+ZPE) values with ΔG values. (See the APPENDIX for more details). For the polymerization reaction, we calculated the energetic span (δE) of the cycle according to the definition of Shaik et al.[25]

In some of the steps during the courses of the reactions studied, ethylene coordinates to or dissociates from the Gd or Al atom. Similarly, the alkyl group in the Al fragment coordinates to or dissociates from the Gd atom. I assumed that such reactions can take place easily as observed in many organometallic reactions and therefore I have not investigated them in detail. In the Figures for the energy profiles such steps are drawn with dotted lines, whereas the steps of which the transition states were determined are with solid lines. The Natural localized molecular orbitals (NLMOs) analysis was performed with the NBO program (NBO Version 6.0)[26] and NLMOs were plotted by using GaussView (Version 5.0.9.).

2.3. Result and discussion

In order for this polymerization to proceed by a CCTP mechanism, in situ formation of such an alkyl intermediate is required. The most probable one is an ^{i}Bu group transfer from aluminum leading to the neutral complex Cp*$_2$Gd–^{i}Bu which could be in equilibrium with the bimetallic species Cp*$_2$Gd(μ–^{i}Bu)$_2$Al(^{i}Bu)$_2$ as shown in eq. (1).

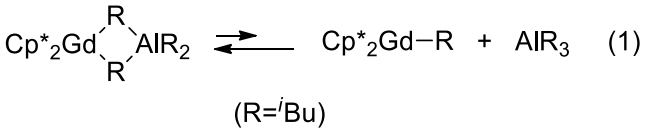

However, as shown in Table 1, the Me analog **1a**/Al(^{i}Bu)$_3$ showed only quite inefficient CCTP activity and was hindered by ca. 50 molar excess of Al(^{i}Bu)$_3$, whereas that is the best ratio for the **2a**/Al(^{i}Bu)$_3$ catalyst system in terms of activity. Thus, Cp*$_2$Gd(μ–^{i}Bu)$_2$Al(^{i}Bu)$_2$ cannot be a candidate that supports the CCTP mechanism in our **2a**/Al(^{i}Bu)$_3$ system.

First, I explored the structure of active species and the possibility of a Gd–alkyl species by DFT calculations, then investigated the mechanism of ethylene polymerization reaction.

Recent experimental and computational studies showed that various ion pairs can be generated in an activation process for polymerization reaction with boron-C_6F_5 compounds such as $B(C_6F_5)_3$ and $[Ph_3C][B(C_6F_5)_4]$ and aluminum alkyl species through Al/B transmetalation.[27,28] Perrin et al., however, adopted $B(C_6F_5)_4^-$ in their DFT calculations for polymerization reactions, to avoid considering various possibilities, although they found stable ion pairs with $Et_2B(C_6F_5)_4^-$ or $AlEt_4^-$.[28] Similarly, in this study we adopted $B(C_6F_5)_4^-$ as an anion.

2.3.1. Reaction of 2a with Al(^{i}Bu)$_3$

On adding Al(^{i}Bu)$_3$ to a toluene solution of **2a**, the blue color immediately turns to green. Assuming that some monomeric active species composed of three components, $[Cp^*_2Gd]^+$, $[B(C_6F_5)_4]^-$, and Al(^{i}Bu)$_3$ are formed, I identified **3a** in Figure 1 as the most stable structure among them. The less stable other possible species are shown in Figure S1. In **3a** the three atoms interacting with Gd cation, i.e. F and two H atoms of isobutyl group, are nearly in the plane that bisects the Cp*–Gd–Cp* axis. Approximately, the plane of the interacting C_6F_5 ring is also oriented in this plane. The calculated binding energy of Al(^{i}Bu)$_3$ to $[Cp^*_2Gd][B(C_6F_5)_4]$ in **3a** is 15.6 kcal/mol.

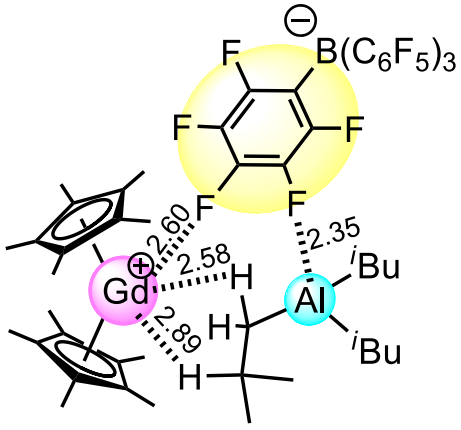

Figure 1. Active species (**3a**). Distances are given in Å.

2.3.2. Possibilities of transformation of 3a to species with a Gd–C(σ) bond.

Having determined the structure of intermediate **3a** formed from **2a** and Al(^{i}Bu)$_3$, we next examined if **3a** can give any species having a Gd–C(σ) bond. If such a species is easily generated, subsequent addition of ethylene would give polymer according to either classical coordination polymerization or the CCTP mechanism.

Alkyl transfer to form neutral Gd metallocene alkyl complexes. Our experiment suggested that even if a species of the type Cp*$_2$Gd–R (R = Me, ^{i}Bu) is generated in the reaction mixture, it stays in the resting state according to eq. (1). DFT calculation showed that formation of such intermediate through reactions eq. (3) and eq. (4) are thermodynamically unlikely in the first place, the products of these reactions being less stable than **3a** by 41.8 and 27.5 kcal/mol, respectively.

$$[Cp^*_2Gd]^+[B(C_6F_5)_4]^- / Al(^iBu)_3\ (\mathbf{3a}) \rightarrow Cp^*_2Gd{-}{}^iBu + [B(C_6F_5)_4]^- \text{ --- } [Al(^iBu)_2]^+ \quad \Delta E+ZPE = 41.8 \text{ kcal/mol)} \quad (3)$$

$$[Cp^*_2Gd]^+[B(C_6F_5)_4]^- / Al(^iBu)_3\ (\mathbf{3a}) \rightarrow Cp^*_2Gd{-}C_6F_5 + B(C_6F_5)_3 + Al(^iBu)_3 \quad \Delta E+ZPE = 27.5 \text{ kcal/mol} \quad (4)$$

Exchange of the alkyl group with a Cp* ligand. Exchange of one of the Cp* ligands in the cationic Gd metallocene with ^{i}Bu in Al(^{i}Bu)$_3$ (eq. (5)) or C_6F_5 group on the $[B(C_6F_5)_4]^-$ moiety (eq. (6)) were calculated.

$$[Cp^*_2Gd]^+[B(C_6F_5)_4]^- / Al(^iBu)_3\ (\mathbf{3a}) \rightarrow [Cp^*Gd{-}{}^iBu]^+\ [B(C_6F_5)_4]^- + [Cp^*Al(^iBu)_2] \quad \Delta E+ZPE = 41.4 \text{ kcal/mol} \quad (5)$$

$$[Cp^*_2Gd]^+[B(C_6F_5)_4]^- / Al(^iBu)_3\ (\mathbf{3a}) \rightarrow [Cp^*Gd{-}C_6F_5]^+\ [Cp^*{-}B(C_6F_5)_3]^- + Al(^iBu)_3 \quad \Delta E+ZPE = 49.6 \text{ kcal/mol} \quad (6)$$

In both cases, the products were found to be extremely less stable than **3a**. Coordination of Cp* ligand in the cationic Gd metallocene therefore appears to be quite strong in nature. The results are summarized in Figure S2 where the energies relative to $[Cp^*_2Gd]^+ + [B(C_6F_5)_4]^- + Al(^iBu)_3$ are shown. Hereafter, all the figures that display energy profiles are scaled with such mixture as 0.0 kcal/mol energy standard. We concluded that $[Cp^*_2Gd]^+$ moiety in **3a** is a quite stable unit and behaves as a part of catalyst in its own form.

2.3.3. Coordination of ethylene and subsequent reactions

When an ethylene molecule approaches to **3a**, three sites of attack may be conceivable (Scheme 3).

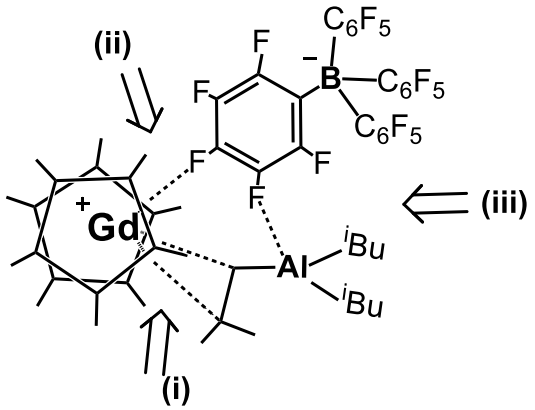

Scheme 3. Three possible sites of attack for the ethylene monomer in **3a**.

Of these, front attack (iii) may be negligible because the approach to Gd center is well guarded by two ^{i}Bu groups on Al and by C_6F_5 groups of borate. Accordingly, we examined ethylene attack from side directions (i) and (ii).

Attack of ethylene on 3a at site (i). Though the Gd center in **3a** is considerably crowded, the local minimum with very weakly coordinated ethylene was found (Figure 2, **4a-i**). The binding energy was very small (1.4 kcal/mol) and Gd---C(ethylene) distances are quite long (4.96 and 5.04 Å, Figure 3), while only slight change in orientation of $[B(C_6F_5)_4]^-$ and $Al(^iBu)_3$ was noted. Another local minimum with stronger coordination of ethylene (**5a-i**, Gd---C(ethylene): 3.06 and 3.27 Å) pushes $Al(^iBu)_3$ away from Gd, Gd---C(^{i}Bu) and Gd---βH(^{i}Bu) being elongated (3.53 and 4.02 Å). The energy level of **5a-i** is 2.6 kcal/mol higher than that of **4a-i**. There are several equilibrium structures with energy that is not so different between **4a-i** and **5a-i**. This shows that the energy surface of the area from **4a-i** to **5a-i** is very flat. The reaction of **5a-i** to **7a-i** requires various structure changes and it is not easy to locate its transition state. Accordingly, instead we performed calculation for $Al(^iBu)_3$ dissociation (**6a-i**) from **5a-i** to investigate the energy required by the ethylene insertion between Gd and $Al(^iBu)_3$, since the re-coordination of $Al(^iBu)_3$ to the backside of coordinated ethylene in **6a-i** can give intermediate **7a-i**. The transition state from **5a-i** to **7a-i**, if exists, probably should be lower in energy than that of **6a-i**. If less stable, the dissociative mechanism through **6a-i** would be followed. As a matter of fact, thus-obtained dissociating state (**6a-i** + $Al(^iBu)_3$) is more stable than the ethylene insertion transition state (**TS78a-i**), indicating that the mechanism, dissociative or associative, does not matter.

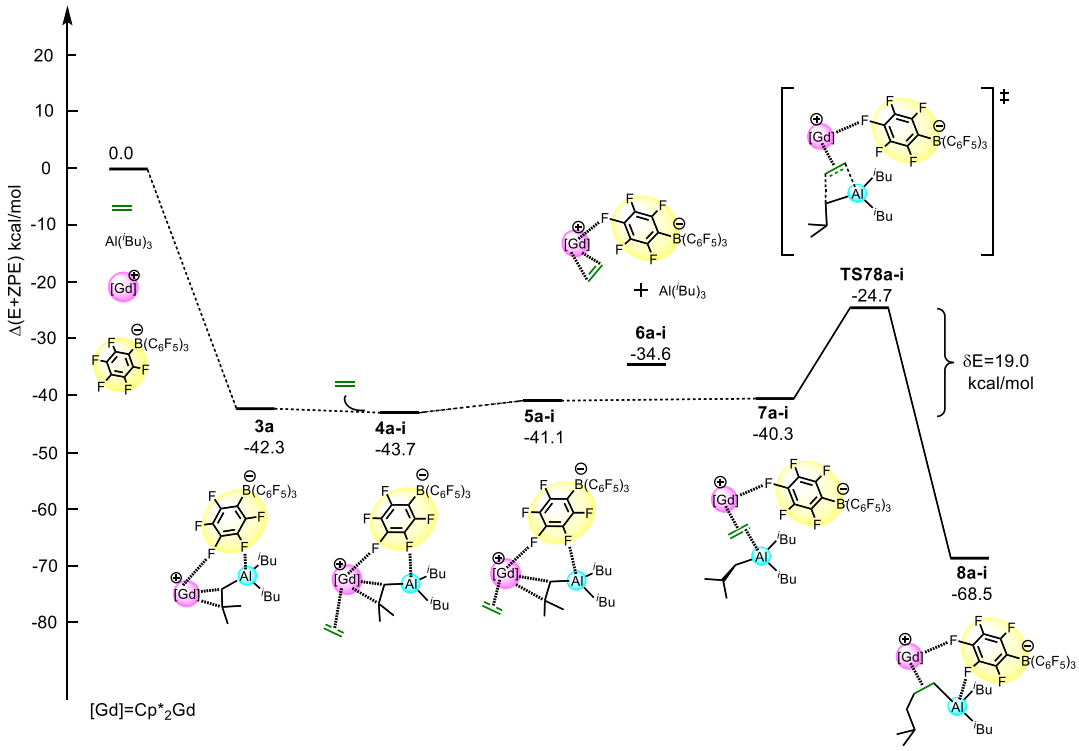

Figure 2. Energy profile (in kcal/mol, E+ZPE in toluene solution) for ethylene coordination at site (i) of **3a**, successive rearrangement and insertion into the Al–C bond. Cp^*_2 ligands are omitted for simplicity.

Starting from the ethylene-separated Gd---Al intermediate **7a-i**, we could find a pathway that enables insertion of ethylene into the Al–C(^{i}Bu) bond to give **8a-i**. The transition state (**TS78a-i**) that connects **7a-i** and **8a-i** is located at 19.0 kcal/mol higher energy level from the most stable intermediate in the reactant side (**4a-i)**.Coordination of a new ethylene molecule to **8a-i** should repeat the propagation cycle and eventually gives polymeryl-Al compound. Nevertheless, hoping to find energetically more feasible pathway for the polymerization, we continued our computational examination for the initial ethylene attack through the other direction of **3a**.

Much effort has been put into exploring activation and propagation mechanisms in cationic catalyst.[29–39] As a result of these efforts, it is generally accepted that the polymerization process is initiated with an anion displacement step, where the first incoming monomer displaces the counter anion in the inner-sphere contact ion pair to form the outer-sphere ion pair of monomer-coordinating intermediate and the counter anion. In this study, we considered that the additional ethylene monomer or alkyl aluminum needs to interfere with the coordination of the counter anion to the Gd cation in order to keep the counter anion away from the Gd cation in toluene solvent. Therefore, the displacement model of the counter anion was examined using a relatively small ethylene molecule as a displacement substrate.

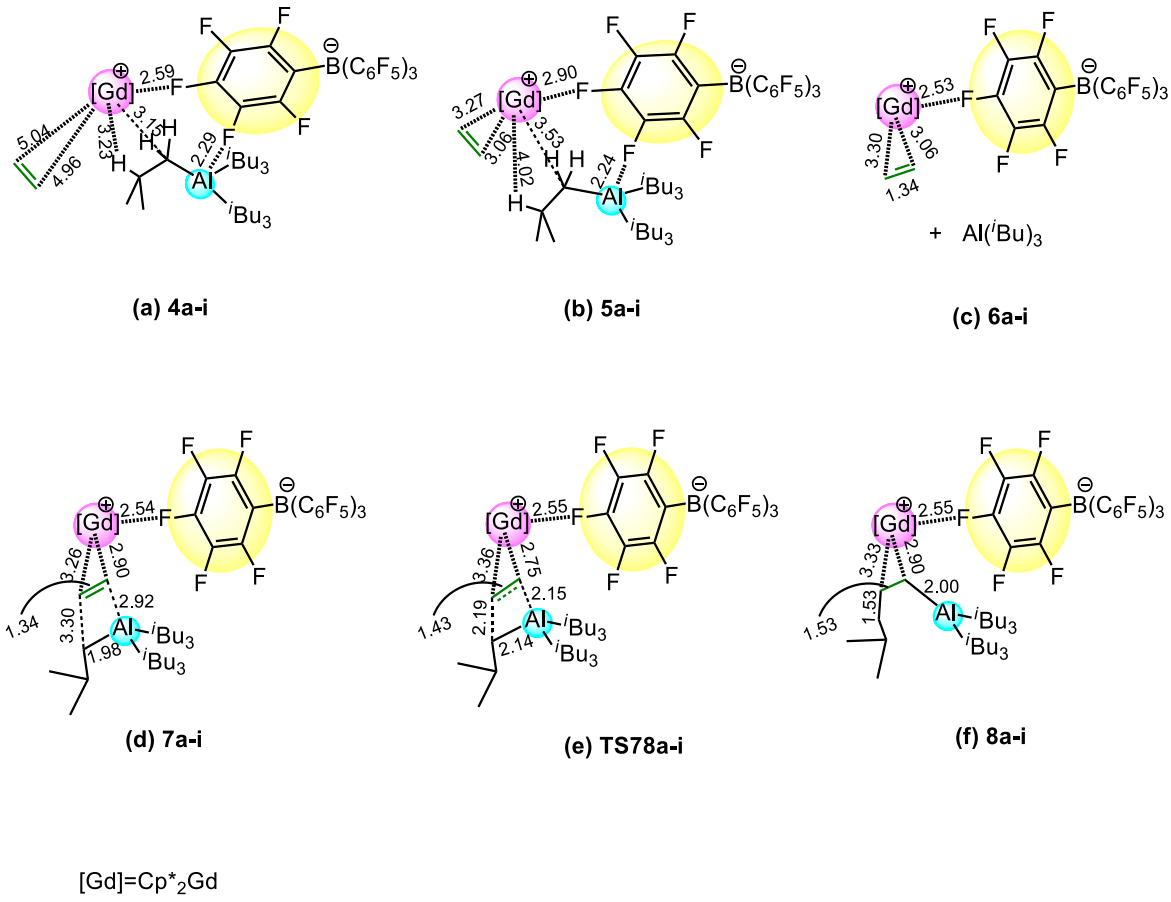

Figure 3. The geometries (distance in Å) of intermediates and transition states in Figure 2.

Attack of ethylene on 3a at site (ii). On approaching to the cationic Gd center through direction (ii), the ethylene molecule firstly gives a local minimum (**4a-ii**, Figure 4) that has very weak interaction to Gd with Gd---C(ethylene) distances of 4.68 and 4.63 Å (Figure 5). The neighboring borate moiety is slightly pushed away from Gd; calculated elongation of the Gd---F distance is from 2.60 Å in **3a** to 2.93 Å in **4a-ii**. Closer approach of this ethylene to Gd eventually lead to dramatic reorientation of the relative position. As shown in Figure 4, the whole reorientation process is energetically flat containing five intermediates, **4a-ii**, **5a-ii**, **6a-ii**, **7a-ii** and **8a-ii**. The process between **4a-ii** to **6a-ii** is considered to be Gd---C(ethylene) distance shortening process and the borate moiety is farthest away from Gd in **6a-ii** (Gd---F 3.34 Å). In **7a-ii**, the Gd---F distance became elongated to 5.22 Å and the borate moiety opens the gate, shifting its interaction from Gd to H of incoming ethylene (F---H(ethylene) 2.44 Å in **7a-ii**). Furthermore, we located a transition state (**TS78a-ii**) connecting **7a-ii** and **8a-ii** with a very small activation energy, a process requiring relatively large structure change. At **TS78a-ii**, one of the C_6F_5 rings in the borate anion rotates toward the ethylene coordinated with Gd. The final product **8a-ii** of this procedure has a unique structure; π-orbital of the coordinated ethylene also interacts with π-orbitals of one of the C_6F_5 rings in the borate anion. The distance of this π–π interaction (between center of the coordinated ethylene and center of one of the C_6F_5 rings in the borate anion) was calculated to be 3.54 Å. The largest energy barrier of 3.7 (= –38.6 – (–42.3)) kcal/mol is found between intermediates **3a** and **8a-ii**. Product **8a-ii** are more stable at 4.3 kcal/mol than **4a-ii** and 3.1 kcal/mol than the relative energies of **3a** + ethylene, respectively. The ethylene pressure (0.8 MPa) we employed in the present reaction would promote the formation of **8a-ii**.

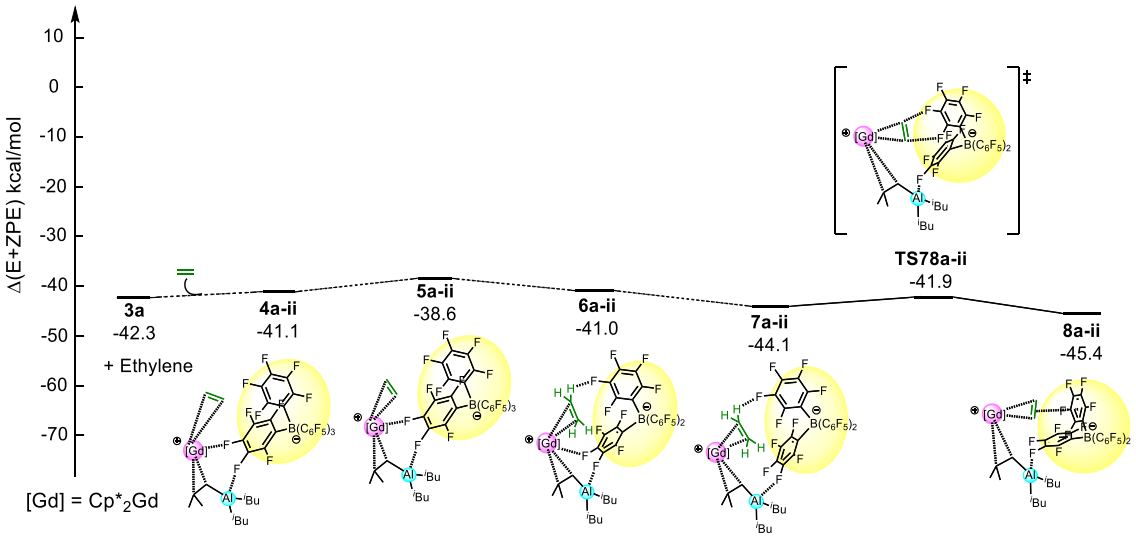

Figure 4. Energy profile (in kcal/mol, E+ZPE in toluene solution) for the coordination of ethylene leading to substitution of the $[B(C_6F_5)_4]^-$ unit. Cp^*_2 ligands are omitted for simplicity.

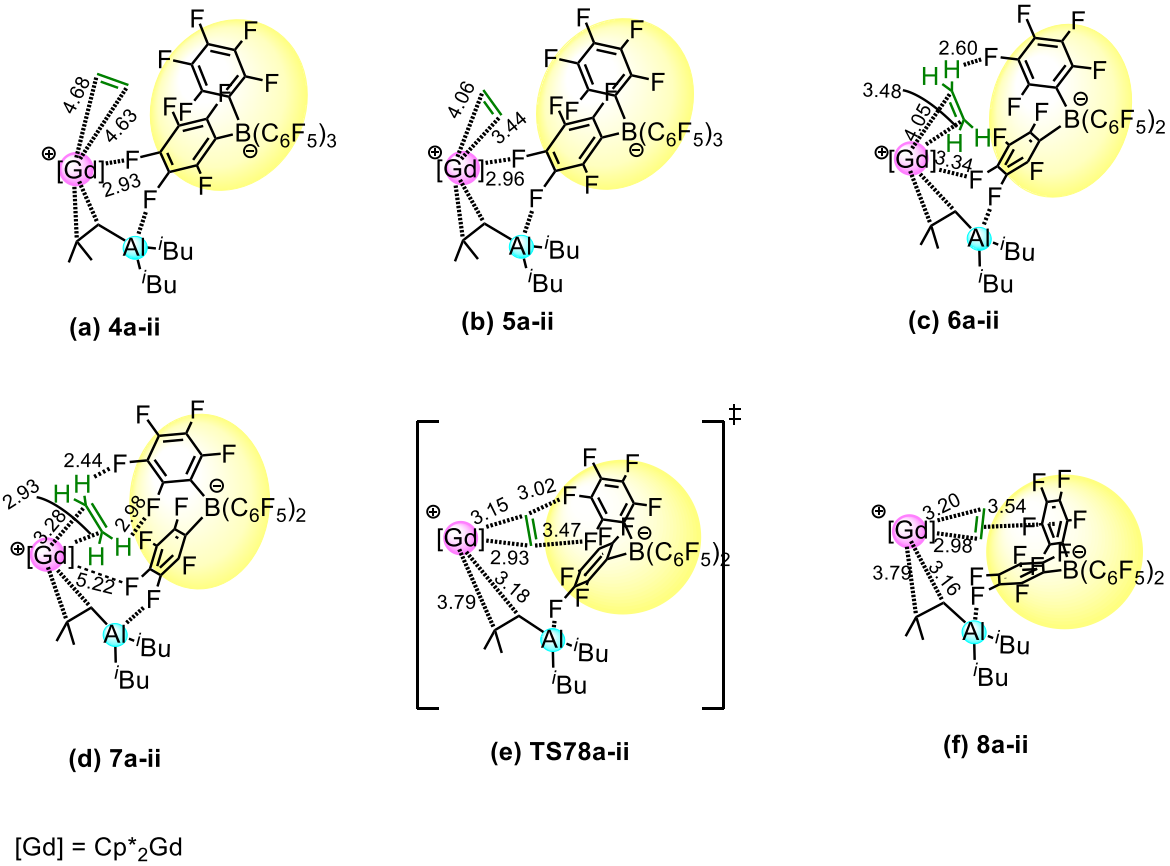

Figure 5. The geometries (distance in Å) of intermediates and transition states in Figure 4.

Attack of another ethylene molecule on 8a-ii at site (i). Formation of **8a-ii** described in the previous section would bring about important change in the environment of cationic Gd center. Electrostatic interaction between Gd and borate becomes weaker and steric congestion in close proximity to Gd must be eased in comparison to the situation in **3a**.

I examined a process similar to that shown in Figure 2, viz. attack of ethylene from the coordinating Al(^{i}Bu)$_3$ side, but starting from **8a-ii** in place of **3a**. The resulting energy diagram is shown in Figure 6 and the geometries of intermediates and transition state are illustrated in Figure 7. First, the conformational change of the ^{i}Bu group coordinated to Gd occurs and Al(^{i}Bu)$_3$ dissociates from Gd to open the gate between ^{i}Bu group and Gd; calculated elongation of the Gd---αH (^{i}Bu) distance is from 2.74 Å in **8a-ii** to 3.94 Å in **9a-ii**. The weak coordination of ethylene (**10a-ii**) slightly destabilizes the starting **8a-ii**. In the process from **9a-ii** to relatively stable **14a-ii**, where ethylene penetrates deeply between Gd and ^{i}Bu nearby borate anion, as found for **3a**, we located three intermediates structures, **10a-ii**, **11a-ii**, and **12a-ii**. The structure changes in this process show that ethylene gradually interrupts between Gd---Al(^{i}Bu)$_3$ and stronger coordination (**14a-ii**) expels Al(^{i}Bu)$_3$ away from Gd. Small energy changes without formation and cleavage of coordinate bond suggest that this takes place easily. Furthermore, we performed calculations for Al(^{i}Bu)$_3$ dissociation (**13a-ii**) from these intermediates for the similar purpose of calculations of **6a-i**. The thus obtained dissociating state (**13a-ii**) is more stable than the ethylene insertion transition state (**TS1617a-ii**), indicating that the mechanism, dissociative or associative, does not matter. In the next step, Al(^{i}Bu)$_3$ migrates from F in borate to ethylene gives **15a-ii** with a slight energy barrier (2.8 kcal/mol), followed by the ethylene insertion through four-centered transition state, **TS1617a-ii**, with an activation energy of 11.4 kcal/mol. These transformations are almost parallel to those of **3a** shown in Figure 2 but the most stable intermediate is now an intermediate

14a-ii. Importantly, the energy barrier (δE) of this process is 13.7 kcal/mol, much smaller than the corresponding value for the transformation shown in Figure 2. Coordination of a new ethylene molecule to the insertion product **17a-ii** would initiate stepwise propagation by repeating similar smooth cycles.

I believe that the procedure illustrated in Figure 6 provides a reasonable route for the present polymerization catalyzed by a mixture of **2a** with excess amount of Al(^{i}Bu)$_3$. Our preliminary molecular dynamics simulation suggests that other species such as Al(^{i}Bu)$_3$ in situ instead of ethylene, could assist borate dissociate from Gd, similar to the result in Figure 4.[40] The reaction be envisaged as direct insertion into an Al–C bond to give Al-terminated polyethylene which is catalyzed by cationic Gd metallocene.

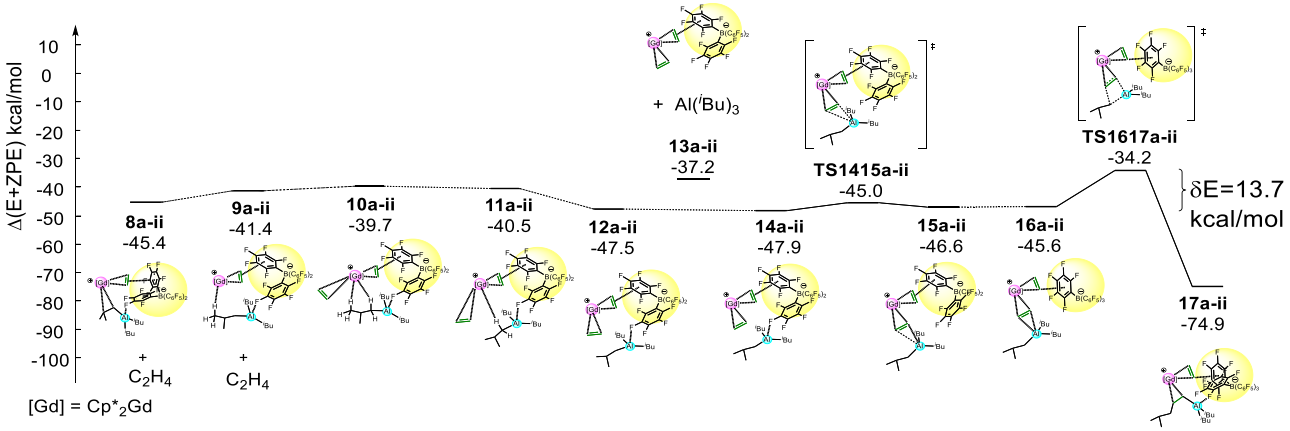

Figure 6. Energy profile (in kcal/mol, E+ZPE in toluene solution) for attack of ethylene from the Al(^{i}Bu)$_3$ side, but starting from **8a-ii.** Cp*$_2$ ligands are omitted for simplicity.

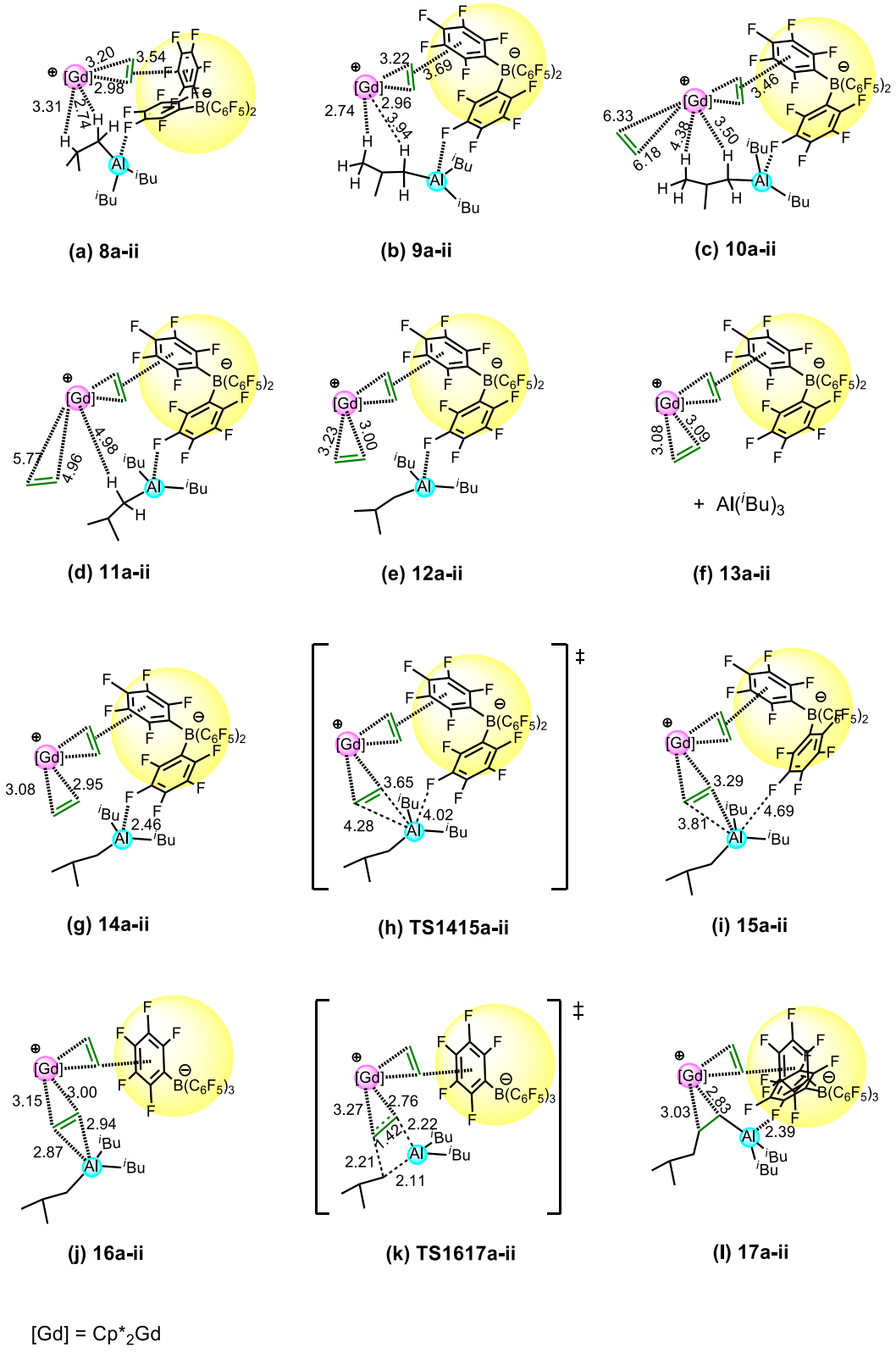

Figure 7. The geometries (distance in Å) of intermediates and transition states in Figure 6.

Exchange of the trialkyl aluminum moiety in intermediate complexes with free aluminum molecules. In the consecutive steps shown in Figure 6, there exists a chance of complete dissociation of Al(^{i}Bu)$_3$ from the complex which may be viewed as substitution of Al(^{i}Bu)$_3$ in **8a-ii** by an incoming ethylene molecule. This stage (**14a-ii**) is reached rather easily by the initial attack of ethylene on **8a-ii** by 10.4 kcal/mol (relative to **12a-ii**). The situation would be similar in further propagation cycles that follow the initiation scheme given in Figure 2. Thus, the exchange of the bound trialkyl aluminum with free one is expected to be occurring smoothly during the propagation, in accord with the observed rather sharp molecular weight distribution as displayed in Table1.[6] The equilibrium between (**8a-ii** + C_2H_4) and (**13a-ii**) may explain why the polymerization activity decreases on addition of too much Al(^{i}Bu)$_3$ to the **2a**/Al(^{i}Bu)$_3$ system (Table1) [6].

2.3.4. Origin of the promotion effect by the lanthanide metal

To assess the contribution of the Gd metal cation in the present polymerization reaction in detail, the calculated transition states for the insertion of ethylene into the Al–C(σ) bond of Al(^{i}Bu)$_3$ were compared with or without the presence of Gd metal cation. Figure 8(a) shows the energy profile and transition state structure for the insertion into free Al(^{i}Bu)$_3$ which takes place in Ziegler "aufbau" conditions. In Figure 8(b), those for the insertion step within the coordination sphere of Gd cation is shown, which we have already seen in Figure 6 (**TS1617a-ii**) but illustrated here in a simpler form for comparison. The activation energy 7.7 (= 19.1–11.4) kcal/mol was smaller when Gd cation is present. Why this happens was elucidated based on the Natural Localized Molecular Orbitals (NLMOs) representation as illustrated in Figure 9. The four-centered transition state for the insertion of free ethylene (**TS12**) has donation and back-donation between Al and ethylene, as illustrated in Figure 9. Note that upon interaction of ethylene with free Al(^{i}Bu)$_3$, ethylene π and π*

orbitals are largely polarized. NLMO-(a) denotes the donation from ethylene polarized π orbital to an empty 3p-orbital of Al and is going to develop the Al–C(2) bond, while NLMO-(b) shows the back-donation from Al–C(0) σ-orbital to polarized π* orbital of ethylene that will eventually form the C(0)–C(1) bond of the product. A similar reaction of Al(^{i}Bu)$_3$ toward ethylene that is pre-coordinated to the Cp*$_2$Gd cation (Figure 8(b)) has a 7.7 kcal/mol lower activation energy. As shown by NLMO-(c), -(d) and -(e) in Figure 9, this reduction in activation energy is brought about by the additional interaction of ethylene π and π* orbitals with empty 5d orbitals of Gd. This stabilizes π and π* orbitals, so that back-donation from Al–C(0) σ-orbital to π* orbital plays more important role in bond exchange than donation from π orbital; based on the results of Natural Bond Orbital (NBO) analysis, the energies of the π and π* orbitals in **TS12** are –0.327 and –0.019 a.u., respectively, whereas those in **TS1617a-ii** are –0.403 and –0.062 a.u., respectively. Also, the longer Al-ethylene distances (2.87 and 2.94 Å) in **16a-ii** compared with those in **1** (2.67 and 2.68 Å) are accounted for in terms of weaker donation from stable π orbital.

It is well-established that in the Diels-Alder reaction the Lewis acid lowers the energies of the lowest unoccupied molecular orbitals of dienophiles such as ketone to accelerate it. The effect of Gd found here is expected to be similar. The interaction of ethylene with Gd apparently reduces polarization in π and π* orbitals in NLMO-(c) and -(d), and therefore the formation of both Al–C(2) and C(0)–C(1) bonds are observed in both NLMOs different from the reaction of free Al(^{i}Bu)$_3$. However, unitary rotation of these NLMOs by 15° gave the orbitals similar to the NLMOs for free Al(^{i}Bu)$_3$, showing that the NLMOs for both reactions demonstrate similar interaction between Al–C(2) and C(0)–C(1) bonds. In addition to the NLMOs for four-centered interaction, we found the NLMO in which bent C(1)–C(2) bond interacts with Gd 5d orbital (Figure 9(e)). This

interaction partly releases strain in the σ bond framework in the four-membered ring structure to result in stabilizing the transition state structure.

The NLMOs for **TS78a-i** and the energies of π and π* orbitals are qualitatively similar to those for **TS1617a-ii** and, therefore, they are not shown. The larger activation energy for **TS78a-i** is mainly caused by the other factor than the orbital interactions. When $Al(^{i}Bu)_3$ approaches the ethylene molecule, the steric contact between non-reacting ^{i}Bu groups and the C_6F_5 group interacting with the Gd atom occurs. Contrary to this, in **TS1617a-ii** the second ethylene molecule makes the borate anion apart from the Gd atom and locates it at the side of $Al(^{i}Bu)_3$, reducing steric hindrance to decrease the activation energy.

Note that in **17a-ii** the strong interaction occurs between F in borate and Al, which misses in **16a-ii** upon the migration of $Al(^{i}Bu)_3$ to coordinated ethylene. This makes the insertion reaction with Gd more exoenergetic and shifts the transition state structure earlier, in addition to the activation of ethylene by Gd.

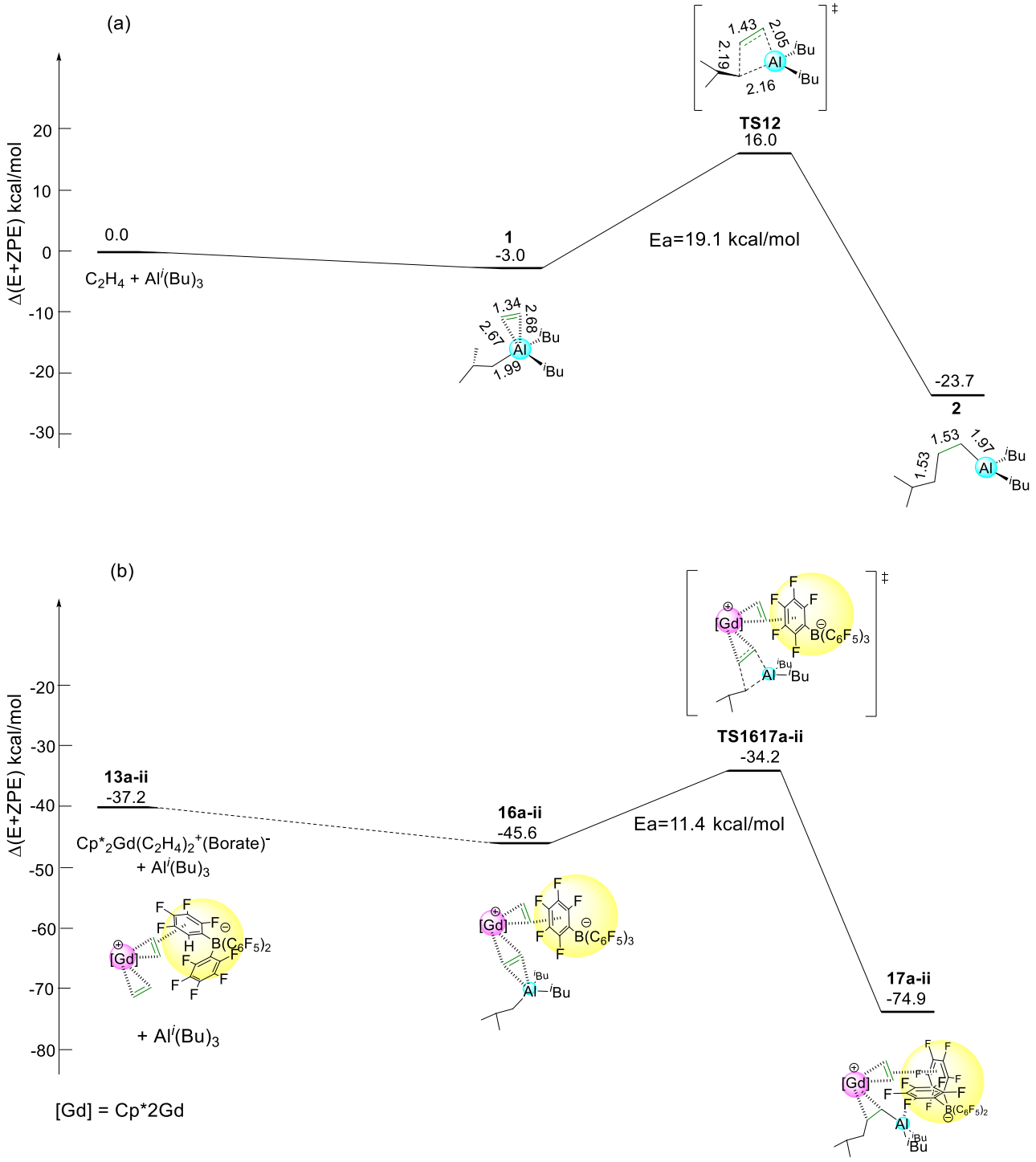

Figure 8. Transition state structures and their energies for the each C=C insertion into the Al–C (σ) bond of Al^iBu_3 (**TS12** and **TS1617a-ii**). For comparison the reaction with $[Cp^*_2Gd]^+$ starts from **13a-ii** with $Al(^iBu)_3$ dissociation. Cp^*_2 ligands are omitted for simplicity.

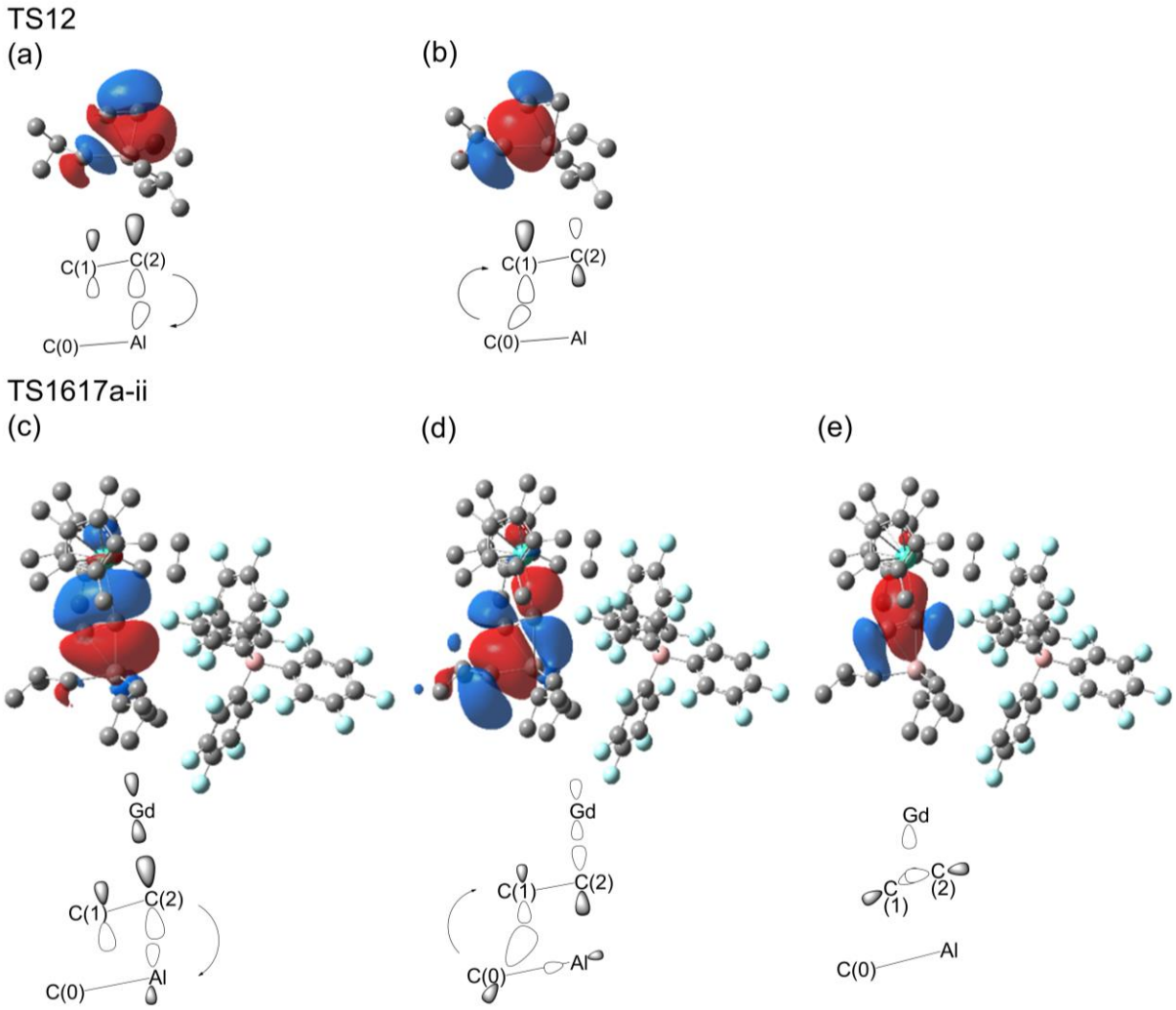

Figure 9. The transition state structures and their NLMO representations with or without the $Cp^*_2Gd^+$ unit. H atom omitted. (a) The donation from ethylene π orbital to an empty 3p-orbital of Al without the $Cp^*_2Gd^+$ unit. (b) The back-donation from Al–C(0) σ-orbital to π^* of ethylene without the $Cp^*_2Gd^+$ unit. (c) The donation from ethylene π to an empty 3p-orbital of Al with the $Cp^*_2Gd^+$ unit. (d) The back-donation from Al–C(0) σ-orbital to π^* of ethylene with the $Cp^*_2Gd^+$ unit. (e) The interaction of the bent C(1)–C(2) σ-orbital with the $Cp^*_2Gd^+$ unit.

2.4. Conclusion

We have already confirmed that the cationic Gd metallocene $[Cp^*_2Gd][B(C_6F_5)_4]$ (**2a**) can promote the polymerization of ethylene under mild conditions upon treatment with a large excess of $Al(^iBu)_3$. Prior quenching, the formed polyethylene exists mainly in the form of [Al]–$(CH_2CH_2)_n$–$CH_2CH(CH_3)_2$ with one Al atom at one end and one ^{i}Bu group at the other end, as suggested by polymers NMR characterization and deuterium labeling experiment[6]. The formation of such fragment is typical of a coordinative chain transfer polymerization (CCTP) mechanism where catalysts based on d- or f-block metal–alkyl complex can react with ethylene and chain transfer agent (CTA) such as alkyl aluminum. However, a big mystery to us was that this cationic metallocene catalyst system does not have a Gd–alkyl group, and the polymerization was unlikely to proceed in a typical CCTP fashion.

In this chapter 2, I have initiated a computational study (DFT calculation) to better understand the initiation and propagation mechanisms with this system. First, I confirmed that the in situ generation of a Gd–alkyl intermediate from **2a** that could insert ethylene monomer was not thermodynamically feasible. Then, I was able to find a reaction path, where the cationic Gd plays a crucial role by assisting ethylene insertion into one Al–C bond from $Al(^iBu)_3$ (Figures 4 and 6). Based on this model, it has been calculated that the contribution of Gd cation lowered the activation energy of ethylene insertion into the Al–C bond by 7.7 kcal/mol. Interaction of π and π* orbitals of ethylene with empty 5d orbitals of Gd was found responsible for this activation energy reduction. Importantly, such transition state is realized via prior separation of the $[Cp^*_2Gd]$ cation and the $[B(C_6F_5)_4]$ counter anion by species such as ethylene monomer (Figures 4 and 6). Although various anions may be generated in polymerization reactions,[18, 19] the qualitative results would be

unchanged, when the form of a borate anion is changed. This is because these results mainly originate from the interaction of ethylene with Gd,

This novel reaction mechanism derived from our theoretical calculation may bring new development to metal complex-catalyzed olefin polymerization, and shed new lights on the role of lanthanide ions. Next, since it has already been experimentally confirmed that this catalyst system is extremely effective for the high-cis 1,4-polymerization of butadiene, [5] I conducted theoretical calculations using butadiene instead of ethylene assuming a reaction route similar to that proposed in chapter 2. It would be interesting to see if this unique mechanism is also valid for butadiene, in which case the theoretical simulation should reproduce the observed high cis selectivity of its polymerization. They are discussed in chaper 3.

APPENDIX

The validity of the discussion for the polymerization reaction using ΔE with ZPE correction was confirmed by investigating the Gibbs free energy profiles in toluene in Figures S3–S6. Also, the Gibbs free energies of the products in the reaction of **2a** with Al(^{i}Bu)$_3$ and in the reaction eqs. (3)–(6) were given in Figures S1 and S2. These free energies were calculated at a pressure of 1 atm and a temperature of 298.15 K. With these free energies we obtained qualitatively the same results to support the discussion with Δ(E+ZPE). An exception is that migration of Al(^{i}Bu)$_3$ to the reacting ethylene molecule, **5a-i** to **7a-i** and **10a-ii** to **14a-ii**, may adopt the dissociative mechanism discussed in the body text.

Furthermore, in order to obtain more reliable energy profile, single-point energy calculations for the structures obtained with the above-mentioned basis set were performed using the larger 6-311G(d,p) basis sets for all atoms but the Gd atom. The results are shown in Figure S1, Figure S2,

Table S1, and S2, in which the smaller and larger basis sets are called basis set 1 and 2, respectively. The energy profiles thus obtained gave qualitatively the same results to support the calculations with the smaller basis set.

1. The Possible Species Produced in the Reaction of 2a with Al(^{i}Bu)$_3$.

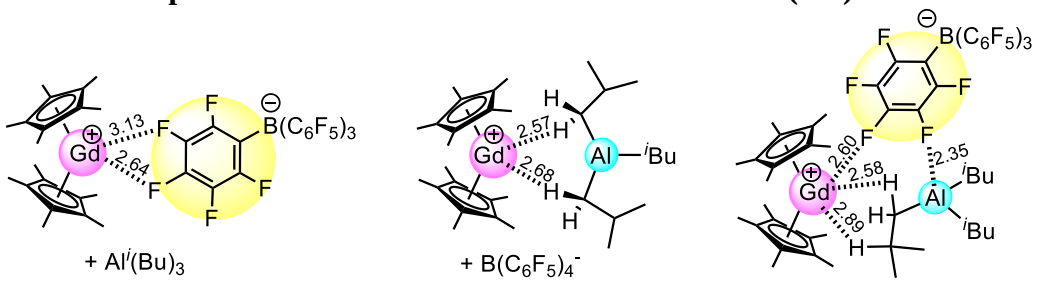

Figure S1. Energies (E+ZPE in toluene solution) of the possible species produced by the reaction of **2a** with Al(^{i}Bu)$_3$ relative to [Cp*$_2$Gd]$^+$ + [B(C$_6$F$_5$)$_4$]$^-$ + Al(^{i}Bu)$_3$ in kcal/mol. The values in parentheses are estimated with basis set 2, and those in brackets are the Gibbs free energies. Distances are given in Å.

2. Possibilities of transformation of 3a to a species with a Gd–C(σ) bond.

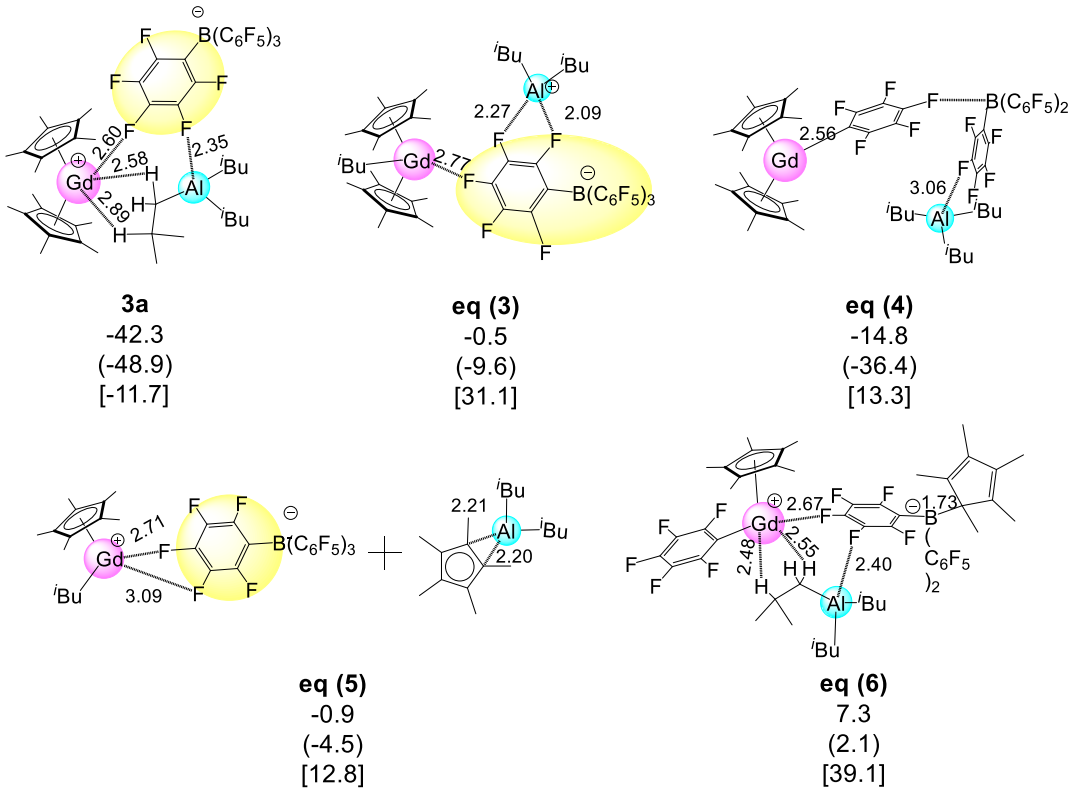

Figure S2. Energies (E+ZPE in toluene solution) of **3a** and the possible species with a Gd–C(σ) bond relative to $[Cp^*_2Gd]^+ + [B(C_6F_5)_4]^- + Al(^iBu)_3$ in kcal/mol. The values in parentheses are estimated with basis set 2 and those in brackets are the Gibbs free energies. Distances are given in Å.

3. Energy profile of the Gibbs free energies in toluene

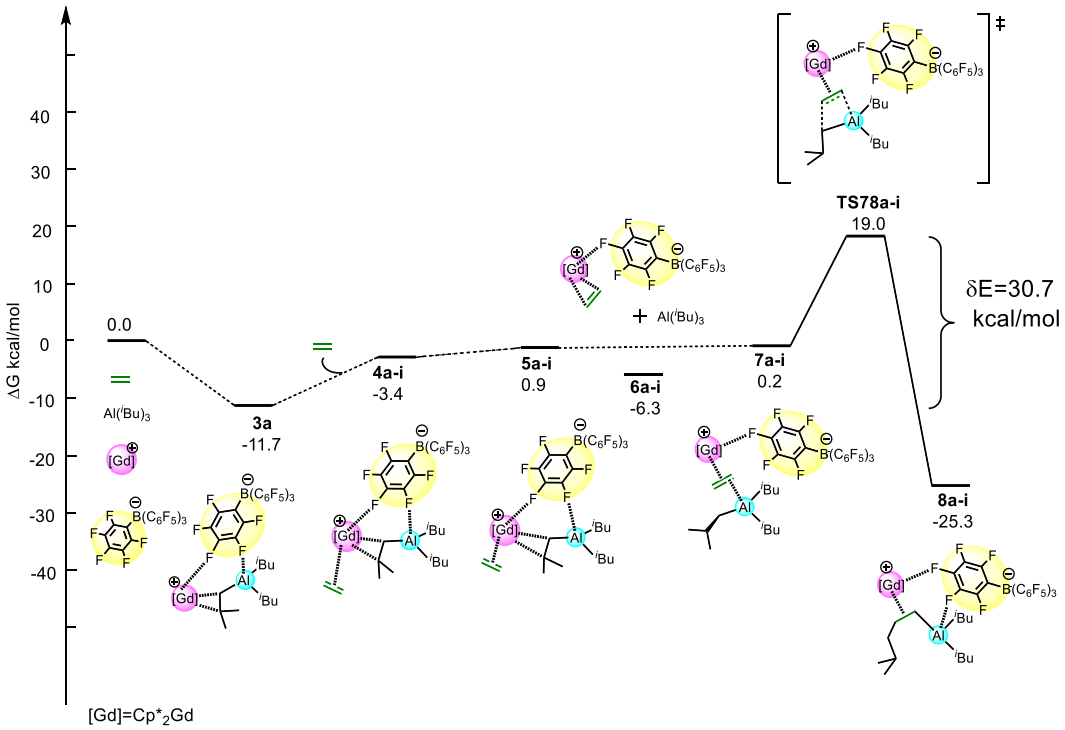

Figure S3. Energy profile (in kcal/mol, the Gibbs free energy in toluene solution) for ethylene coordination at site (i) of **3a**, successive rearrangement and insertion into the Al–C bond. Cp^*_2 ligands are omitted for simplicity.

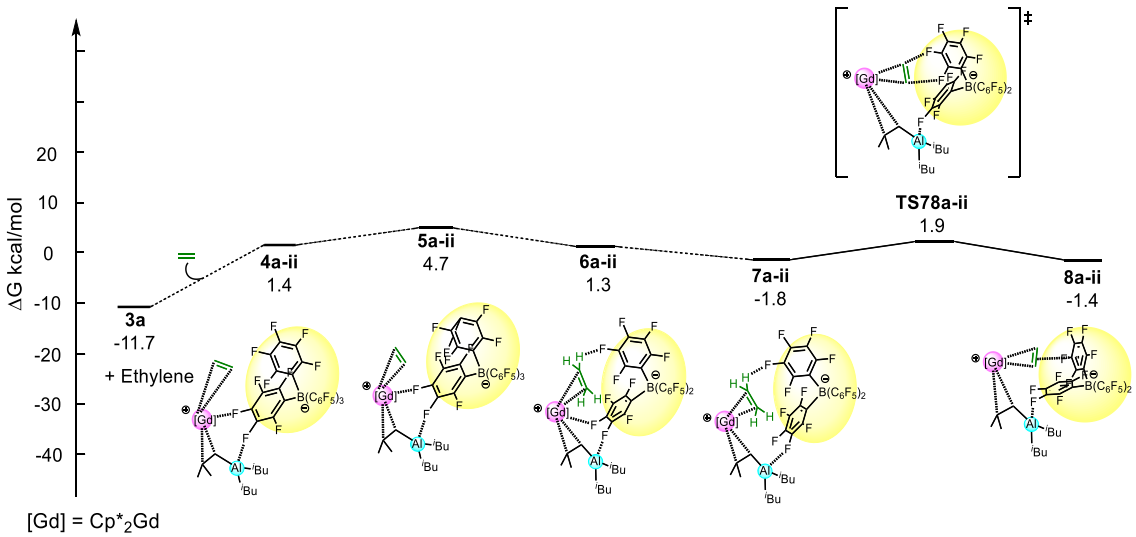

Figure S4. Energy profile (in kcal/mol, the Gibbs free energy in toluene solution) for the coordination of ethylene leading to substitution of the $[B(C_6F_5)_4]^-$ unit. Cp^*_2 ligands are omitted for simplicity.

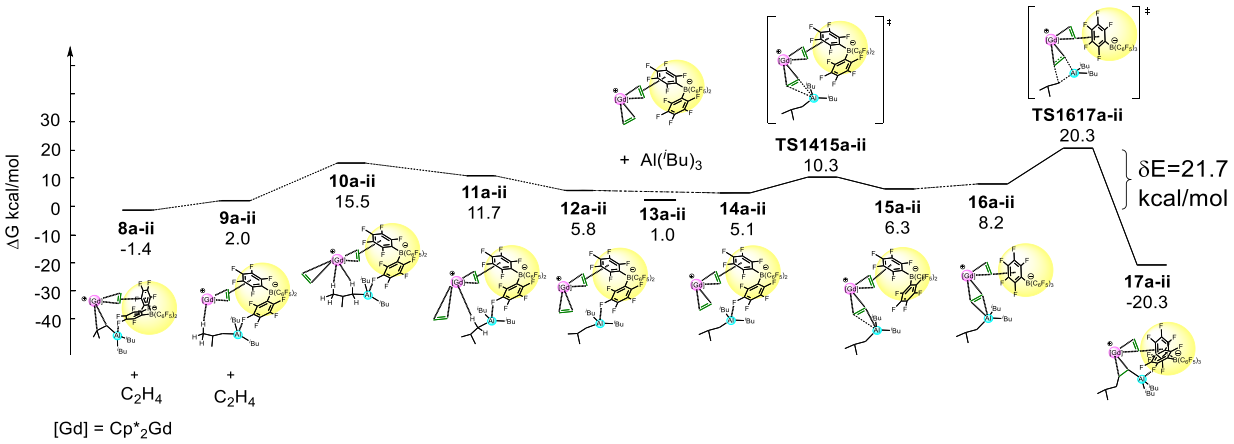

Figure S5. Energy profile (in kcal/mol, the Gibbs free energy in toluene solution) for attack of ethylene from the $Al(^iBu)_3$ side, but starting from **8a-ii**. Cp^*_2 ligand is omitted for simplicity.

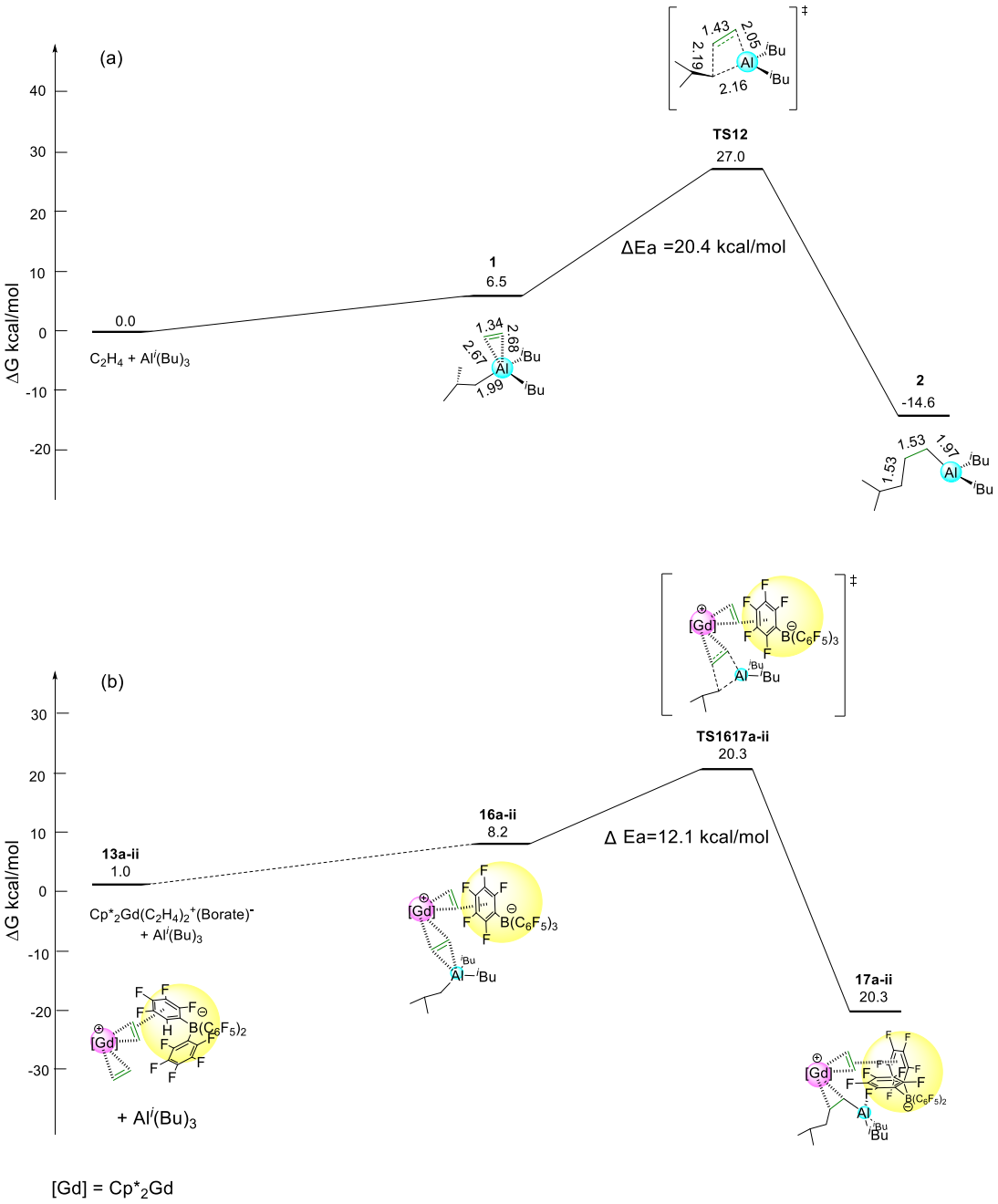

Figure S6. Transition state structures and their energies (in kcal/mol, the Gibbs free energy in toluene solution) for the each C=C insertion into the Al–C (σ) bond of Al(^{i}Bu)$_3$ (**TS12** and **TS1617a-ii**). For comparison the reaction with [Cp*$_2$Gd]$^+$ starts from **13a-ii** with Al(^{i}Bu)$_3$ dissociation. Cp*$_2$ ligands are omitted for simplicity.

4. Single Point Energy Calculations of Selected Intermediates and Transition States with Larger Basis Set.

Table S1. Energies of selected intermediates and transition states relative to $[Cp^*_2Gd]^+ + [B(C_6F_5)_4]^- + Al(^iBu)_3$ and energetic spans (δE) in (a) Figure 2, (b) Figure 4, and (c) Figure 6. All the values are estimated with basis set 2 and in kcal/mol.[a]

[a] single point energy calculations at the structures optimized with basis set 1.

[b] zero-point energy correction.

(a)

E+ZPE[b]		δE
4a-i	**TS78a-i**	
–53.4	–27.7	25.7

(b)

E+ZPE[b]						δE
3a	**4a-ii**	**5a-ii**	**6a-ii**	**7a-ii**	**TS78a-ii**	
–48.9	–51.9	–49.4	–53.0	–53.4	–54.7	2.5 (= –49.4 – (–51.9))

(c)

E+ZPE[b]						δE
12a-ii	**13a-ii**	**14a-ii**	**15a-ii**	**16a-ii**	**TS1617a-ii**	
–60.3	–45.8	–61.0	–60.5	–60.0	–46.3	14.6 (= –46.3 – (–61.0))

Table S2. Activation energies in kcal/mol, calculated using basis set 2, for C=C insertion into the Al–C (σ) bond of Al(^{i}Bu)$_3$ in Figure 8.

	Activation energy (Ea)
without Cp*$_2$Gd$^+$	21.7
with Cp*$_2$Gd$^+$	13.7

References

[1] For a recent review on polymerization of conjugated dienes by Group 3 single-site catalysts, see: J. Huang, Z. Liu, D. Cui, X. Liu, *ChemCatChem.* **2018**, 10, 42.

[2] For reviews on the controlled coordinative chain transfer polymerization (CCTP) of ethylene, see: a) R. Kempe, Chem. Eur. J. **2007**, *13*, 2764. b) A. Valente, A. Mortreux, M. Visseaux, P. Zinck, *Chem. Rev.* **2013**, *113*, 3836. c) D. J. Walsh, M.G. Hyatt, S. A. Miller, D. Guironnet *ACS Catalysis* **2019**, *9*, 11153.

[3] W.J. Evans, L.R. Chamberlain, T.A. Ulibarri, J.W. Ziller, *J. Am. Chem. Soc.* **1988**, *110*, 6423.

[4] a) S. Kaita, Z. Hou, Y. Wakatsuki, *Macromolecules* **1999**, *32*, 9078. b) S. Kaita, Z. Hou, Y. Wakatsuki, *Macromolecules* **2001**, *34*, 1539. (c) Z. Hou, S. Kaita, Y. Wakatsuki, *Pure and Applied Chemistry* **2001**, *73*, 291.

[5] a) S. Kaita, Z. Hou, M. Nishiura, Y. Doi, J. Kurazumi, A.C. Horiuchi, Y. Wakatsuki, *Macromol. Rapid Commun.* **2003**, *24*, 179. b) S. Kaita, M. Yamanaka, A.C. Horiuchi, Y. Wakatsuki, *Macromolecules* **2006**, *39*, 1359.

[6] R. Fukushima, O. Tardif, S. Kaita, Y. Wakatsuki, N. Koga, *Chem. Asian J.* **2021**, *16*, 1403.

[7] M. Bochmann, S.J. Lancaster, *J. Organomet. Chem.* **1995**, *497*, 55.

[8] J.M. Camara, R.A. Petros, J.R. Norton, *J. Am. Chem. Soc.* **2011**, *133*, 5263.

[9] M. van Meurs, G.J.P Britovsek, V.C. Gibson, *J. Am. Chem. Soc.* **2005**, *127*, 9913.

[10] F. Wang, C. Zhang, Y. Hu, X. Jia, C. Bai, X. Zhang, *Polymer* **2012**, *53*, 6027.

[11] C. Boisson, V. Monteil, D. Ribour, R.F. Spitz, F. Barbotin, *Macromol. Chem. Phys.* **2003**, *204*, 1747.

[12] Z. Wang, *Ziegler Alcohol Synthesis in Comprehensive Organic Name Reactions and Reagents*, John Wiley & Sons, Inc., **2010**, pp.3134–3138.

[13] J. S. Kim, L. M. Wojcinski, S. Liu, J. C. Sworen, A. Sen, *J. Am. Chem. Soc.* **2000**, *122*, 5668.

[14] M.P. Coles, R.F Jordan, *J. Am. Chem. Soc.* **1997**, *119*, 8125.

[15] G. Talarico, V. Busico, P.H.M Budzelaar, *Organometallics* **2001**, *20*, 4721.

[16] N. Ghorbani, N. Mahdizadeh Ghohe, S. Torabi, B.F. Yates, A. Ariafard, *Organometallics* **2013**, *32*, 1687.

[17] Gaussian 09, Revision D.01, M. J. Frisch, G.W. Trucks, H. B. Schlegel, G.E. Scuseria, M. A. Robb, J. R. Cheeseman, G. Scalmani, V. Barone, B. Mennucci, G. A. Petersson, H. Nakatsuji, M. Caricato, X. Li, H.P. Hratchian, A. F. Izmaylov, J. Bloino, G. Zheng, J. L. Sonnenberg, M. Hada, M. Ehara, K. Toyota, R. Fukuda, J. Hasegawa, M. Ishida, T., Nakajima, Y. Honda, O. Kitao, H. Nakai, T. Vreven, J. A. Jr Montgomery, J. E. Peralta, F. Ogliaro, M. Bearpark, J. J. Heyd, E. Brothers, K. N. Kudin, V. N. Staroverov, T. Keith, R. Kobayashi, J. Normand, K. Raghavachari, A. Rendell, J. C. Burant, S. S. Iyengar, J. Tomasi, M. Cossi, N. Rega, J. M. Millam, M. Klene, J. E. Knox, J. B. Cross, V. Bakken, C. Adamo, J. Jaramillo, R. Gomperts, R. E. Stratmann, O. Yazyev, A. J. Austin, R. Cammi, C. Pomelli, J. W. Ochterski, R. L. Martin, K. Morokuma, V. G. Zakrzewski, G. A. Voth, P. Salvador, J. J. Dannenberg, S. Dapprich, A. D. Daniels, O. Farkas, J. B. Foresman, J. V. Ortiz, J. Cioslowski, D. J. Fox, Gaussian, Inc., Wallingford CT, **2013**.

[18] a) Y. Zhao, D. G. Truhlar, J. Chem. Theory Comput. **2009**, 5, 324; b) Y. Zhao, D. G. Truhlar, *Acc. Chem. Res.* **2008**, 41, 157.

[19] M. Dolg, H. Stoll, A. Savin, H. Preuss, *Theor. Chim. Acta* **1989**, *75*, 173.

[20] T. H. Dunning Jr., P. J. Hay, in *Modern Theoretical Chemistry*, Vol. 3 (Eds.: H. F. Schaefer III), Plenum, New York, **1977**, pp. 1−28.

[21] M. M. Francl, W. J. Pietro, W. J. Hehre, J. S. Binkley, M. S. Gordon, D. J. DeFrees, J. A. Pople, *J. Chem. Phys.* **1982**, *77*, 3654.

[22] W. J. Stevens, H. Basch, M. Krauss, *J. Chem. Phys.* **1984**, *81*, 6026.

[23] A. V. Marenich, C. J. Cramer, D. G. Truhlar, *J. Phys. Chem. B* **2009**, *113*, 6378.

[24] K. Ando, K. Morokuma, *Theor. Chem. Acc.* **2011**, *130*, 323.

[25] S. Kozuch, S. Shaik, *Acc. Chem. Res.* **2011**, *44*, 101.

[26] E.D. Glendening, C.R. Landis, F. Weinhold, *J. Comput. Chem.* **2013**, *34*, 1429.

[27] D. Mathis, E. P.A. Couzijn, P.Chen, *Organometallics* **2011**, *30*, 3834.

[28] L. Verrieux, J. Thuilliez, F. J. B. Dominique, C. Boisson, M. N. Poradowski, L. Perrin, *ACS Catal*. **2020**, *10*, 12359.

[29] M.S.W. Chan, T.A. Ziegler, *Organometallics* **2000**, *19*, 5182.

[30] Z. Xu, K. Vanka, T. Ziegler, *Organometallics* **2004**, *23*, 1, 104.

[31] S.-Y. Yang, T. Ziegler, *Organometallics* **2006**, *25*, 887.

[32] C.R., Landis, K.A. Rosaaen, D.R. Sillars, *J. Am. Chem. Soc.* **2003**, *125*, 1710.

[33] M.-C. Chen, T.J. Marks, *J. Am. Chem. Soc.* **2001**, *123*, 11803.

[34] C.N. Rowley, T.K. Woo, *Organometallics* **2011**, *30*, 2071.

[35] A. Laine, B.B. Coussens, J.T. Hirvi, A. Berthoud, N. Friederichs, J.R. Severn, M. Linnolahti, *Organometallics* **2015**, *34*, 2415.

[36] R. Parveen, T.R. Cundari, J.M. Younker, G. Rodriguez, *Organometallics* **2020**, *39*, 2068.

[37] X. Wang, G. Zhou, B. Liu, Y. Luo, *Organometallics* **2018**, *37*, 882.

[38] K. Matsumoto, K.S. Sandhya, M. Takayanagi, N. Koga, M. Nagaoka, *Organometallics* **2016**, *35*, 4099.

[39] N. Misawa, Y. Suzuki, S. Saha, N. Koga, M. Nagaoka, *Organometallics* **2021**, *40*, 48.

[40] Unpublished results.

Chapter 3

Non-π-Allyl Mechanism for the 1,4-cis-Butadiene Polymerization: Theoretical Study of Polymerization via Insertion of Butadiene into Al–C Bond with Cationic Gadolinium Metallocene

3.1. Introduction

The stereoselective polymerization of conjugated dienes catalyzed by transition metal complexes has been the subject of much academic and industrial research due to its utility as synthetic rubbers.[1][2] Controlled *cis*-1,4-polymerization of butadiene is particularly important for the rubber industry.[2]

As discussed in Chapter 1, several mechanisms have been proposed for the stereospecific polymerization mechanism of butadiene, which basically consist of two steps: coordination of the monomer to the active site and insertion into the metal–C bond.[2(b),[9-11] The coordination mode of the 1,3-dienes to the central metal is variable, and these coordinated butadiene monomers insert into the metal–C bond, forming metal-η^3-allyl end group. There are two isomers of the π–allyl species, *anti* and *syn*, which can be interconverted via the σ–allyl. It is generally known that stereoselectivity is affected by the *syn-anti* isomerization of the π–allyl and the metal coordination of the penultimate C=C bond.[9(i),(j)]

It has been reported that the reaction of $Cp^*_2Ln(\mu\text{-}Me)_2AlMe_2$ (**1**) with $[Ph_3C][B(C_6F_5)_4]$ gives dimeric metallocene cations bridged by the Ln---F interaction, $\{[Cp^*_2Ln][B(C_6F_5)_4]\}_2$ (**2**, Ln = Gd(**a**), Nd(**b**), Pr(**c**)) and **2b** and **2c** were structurally characterized (Scheme 1).[12,13]

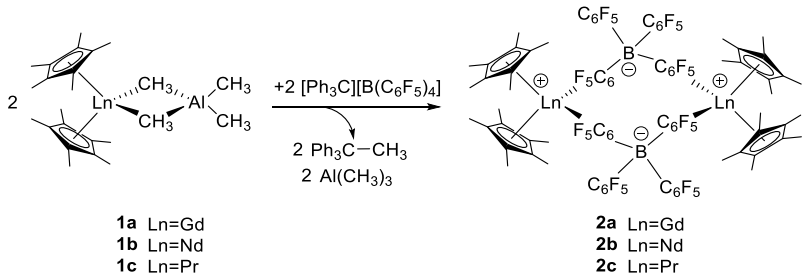

Scheme 1. Synthesis of $\{[Cp^*_2Ln][B(C_6F_5)_4]\}_2$ (Ln = Gd, Nd, Pr).

Interestingly, by adding an excess amount of trialkyl aluminum to **2a** or **2b**, the formation of 1,4-*cis* polybutadiene has been realized. In particular, Gd complex **2a** exhibited extremely high catalytic activity and provided perfectly regulated 1,4-*cis* polybutadiene (1,4-*cis* selectivity > 99.9% at −78 °C).[14] Assuming that **2a** has the similar structure as those of **2b** and **2c**, we became interested in the mechanism of butadiene polymerization with its mixture of **2a** and trialkyl aluminum. The most interesting point was that the Ln–alkyl or –hydride bond, at which a butadiene monomer would normally insert to start the polymerization, is absent. Even if such a bond could be generated *in situ*, it seems highly unlikely that the η^3-allyl end group is involved, which would be formed by the insertion of the first butadiene into the Ln–alkyl bond; $Cp^*_2Sm(\eta^3$-$CH_2CHCHMe)$ and related samallocene-η^3-allyl complexes have been isolated and reported to be inert for any further reactions with butadiene.[15]-[17]

In Chapter 2, to elucidate the mechanism of this polymerization, I reported the computational study of the polymerization of ethylene, the simplest monomer, instead of butadiene. The experiments showed that, when combined with an excess amount of $Al(^iBu)_3$, **1a**/borate or **2a** efficiently produces polyethylene at 80 ℃ under 0.8 MPa pressure of ethylene[18]. Because no Gd–alkyl species appears to be involved, a mechanism with conventional coordinative chain transfer polymerization (CCTP) [19]-[24] is not feasible. Density functional theory (DFT) analyses indicate a

novel mechanism in which the cationic Gd plays a crucial role by coordinating ethylene and assists the insertion of the coordinated ethylene into Al–C bond (Figure 1).

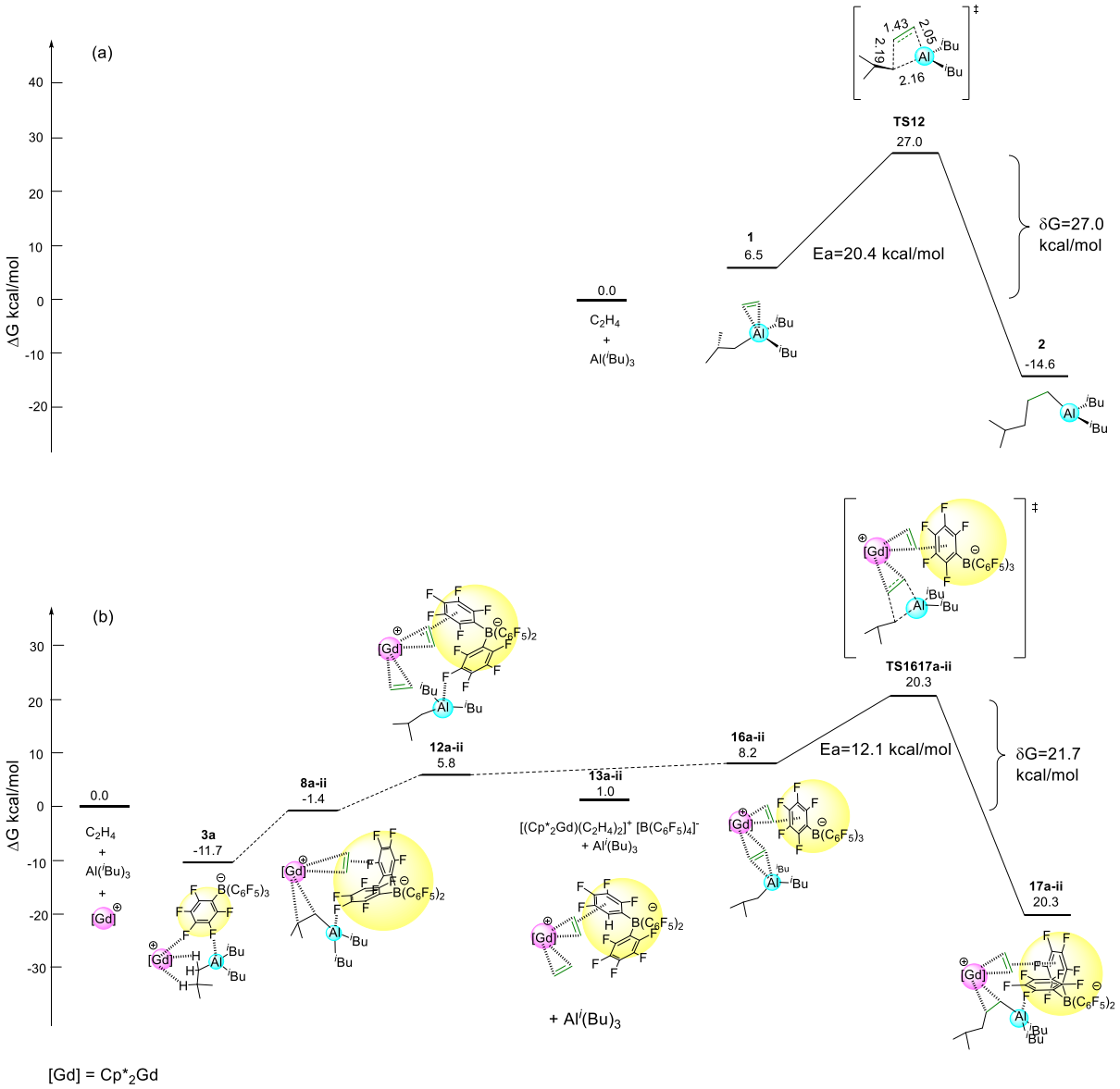

Figure 1. Energy profile (in kcal/mol, the Gibbs energy in toluene solution) for the each C=C insertion into the Al–C (σ) bond of Al(^{i}Bu)$_3$ without [Cp*$_2$Gd]$^+$ (a) and with [Cp*$_2$Gd]$^+$ (b).[18] Cp*$_2$ ligands are omitted for simplicity.

In this chapter, I extended the mechanism of ethylene polymerization by the **2a**/Al(^{i}Bu)$_3$ system (chapter 2 and Figure 1) to butadiene polymerization and report computational study on the specific 1,4-*cis* polymerization of butadiene with this catalytic system.

3.2. Computational details

All calculations were performed with the Gaussian 09 program.[39] The DFT method with M06 hybrid meta functional[40] was utilized for geometry optimization and vibrational frequency calculations. Since 4f orbitals are much smaller than 6s and 5d orbitals, it is generally accepted that 4f orbitals are not responsible for the chemical bonds of lanthanide metal complexes. Therefore, the Gd atom was treated with the Stuttgart-Dresden quasi-relativistic large core effective core potential (ECP) and the associated basis sets.[41] D95V(d,p)[42] was used for the C and H atoms of Cp* and ^{i}Bu groups and butadiene molecule and the 6-31G(d,p) basis set[43] was used for Al atom to which D95V(d,p) is not available. To save computational time, CEP-31G basis set[44] was used to B, C and F atoms of $[B(C_6F_5)_4]^-$, where the 1s electrons of those atoms were replaced by the ECPs. The solvation effects were considered in geometry optimization calculations with PCM method.[45] Toluene (ε=2.37) was employed as a solvent in the PCM method. Transition state structures were checked by frequency calculations to prove that they were saddle points of order 1 and equilibrium structures were checked to have no imaginary frequency. Furthermore, the transition state structure was relaxed initially with the intrinsic reaction coordinate (IRC) calculations and then with geometry optimization calculations, to confirm that it does indeed connect the corresponding local minimum structures. On the other hand, the search for reaction pathways not involving $[Cp^*_2Gd]^+$ unit was performed by applying the AFIR method and saddle-point optimization at the same level of GRRM[46] as the DFT calculations with the Gaussian 09

described above. In the present work, all required computations for the GRRM program were performed along with Gaussian 09 program. Energy values correspond to Gibbs energy given in kcal/mol estimated at 298 K and 1atm. Enthalpy and entropy contributions are estimated within the harmonic oscillator approximation. We calculated the energetic span (δG) of the cycle according to the definition of Shaik et al.[47]

Using the above method, I investigated the mechanism of butadiene polymerization reaction. In some of the steps during the courses of the reactions studied, butadiene coordinates to or dissociates from the Gd or Al atom. Similarly, the alkyl group in the Al fragment coordinates to or dissociates from the Gd atom. I assumed that such reactions can take place easily as observed in many organometallic reactions and therefore I have not investigated them in detail. In the Figures for the energy profiles such steps are drawn with dotted lines, whereas the steps of which the transition states were determined are with solid lines. The Natural localized molecular orbitals (NLMOs) analysis was performed with the NBO program (NBO Version 6.0)[48] and NLMOs were plotted by using GaussView (Version 6.1.1.).

3.3. Results and discussion

Many previous studies have suggested displacement of the counter anion during polymerizations to enhance catalysis.[25]-[38] In the previous DFT analysis of the polymerization of ethylene, it was found that the $[B(C_6F_5)_4]^-$ exists in the vicinity of the $[Cp^*_2Gd]^+$ and interacts with the $[Cp^*_2Gd]^+$, but it is not directly involved in the monomer insertion reaction (Figure 1 (b)).[18] My preliminary molecular dynamics simulation suggests that other species such as $Al(^iBu)_3$ and monomers in situ could assist the $[B(C_6F_5)_4]^-$ unit to dissociate from Gd, and it was also observed that a butadiene monomer has a stronger dissociation-assisting effect than an ethylene monomer.[49] Thus, I decided

to investigate the polymerization mechanism without the counter anion to save computational time. I investigate the mechanism of butadiene polymerization with adopting the previously estimated active species without the $[B(C_6F_5)_4]^-$ (Figure 2). [18] Based on the mechanism I also analyzed the stereoselective polymerization of 1,3-butadiene.

3.3.1 Adduct of cationic gadolinium metallocene with Al(^{i}Bu)$_3$

While **3a** in Figure 2 has already identified as active species in the reaction with $[B(C_6F_5)_4]^-$, the structure determination of active species by removing $[B(C_6F_5)_4]^-$ and ethylene monomer from **3a** and **8a-ii** showed that **4a** is a more stable active species. In **4a**, the distance between Gd and Al(^{i}Bu)$_3$ is closer than that in **8a-ii** and the β-H of another isobutyl group of Al(^{i}Bu)$_3$ interacts with Gd.

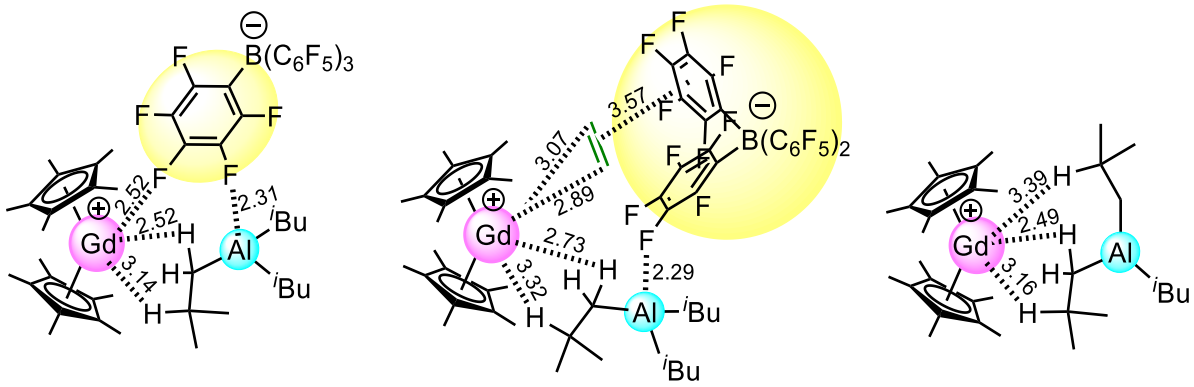

Figure 2. The structures (distance in Å) of intermediates. (a) Active species **3a**. (b) Active species **8a-ii** with $[Cp^*_2Gd]^+$ and $[B(C_6F_5)_4]^-$ separated by ethylene monomer. (c) Active species **4a** obtained by removing $[B(C_6F_5)_4]^-$ and ethylene monomer from **8a-ii**.

3.3.2. Initiation step of polymerization

I first examined the structures in the case of s-*trans*- and s-*cis*-butadiene coordination to $[Cp^*_2Gd]^+$, and found that the s-*trans*-butadiene-coordinated complex was 4.1 kcal/mol more stable than s-*cis*-butadiene-coordinated complex. s-*Trans*-butadiene is 2.9 kcal/mol more stable than s-*cis*-butadiene, indicating that the binding energy of the s-*trans* complex is 1.2 kcal/mol larger. This is due to the greater steric contact of s-*cis*-butadiene with $[Cp^*_2Gd]^+$ in $[Cp^*_2Gd(s\text{-}cis\text{-butadiene})]^+$ complex (Table S1 and Figure S1). Therefore, the butadiene coordination in the following is assumed to be s-*trans*-butadiene coordination. The reaction of an s-*trans*-butadiene molecule with the above-mentioned bimetallic species **4a** starts with the formation of complex **5a** (Figure 3), in which coordination of an s-*trans*-butadiene pushes $Al(^iBu)_3$ away from Gd, the distance between Gd and β-H(^{i}Bu) being elongated (4.22 Å). **5a** is 3.9 kcal/mol higher in Gibbs energy than that of **4a** due to entropy loss.

In the propagation step of ethylene polymerization, we found that the insertion reaction proceeds from the intermediate in which an ethylene molecule is sandwiched by $[Cp^*_2Gd]^+$ and $Al(^iBu)_3$ (**16a-ii** in Figure 1). The reactant **7a** of the butadiene insertion is such an intermediate and formed in the reaction of **5a**. The reaction of **5a** to **7a** is, however, not easy to follow in detail, because the various structure changes would occur in its reaction pathway. Accordingly, to estimate the energy required by the formation of **7a** from **5a**, I instead performed the calculations for $Al(^iBu)_3$ dissociation from **5a** to give **6a**. This is because the re-coordination of free $Al(^iBu)_3$ to the backside of coordinated butadiene in **6a** can give intermediate **7a**. Thus-obtained dissociating state (**6a** + $Al(^iBu)_3$) is more stable than **5a**. In intermediate **7a**, one C=C bond of the butadiene monomer is coordinated to the reaction center, Al, while the other C=C bond is coordinated to the central metal of the catalyst, Gd. Starting from intermediate **7a**, I found a

pathway to obtain **8a** by insertion of butadiene into the Al–C(*i*Bu) bond. The transition state (**TS78a**) that connects **7a** and **8a** is located at an energy level being 21.5 kcal/mol higher than the most stable intermediate in the reactant side (**6a**). Furthermore, the insertion product in **8a**, (6-methylhept-1-en-3-yl)Al(*i*Bu)$_2$ (**9^t**), dissociates from [Cp$^*_2$Gd]$^+$, being endergonic by 4.6 kcal/mol (= (−12.0) − (−16.6)). This energy barrier was by far lower than the barrier for insertion reactions, so it was expected to occur easily.

Prior to the next butadiene insertion with a head-to-tail coupling observed experimentally, a 1,3-sigmatropic rearrangement of the Al(*i*Bu)$_2$ unit is required. This rearrangement could make both *cis*- and *trans*-forms. In the next section, I estimate the energy barrier required for a series of 1,3-shift and conformational change.

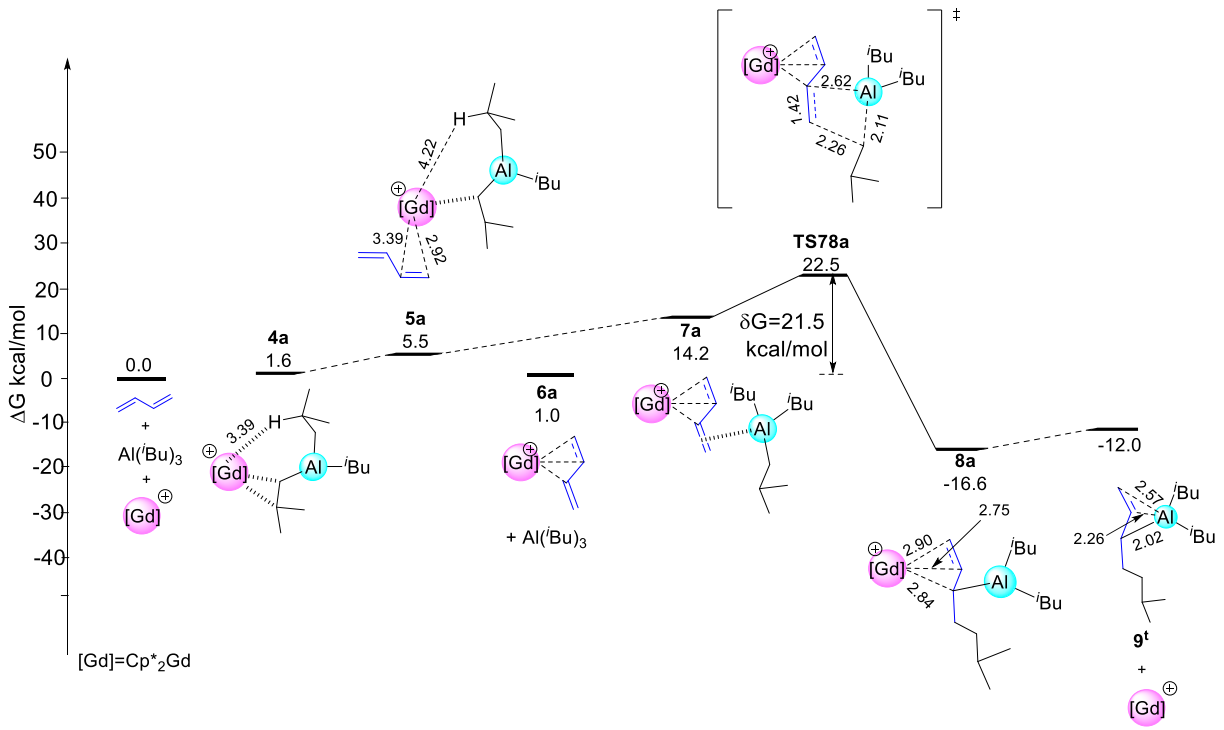

Figure 3. Energy profile (in kcal/mol, Gibbs energy in toluene solution) for butadiene coordination

to **4a**, successive rearrangement and insertion into the Al–C bond. Cp*$_2$ ligands are omitted for simplicity. H atom of one of ^{i}Bu groups is explicitly shown as β-H in the body text.

3.3.3. Isomerization of dissociated growing chains

The insertion product (**9^t**) dissociated from [Cp*$_2$Gd]$^+$ is assumed to cause C2–C3 bond rotation and the 1,3-sigmatropic rearrangement of the Al(^{i}Bu)$_2$ unit in this reaction system as shown in Figure 4. The energy barrier required for the rotation around the C2–C3 bond that gives **9^c** was calculated to be about 10 kcal/mol. Furthermore, the 1,3-sigmatropic rearrangement of Al(^{i}Bu)$_2$ unit occurs smoothly in both **9^t** and **9^c**, leading to **10-*trans*** and **10-*cis***, respectively. The energy barriers for these processes shown in Figure 4 are significantly lower than that of the initiation reaction, and thus they are expected to occur easily in this reaction system.

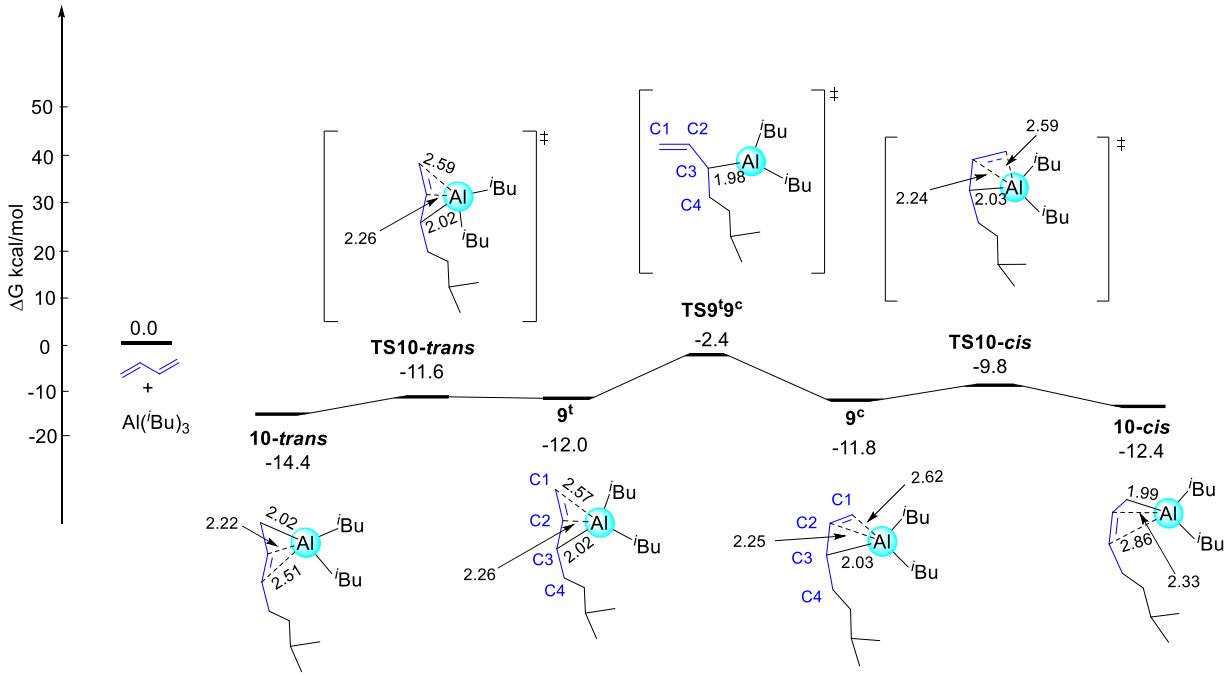

Figure 4. Energy profile (in kcal/mol, Gibbs energy in toluene solution) for the rotation of C2–C3 bond and the 1,3-sigmatropic rearrangement of the Al(^{i}Bu)$_2$ unit in the insertion product.

3.3.4. The propagation step in polymerization

Based on the results in the initiation step mentioned above as well as those for ethylene polymerization,[18] it was reasonably assumed that butadiene polymerization proceeds via an intermediate with butadiene sandwiched by Gd and Al. For chain propagation, the reaction of each of the four insertion product isomers (**9^{t}**, **9^{c}**, **10-*trans*** and **10-*cis*** in Figure 4) with a second s-*trans*-butadiene monomer was investigated. The calculations showed that the reactions of **10-*trans*** and **10-*cis*** with the butadiene monomer pass through the four-centered transition state, while the reactions **9^{t}** and **9^{c}** pass through the eight-membered ring transition state (Figure 5). The energy profiles and structures of these four propagation pathways are shown in Figures 6, 7, 8 and 9.

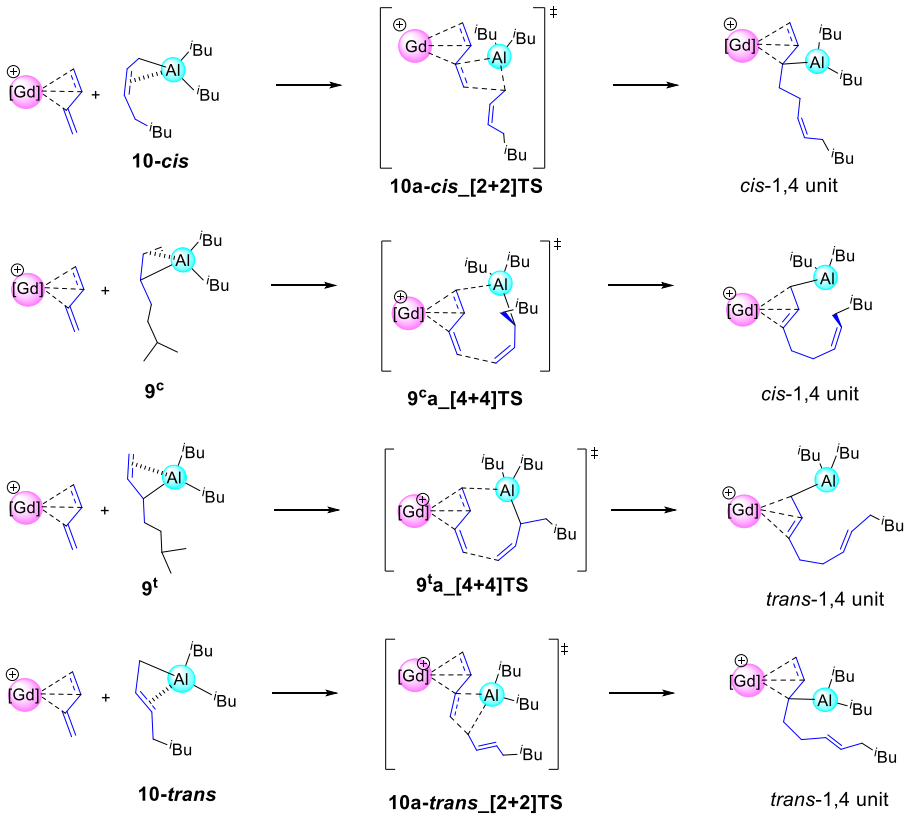

Figure 5. Four possible pathways of the reactions of initial insertion product **9^{t}** and their isomers with $[Cp^*_2Gd(C_4H_6)]^+$. Cp^*_2 ligands are omitted for simplicity.

The energy barrier for **10-*trans*** leading to **10a-*trans*_[2+2]P** with a *trans*-1,4 unit via **10a-*trans*_[2+2]TS** was 23.8 kcal/mol (=9.4−(−14.4)). On the other hand, the energy barrier, relative to the most stable **10-*trans***, for the formation of *cis*-1,4 unit via **10a-*cis*_[2+2]TS** was 26.0 kcal/mol (= 11.6 − (−14.4)). The transition state, **10a-*trans*_[2+2]TS**, for **10-*trans*** leading to **10a-*trans*_[2+2]P** with a *trans*-1,4 unit, is 2.2 kcal/mol is more stable than **10a-*cis*_[2+2]TS** from **10-*cis***, showing that the reaction giving the *trans* form product is more favorable. This is mainly due to the structural difference between *cis* and *trans* configurations, which makes the *cis* form less stable than the *trans* form.

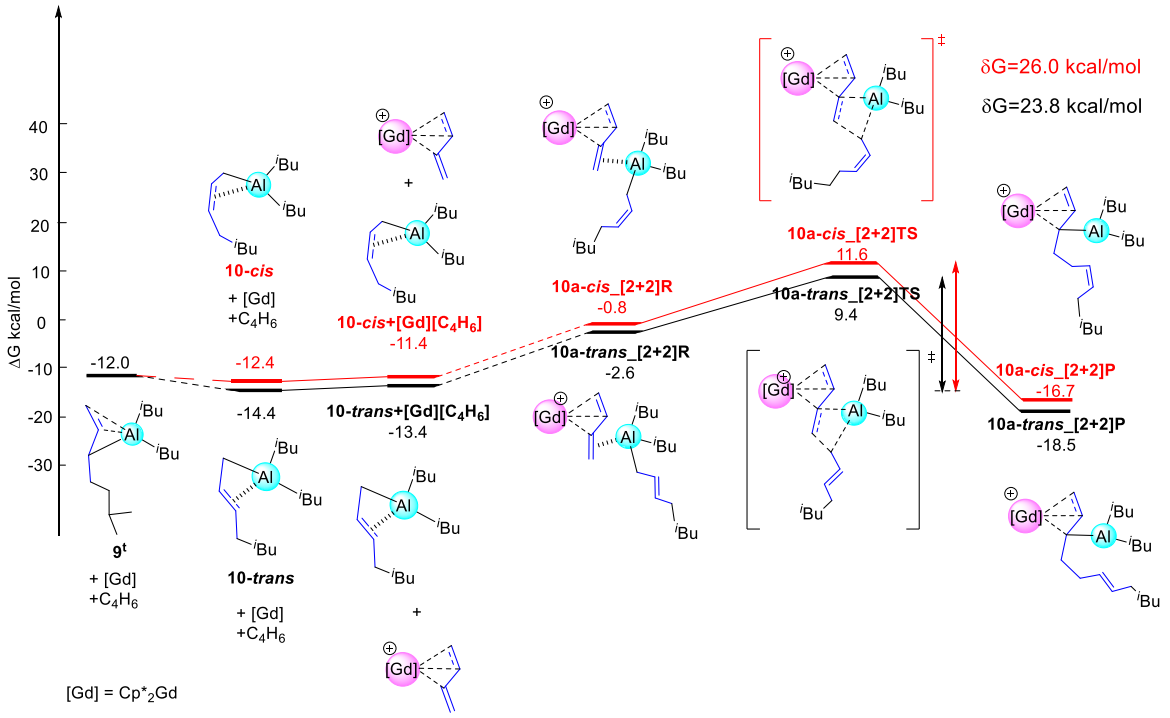

Figure 6. Energy profile (in kcal/mol, Gibbs energy in toluene solution) for butadiene insertion via four-centered transition state**.** Cp^*_2 ligands are omitted for simplicity.

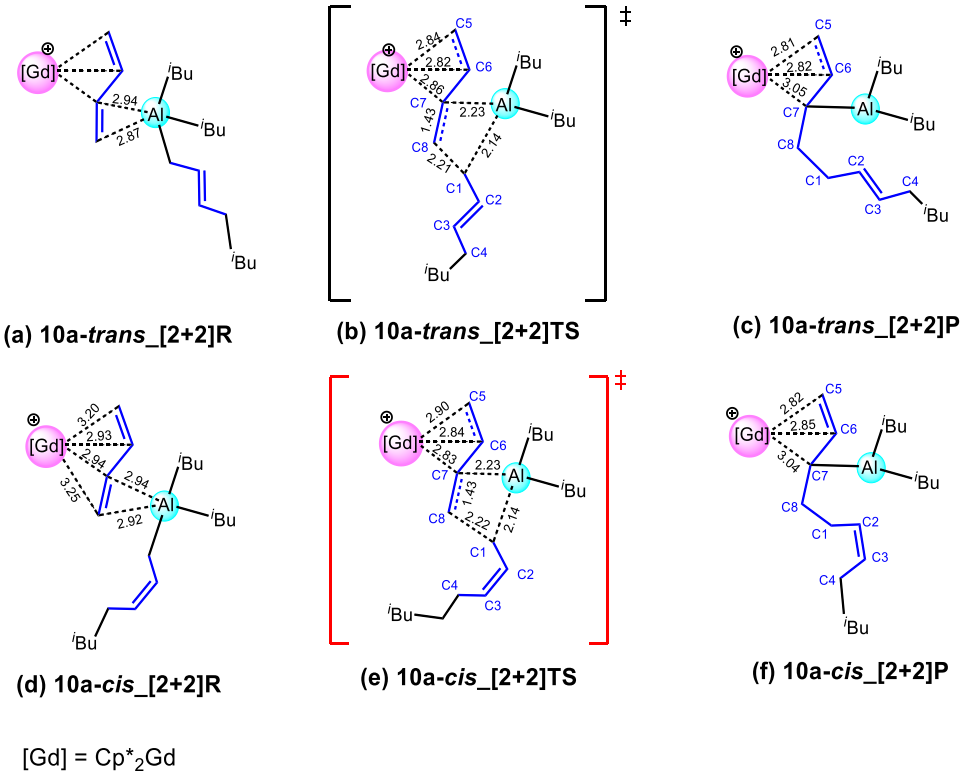

Figure 7. The structures (distance in Å) of intermediates and transition states in Figure 6.

In **9^t** and **9^c**, *trans*-1,4 and *cis*-1,4 units are generated through the eight-membered ring transition state, respectively. These results are shown in Figure 8. Comparing the above four transition states, the eight-membered ring transition states are more stable than the four-centered transition states. This is presumably because the four-centered transition states are more distorted than the eight-membered ring transition states. The energy barrier for **9^t** to produce a *trans*-1,4 unit via **9^{t}a_[4+4]TS** is 19.5 kcal/mol (= 7.5 − (−12.0)), whereas that for the formation of *cis*-1,4 units from **9^c** via **9^{c}a_[4+4]TS** is 18.1 kcal/mol (= 6.1 − (−12.0)). The formation of *cis*-1,4 unit is 1.4 kcal/mol more favorable than that of *trans*-1,4 unit. The distance between Al(^{i}Bu)$_2$ and the end of the chain in **9^{t}a _[4+4]TS** is shorter than that in **9^{c}a_[4+4]TS**, thereby causing greater steric effect. The above calculations suggest that the *cis*-1,4 units are produced through **9^{c}a_[4+4]TS**. Therefore,

we calculated the Boltzmann factors to estimate the probability of their existence, and confirmed that the probability of producing *cis*-1,4 units through **9^{c}a_[4+4]TS** is as high as about 91%. The calculated results are consistent with the experimental results in favor of 1,4-*cis* selectivity (97.3% at 25 °C in toluene). In addition, it has already been experimentally shown that the 1,4-*cis* selectivity is strongly affected by the bulkiness of the alkylalminum, i.e., Al(^{i}Bu)$_3$ (97.3%) > Al(^{i}Bu)$_2$H (96.1%) > AlEt$_3$ (73.9%) > AlMe$_3$ (60.2%).[14] This experimental result is also explainable in view of the steric effect caused between the alkyl group of the AlR$_2$ and the end of the chain in **9^{t}a _[4+4]TS** described above.

In the following steps during the propagation of polymers, as discussed above for the first monomer insertion in Figure 3, the insertion product must isomerize to have a 1-substituted 2-propenyl group on Al. Accordingly, the second monomer insertion product (**11-*trans***) in **9^{c}a_[4+4]P** dissociates from [Cp*$_2$Gd]$^+$, a process being endergonic by 9.4 kcal/mol (= (−20.0) − (−29.4)), and it adopts the 1,3-sigmatropic rearrangement of the Al(^{i}Bu)$_2$ unit and C6–C7 bond rotation (Figure 10). The energy barriers calculated are 3.8 and 8.2 kcal/mol for the rearrangement of **11-*trans*** to **12^{t}** due to the 1,3-sigmatropic rearrangement of the Al(^{i}Bu)$_2$ unit and the conformation change from **12^{t}** to **12^{c}** due to C6–C7 bond rotation, respectively. The energy barrier for the 1,3-sigmatropic rearrangement in the second monomer insertion product (3.8 kcal/mol) is 1.0 kcal/mol higher than in the first (2.8 kcal/mol). The interaction between Al and C6=C7 bond in **11-*trans*** is weaker than that between Al and C2=C3 bond in **10-*trans*** due to the interaction of Al(^{i}Bu)$_2$ with the C1–C2=C3–C4–^{i}Bu end of the chain. Presumably, this makes the energy required by the migration of Al(^{i}Bu)$_2$ from C5 to C7 lager. The conformational changes of these insertion products are by far lower than the energy barriers for the propagation, and thus are

expected to occur easily in the reaction system. Subsequent propagation would proceed by repeating the same cycle as in Figure 8 with *cis* configuration being more favorable.

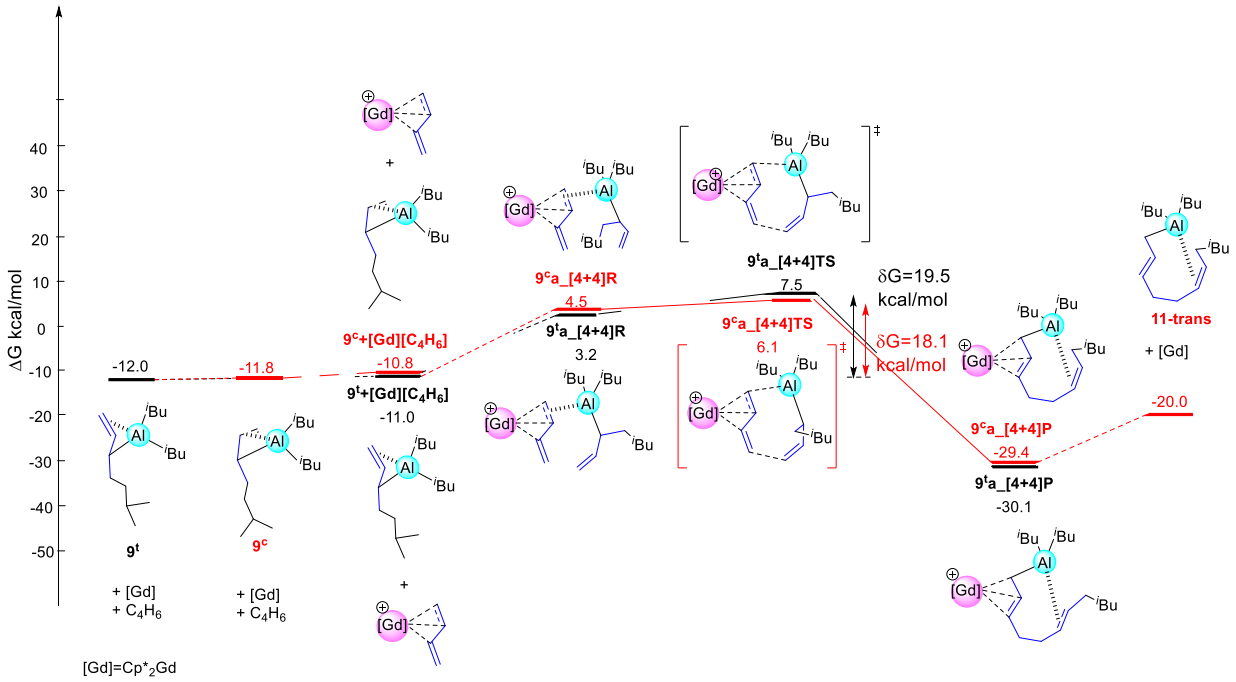

Figure 8. Energy profile (in kcal/mol, Gibbs energy in toluene solution) for butadiene insertion via eight-membered ring transition state**.** Cp^*_2 ligands are omitted for simplicity.

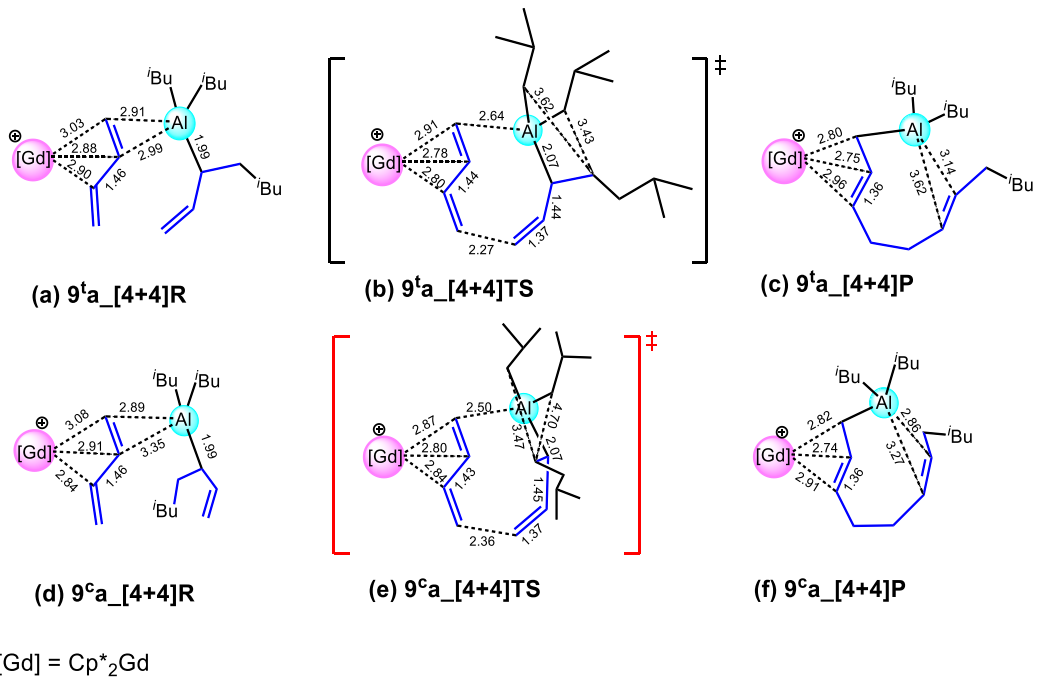

Figure 9. The structures (distance in Å) of intermediates and transition states in Figure 8.

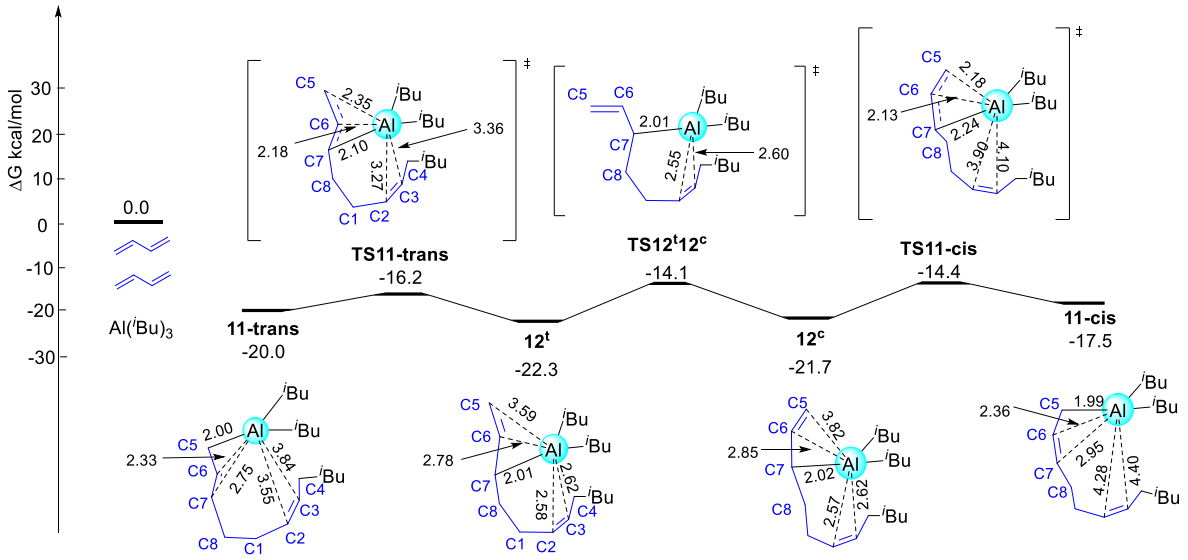

Figure 10. Energy profile (in kcal/mol, Gibbs energy in toluene solution) for the rotation of C6–C7 bond and the 1,3-sigmatropic rearrangement of the Al(^{i}Bu)$_2$ unit.

3.3.5. Orbital analysis of the effect of Gd cation

To evaluate in detail the contribution of the Gd cation in the current butadiene polymerization, we compared the insertion of s-*trans* butadiene into the Al–C(σ) bond of the growing chain in the presence and absence of $[Cp^*_2Gd]^+$. Figure 11(a) shows the energy profile and transition state structure for the butadiene insertion into the growing chain of **9^c** in the absence of $[Cp^*_2Gd]^+$, and Figure 11(b) shows those for the insertion step in the presence of $[Cp^*_2Gd]^+$. The latter has already demonstrated in Figure 8 (**9^{c}a_[4+4]TS**) but only important structures are extracted here for comparison. The activation energy in the presence of $[Cp^*_2Gd]^+$ is 14.2 (= 15.8 − 1.6) kcal/mol smaller than in its absence. The reason of this difference was analyzed based on the Natural Localized Molecular Orbitals (NLMOs) representation as done in our previous study for ethylene polymerization.[18] The NLMOs are illustrated in Figure 12. The eight-membered ring transition state (**9^c_[4+4]TS**) for the insertion of s-*trans* butadiene without $[Cp^*_2Gd]^+$ has donation and back-donation between Al and s-*trans* butadiene. Note that upon interaction of butadiene with the growing chain, butadiene occupied π orbitals are localized on the C(5)=C(6) or C(7)=C(8) regions. NLMO-(a) denotes the donation from one of them localized on the C(5)=C(6) bond to an vacant 3p orbital of Al, indicating that an Al–C(5) bond is being formed, whereas NLMO-(b) shows the back-donation from C(1)–C(2) π-orbital to π* LUMO of butadiene that will finally form the C(1)–C(8) bond of the product. NLMO-(c) shows the mixing of Al–C(3) σ-orbital and C(1)–C(2) π* orbital to form the C(2)–C(3) π bond and to cleave the Al–C(3) σ-bond. In the presence of $[Cp^*_2Gd]^+$, a similar reaction of **9^c** toward butadiene (Figure 11(b)) shows a 14.2 kcal/mol decrease in activation energy. As shown by NLMO-(d), -(e) and -(f) in Figure 12, this reduction in activation energy is brought about by the additional interaction of butadiene π and π* orbitals with vacant Gd 5d orbitals, which stabilizes π and π* orbitals

and effectively attracts π electrons to C(5)–C(6) bond (NLMO-(d)). The interaction of Gd 5d orbitals with C(6)–C(7) component of π∗-orbital increases the electrophilicity of C(7)–C(8) bond to enhance the back-donation shown in NLMO-(e). Furthermore, the $[Cp^*_2Gd]^+$ stabilizes the eight-membered ring transition state electrostatically. Besides, the longer Al–butadiene distances (2.89 and 3.35 Å) in **9^{c}a_[4+4]R** compared with those in **9^c_[4+4]R** (2.54 and 2.80 Å) are ascribed to weaker donation from stabilized π orbital.

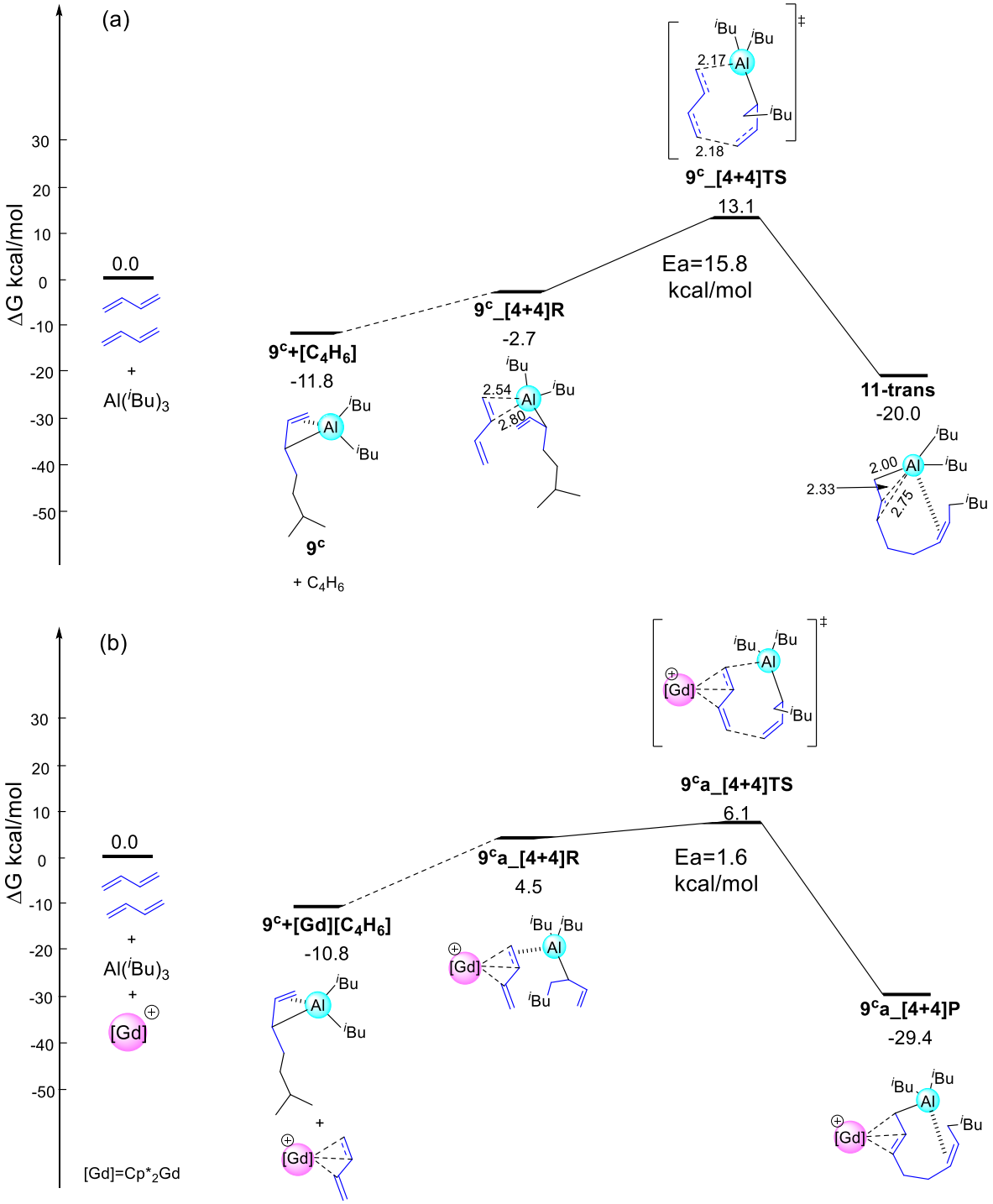

Figure 11. Transition state structures (**9ᶜ_[4+4]TS** and **9ᶜa_[4+4]TS**) and their energies (in kcal/mol, Gibbs energy in toluene solution) for the each butadiene insertion into the Al–C (σ) bond

of growing chain, (a) without $[Cp^*_2Gd]^+$ and (b) without $[Cp^*_2Gd]^+$. Cp^*_2 ligands are omitted for simplicity.

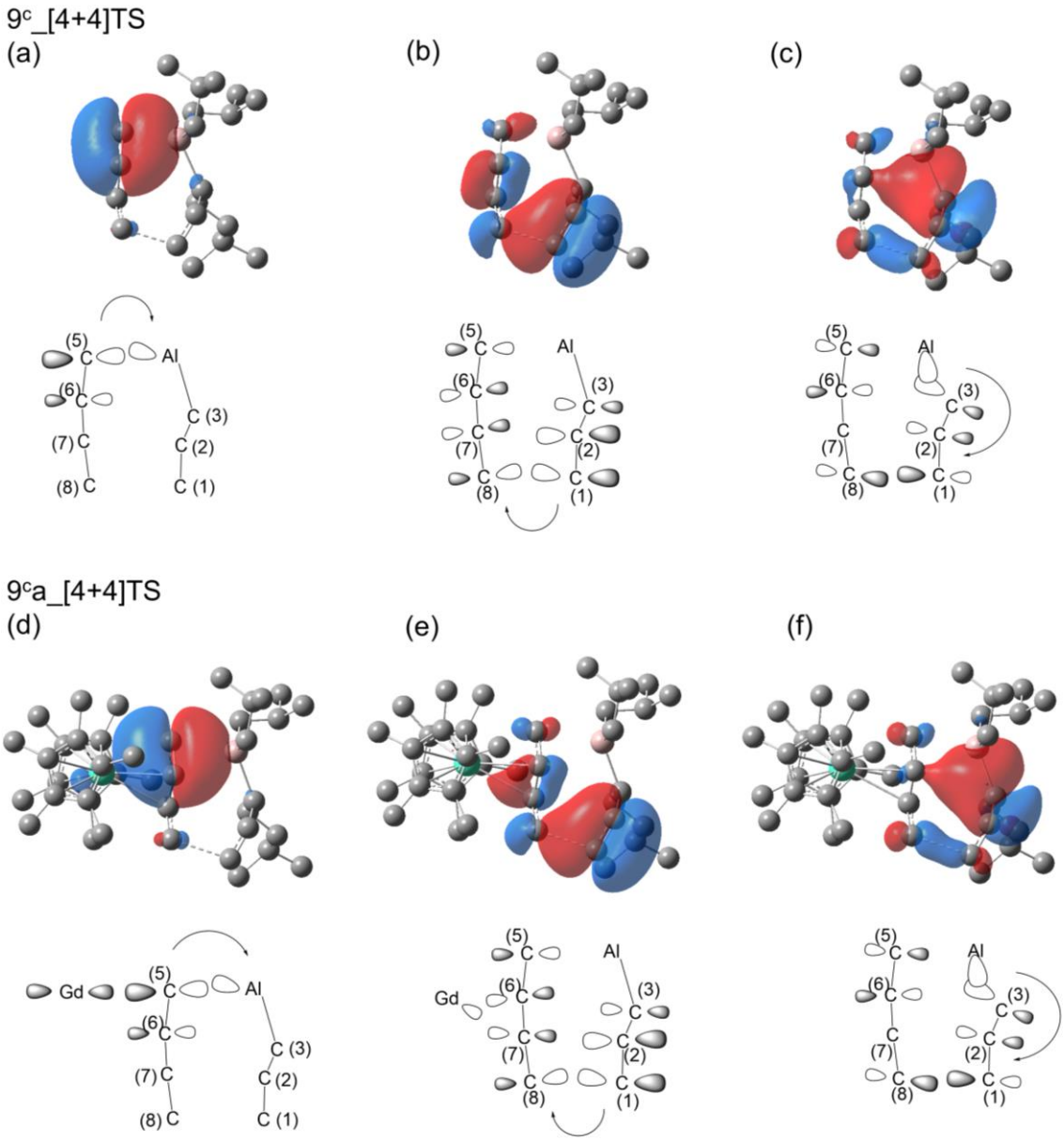

Figure 12. The transition state structures and their NLMO representations with or without $[Cp^*_2Gd]^+$. H atoms are omitted. (a) The donation from butadiene π orbital to an empty 3p-orbital of Al without $[Cp^*_2Gd]^+$. (b) The back-donation from C(1)–C(2) π-orbital to π^* of butadiene

without $[Cp^*_2Gd]^+$. (c)The mixing of Al–C(3) σ-orbital and C(1)–C(2) π^*-orbital to form C(2)–C(3) π bond without $[Cp^*_2Gd]^+$. (d) The donation from butadiene π to an empty 3p-orbital of Al with $[Cp^*_2Gd]^+$. (e) The back-donation from C(1)–C(2) π-orbital to π^*-orbital of butadiene with $[Cp^*_2Gd]^+$. (f) The mixing of Al–C(3) σ-orbital and C(1)–C(2) π^*-orbital to form C(2)–C(3) π bond with $[Cp^*_2Gd]^+$ and cleave Al–C(3) σ-bond.

3.4. Conclusion

In this chapter, I extended the mechanism of ethylene polymerization by the **2a**/Al(^{i}Bu)$_3$ system [18] (Figure 1) to butadiene polymerization and report computational study on the specific 1,4-*cis* polymerization of butadiene with this catalytic system. In the initiation reaction, I was able to find a reaction path, where the cationic Gd plays a crucial role as assisting butadiene insertion into one Al–C bond from Al(^{i}Bu)$_3$ via the four-centered transition state similar to ethylene polymerization (Figures 3). The insertion product dissociated readily from [Cp*$_2$Gd]$^+$ and isomerization from the *trans*-1,4 unit to the *cis*-1,4 unit with a 1,3-sigmatropic rearrangement was also easily achieved. In the propagation, I found not only reaction pathways via the four-centered transition states, but also those via more stable eight-membered ring transition states. This mechanism of butadiene polymerization via the eight-membered ring transition state (**9^{c}a_[4+4]TS**) could explain the experimental results showing specific 1,4-*cis* selectivity. According to the proposed mechanism, the specific 1,4-*cis* selectivity of this catalyst system is due to the steric effect between the growing chain and the ^{i}Bu groups of Al(^{i}Bu)$_2$ unit. This is consistent with the experimental fact that the 1,4-*cis* selectivity is strongly affected by the bulkiness of the alkylaluminum.[14]

The activation energy of the butadiene insertion reaction through the eight-membered ring transition state (**9^{c}a_[4+4]TS**) is 1.6 kcal/mol, which is 14.2 kcal/mol smaller than that in the absence of [Cp*$_2$Gd]$^+$. This is due to the interaction of π and π* orbitals of butadiene with empty 5d orbitals of Gd.

This novel reaction mechanism derived from my theoretical calculations is expected to lead to new developments in metal complex-catalyzed olefin polymerization, and shed new lights on the role of lanthanide ions. This catalyst system is capable of not only homopolymerization such as polyethylene and polybutadiene, but also olefin-diene copolymerization by combining them. It

would be interesting to investigate the microstructure of olefin-diene copolymerization with theoretical calculations. It is expected that catalyst design based on this mechanism will lead to the development of new copolymers.

APPENDIX

1. Free Butadiene and Its Complex with $[Cp^*_2Gd]^+$.

Table S1. Relative energies of s-*trans*- and s-*cis*-butadiene in toluene in kcal/mol.

	s-*trans*-butadiene	s-*cis*-butadiene
Gibbs energy	0.0	2.9
E+ZPE	0.0	3.1

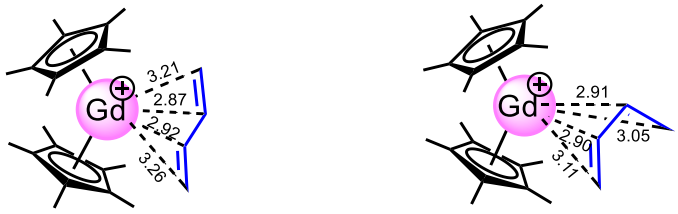

s-*Trans*-butadiene
(0.0 kcal/mol)
[0.0 kcal/mol]

s-*Cis*-butadiene
(4.1 kcal/mol)
[2.4 kcal/mol]

Figure S1. Optimized structures of $[Cp^*_2Gd(s\text{-}trans\text{-butadiene})]^+$ and $[Cp^*_2Gd(s\text{-}cis\text{-butadiene})]^+$ (distances in Å). Energies shown are energy in toluene solution relative to s-*trans*-butadiene with $[Cp^*_2Gd]^+$ unit. The values in parentheses are estimated with the Gibbs energies and those in brackets are the E+ZPE.

2. Potential Energy Profiles Including Zero-point Energy Corrections.

The validity of the discussion for the polymerization reaction mechanism using the Gibbs energies was confirmed by investigating the potential energy profiles including zero-point energy corrections (Δ(E+ZPE) profiles) in toluene in Table S1 and Figures S1-S7. The entropic effects calculated with textbook equations for ideal-gas molecules mainly come from the relative translation and rotation of the components. In solution, however, they are quenched, because components are individually solvated.[50] Therefore, I compared Δ(E+ZPE). With these Δ(E+ZPE) I obtained qualitatively the same results to support the discussion with Gibbs energies.

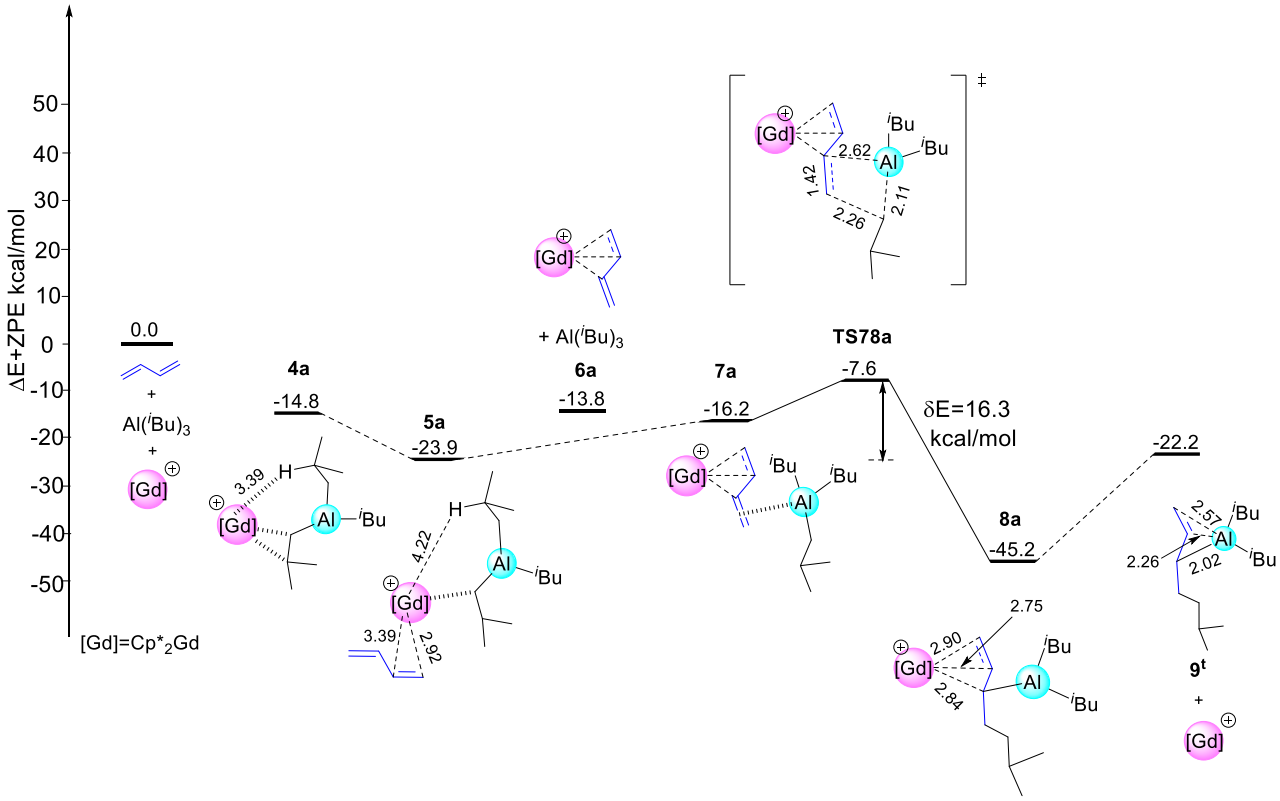

Figure S2. Energy profile (in kcal/mol, E+ZPE in toluene solution) for butadiene coordination to **4a**, successive rearrangement and insertion into the Al–C bond. Cp^*_2 ligands are omitted for simplicity. H atom of one of ^{i}Bu groups is explicitly shown as β-H in the body text.

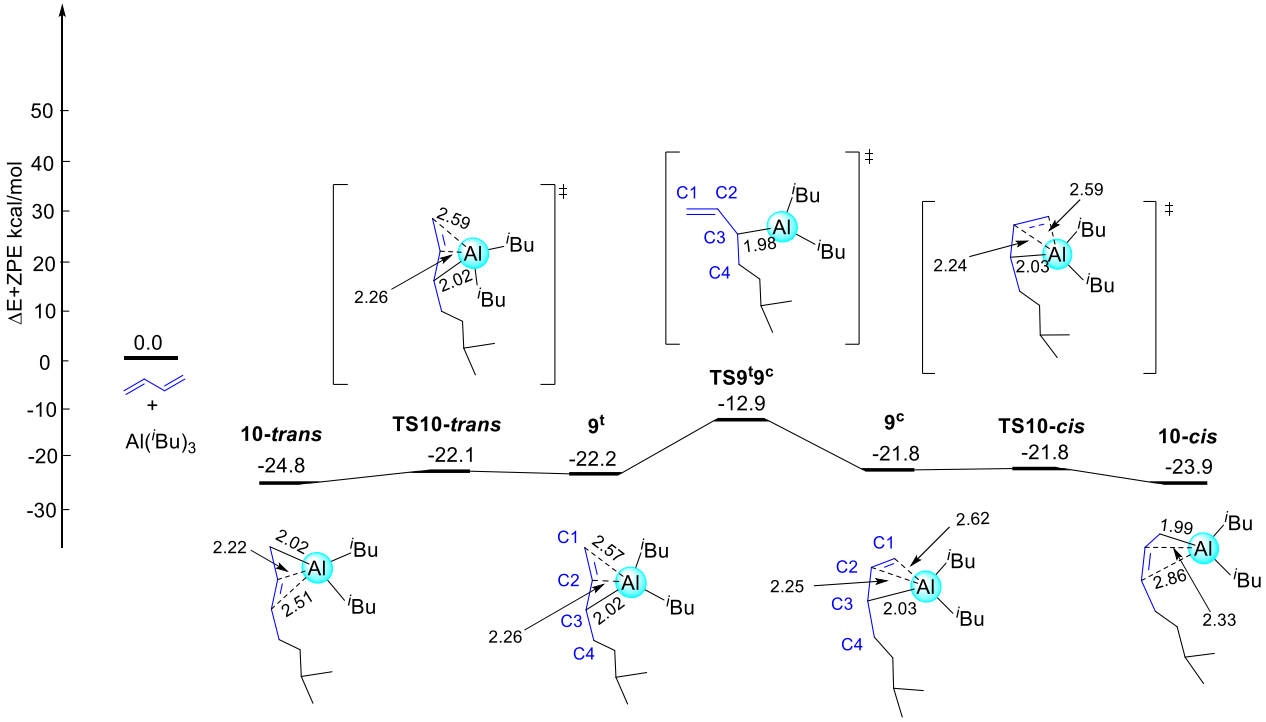

Figure S3. Energy profile (in kcal/mol, E+ZPE in toluene solution) for the rotation of C2–C3 bond and the 1,3-sigmatropic rearrangement of the Al(^{i}Bu)$_2$ unit in the insertion product.

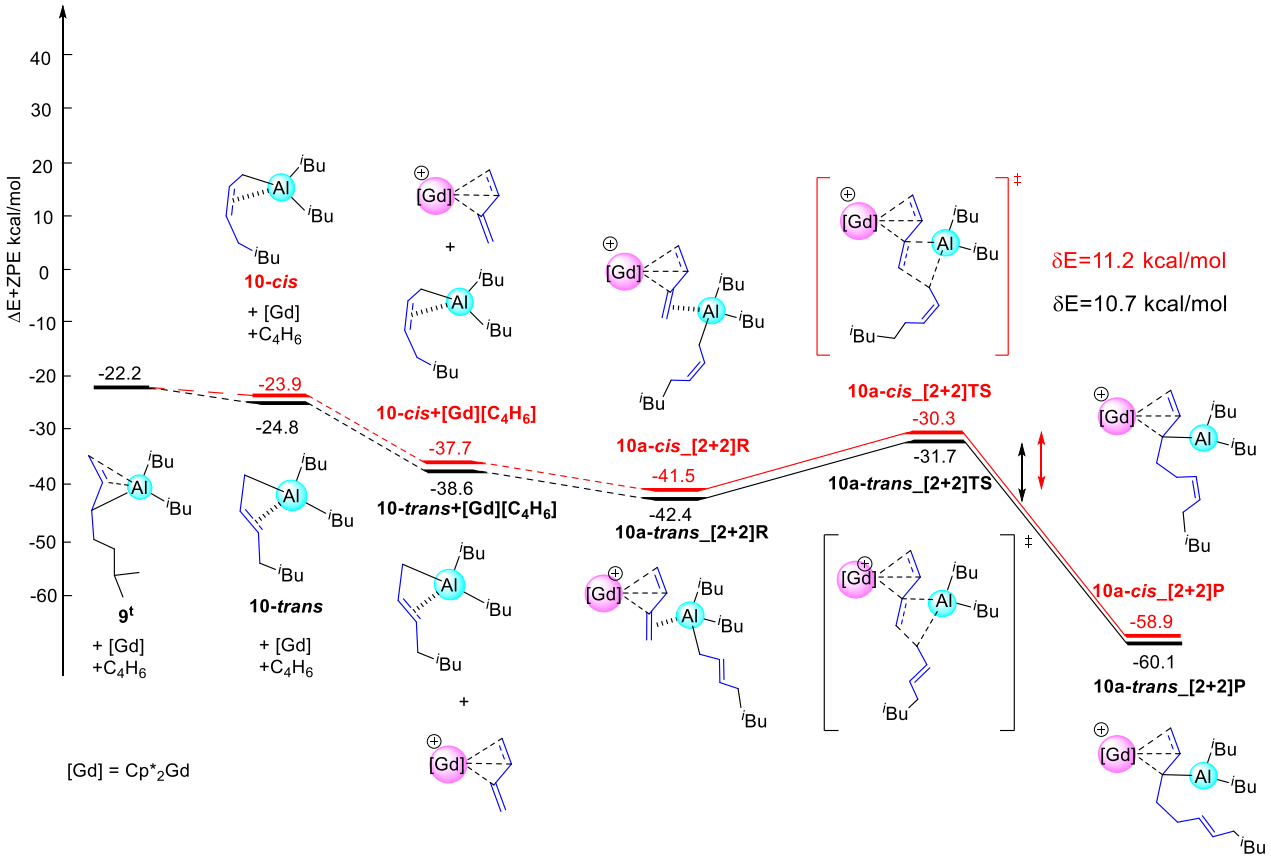

Figure S4. Energy profile (in kcal/mol, E+ZPE in toluene solution) for butadiene insertion via four-centered transition state. Cp^*_2 ligands are omitted for simplicity.

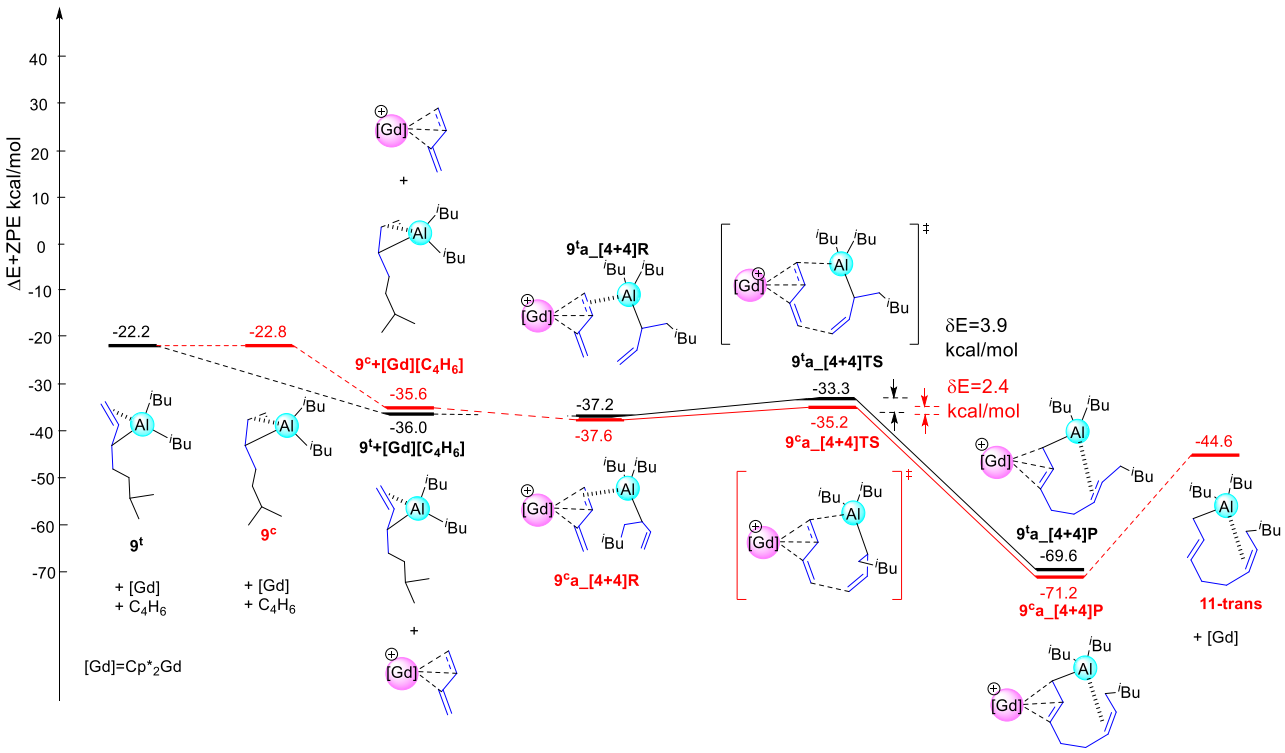

Figure S5. Energy profile (in kcal/mol, E+ZPE in toluene solution) for butadiene insertion via eight-membered ring transition state. Cp^*_2 ligands are omitted for simplicity.

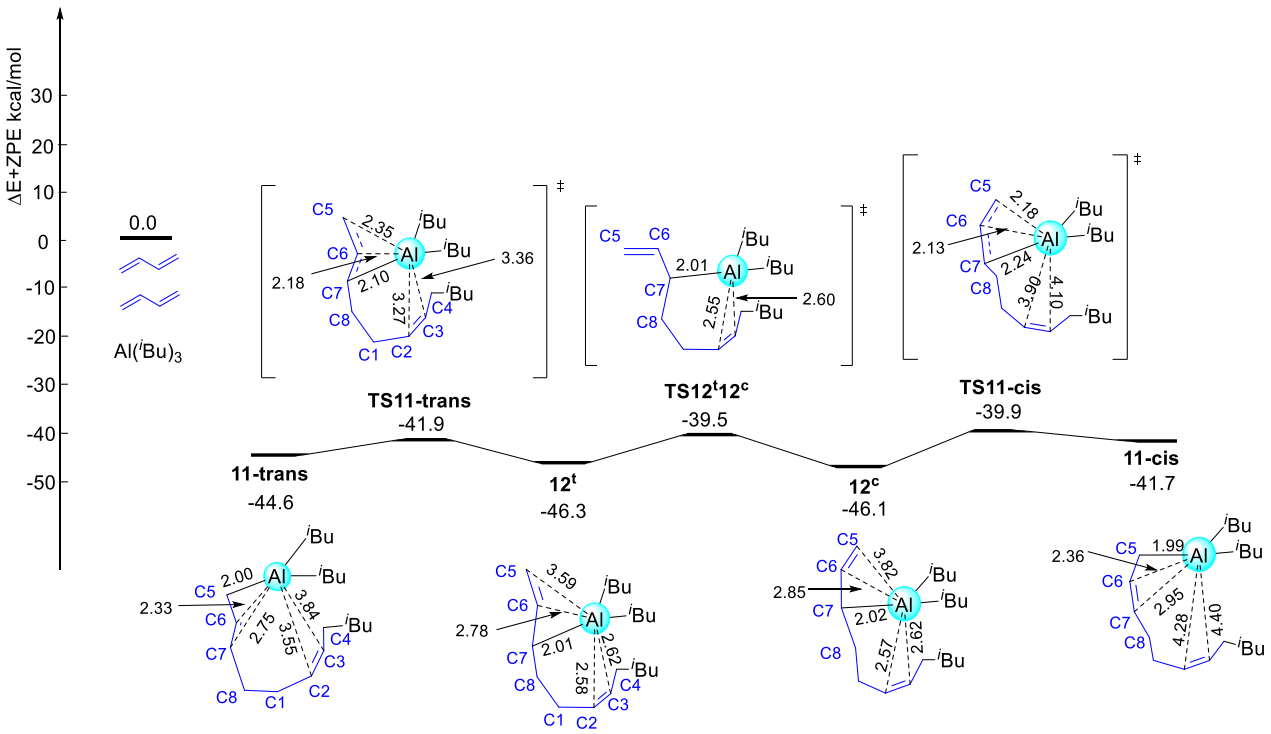

Figure S6. Energy profile (in kcal/mol, E+ZPE in toluene solution) for the rotation of C6–C7 bond and the 1,3-sigmatropic rearrangement of the Al(^{i}Bu)$_2$ unit.

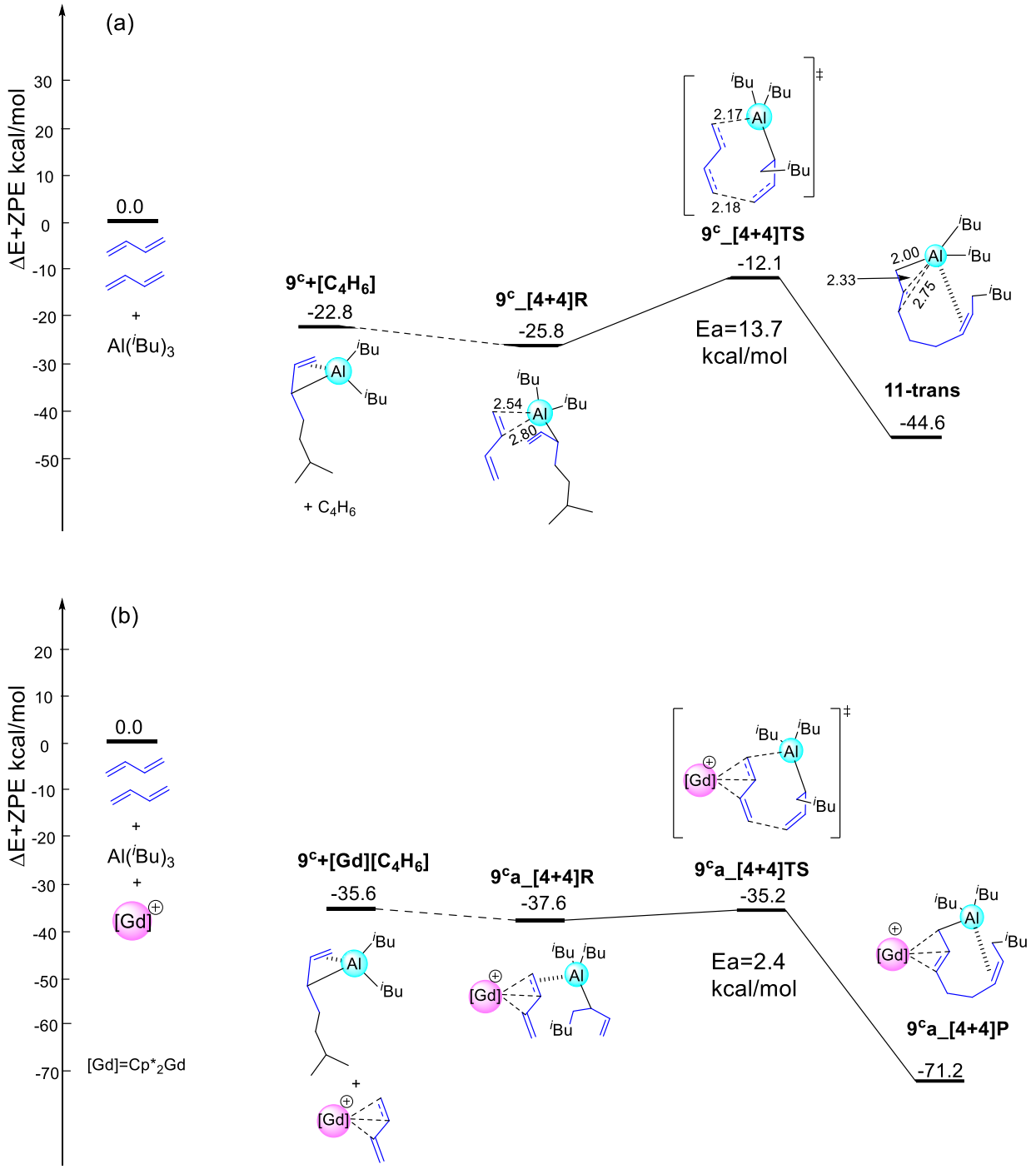

Figure S7. Transition state structures (**9^{c}_[4+4]TS** and **9^{c}a_[4+4]TS**) and their energies (in kcal/mol, E+ZPE in toluene solution) for the each butadiene insertion into the Al–C (σ) bond of growing chain, (a) without $[Cp^*_2Gd]^+$ and (b) without $[Cp^*_2Gd]^+$. Cp^*_2 ligands are omitted for simplicity.

3. Single Point Energy Calculation of 9^{c}a_[4+4]TS and ^{9t}a_[4+4]TS with Different Methods.

In addition to the validity of the above, basis sets and functional, calculation of Gibbs energies requires special attention. In order to make more reliable comparison regarding the setereoselectivity in the proposed polymerization mechanism, several single-point energy calculations were performed for the structures of **9^{c}a_[4+4]TS** and **9^{t}a_[4+4]TS** obtained using the method in the computational details (method 1). The energy difference between these two structures is the most important issue here. The vibrational frequencies were taken from the calculations with the smaller basis set, to evaluate the zero point energies and thermal corrections. The results are shown in Table S2. Entry 1 was performed using the larger 6-311G(d,p) basis sets for all atoms but the Gd atom. Entry 2 was performed using the Grimme's D3 dispersion model [51] with M06 functional. It is generally well-known that as the system get larger, the number of low energy normal modes increases dramatically, making it difficult to estimate the vibrational entropy using a harmonic oscillator approximation. Therefore, entries 3 and 4 were performed using the Truhlar's quasi-harmonic (qh) entropy correction [52] with a cut-off frequency of 100 cm^{-1} and the Grimme's rigid-rotor-harmonic-oscillator approximation,[53] respectively. These energies thus obtained gave qualitatively the same results to support the calculations with the method 1.

Table S2. Relative Gibbs energies of selected transition states in Figure 8.

entry	Calculation method	Relative Gibbs energy [a] (kcal/mol)	
		9^{t}a_[4+4]TS	**9^{c}a_[4+4]TS**
1	Larger Basis set	0.0	–1.8
2	M06+D3 [b]	0.0	–2.0
3	quasi-harmonic approach [c]	0.0	–1.1
4	RRHO approximation [d]	0.0	–1.4

a Single point energy calculations at the structures optimized with method 1.

b Corrected for dispersion forces using the Grimme's D3 dispersion model.

c Corrected for low energy vibrations using a quasi-harmonic approach.

d Corrected for low energy vibrations using a rigid-rotor-harmonic-oscillator approximation

References

[1] (a) L. Porri, A. Giarrusso, in *Comprehensive Polymer Science,* Vol. 4, Pergamon, Oxford, UK, **1989**, p. 53–108. (b) R.Taube, G. Sylvester, in *Applied Homogeneous Catalysis with Organometallic Compounds*, Vol. 1 (Eds.: B. Cornils, W. A. Herrmann), VCH, Weinheim, **1996**, pp. 280–318.

[2] (a) L. Porri, A. Giarrusso, G. Ricci, *Prog. Polym. Sci.* **1991**, *16*, 405. (b) S. K.-H. Thiele, D. R. Wilson, *J. Macromol. Sci. Part C: Polym. Rev.* **2003**, *4*, 581. (c) J. Huang, Z. Liu, D. Cui, X. Liu, *ChemCatChem.* **2018**, *10*, 42.

[3] (a) L. Oliva, P. Longo, A. Grassi, P. Ammendola, C. Pellecchia, *Makromol. Chem., Rapid Commun.* **1990**, *11*, 519. (b) G. Ricci, S. Italia, A. Giarrusso, L. Porri, *J. Organomet. Chem.* **1993**, *451*, 67. (c) G. Ricci, L. Porri, A. Giarrusso, *Macromol. Symp.* **1995**, *89*, 383. (d) G. Ricci, C. Bosisio, L. Porri, *Macromol. Rapid Commun.* **1996**, *17*, 781.

[4] (a) A. Miyazawa, T. Kase, K. Soga, *J. Polym. Sci., Polym. Chem.* **1999**, *37*, 695. (b) A. Miyazawa, T. Kase, K. Soga, *Macromolecules* **2000**, *33*, 2796. (c) A. Miyazawa, T. Kase, K. Hashimoto, J. Choi, T. Sakakura, J. Jizhu, *Macromolecules* **2004**, *37*, 8840.

[5] W. Kaminsky, B. Hinrichs, D. Rehder, *Polymer* **2002**, *43*, 7225.

[6] Z. Shen, J. Ouyang, F. Wang, Z. Hu, F. Yu, B. Qian, *J. Polym. Sci., A, Polym. Chem.* **1980**, *18*, 3345.

[7] A. Oehme, U. Gebauer, K.Gehrke, M. D. Lechner, *Angew. Makromol. Chem*. **1996**, *235*, 121.

[8] R. P. Quirk, A. M. Kells, K. Yunlu, J.-P. Cuif, *Polymer*, **2000**, *41*, 5903.

[9] (a) C. Boisson, F.Barbotin, R. Spitz, *Macromol. Chem. Phys.* **1999**. *200*. 1163. (b) F. Barbotin, V. Monteil, M.-F. Llauro, C. Boisson, R. Spitz, *Macromolecules* **2000**, *33*, 8521. (c) S. Maiwald, H. Weißenborn, C. Sommer, G. Müller, R. Taube, *J. Organomet. Chem.* **2001**, *640*,

1. (d) S. Maiwald, H. Weißenborn, C. Sommer, G. Müller, R. Taube, *Macromol. Chem. Phys.* **2001**. *202*. 1446. (e) S. Maiwald, H. Weißenborn, C. Sommer, G. Müller, R. Taube, *Macromol. Chem. Phys.* **2002**. *203*. 1029. (f) L. Friebe, O. Nuyken, H. Windisch, W. Obrecht, *Macromol. Chem. Phys.* **2002**. *203*. 1055. (g) J. Thuilliez, V. Monteil, R. Spitz, C. Boisson, *Angew. Chem. Int. Ed.* **2005**, *44*, 2593. (h) A. R. O'Connor, P. S. White, M. Brookhart, *J. Am. Chem. Soc.* **2007**, *129*, 4142. (i) J. Furukawa, *Pure Appl. Chem.* **1975**, *42*, 495. (j) E. Kobayashi, S. Kaita, S. Aoshima, J. Furukawa, *J. Polym. Sci. Part A: Polymer Chemistry*, **1995**, *33*, 2175.

[10] (a) S. Tobisch, H. Bögel, R. Taube, *Organometallics* **1996**, *15*, 3563. (b) G. Guerra, L. Cavallo, P. Corradini, R. Fusco, *Macromolecules* **1997**, *30*, 677. (c) A. Peluso, R. Improta, A. Zambelli, *Macromolecules* **1997**, *30*, 2219. (d) S. Tobisch, H, Bögel, R. Taube, *Organometallics* **1998**, *17*, 1177. (e) S. Tobisch, R.Taube, *Organometallics* **1999**, *18*, 3045. (f) S. Tobisch, R. Taube, *Organometallics* **1999**, *18*, 5204. (g) A. Peluso, R. Improta, A. Zambelli, *Organometallics* **2000**, *19*, 411. (h) C. Costabile, G. Milano, L. Cavallo, G. Guerra, *Macromolecules*, **2001**, *34*, 7952. (i) S. Tobisch, *Chem. Eur. J.* **2002**, *8*, 4756. (j) S. Tobisch, *Acc. Chem. Res.* **2002**, *35*, 96. (k) S. Tobisch, *J. Mol. Struc: TEOCHEM* **2006**, *771*, 171. (l) C. Costabile, S. Pragliola, L. Pelosi, P. longo, *Polymer*, **2007**, *48*, 3059.

[11] L. Zhang, M. Nishiura, M. Yuki, Y. Luo, Z. Hou, *Angew. Chem. Int. Ed.* **2008**, *47*, 2642.

[12] (a) S. Kaita, Z. Hou, Y. Wakatsuki, *Macromolecules* **1999**, *32*, 9078. b) S. Kaita, Z. Hou, Y. Wakatsuki, *Macromolecules* **2001**, *34*, 1539. (c) Z. Hou, S. Kaita, Y. Wakatsuki, *Pure and Applied Chemistry* **2001**, *73*, 291.

[13] S. Kaita, Z. Hou, M. Nishiura, Y. Doi, J. Kurazumi, A.C. Horiuchi, Y. Wakatsuki, *Macromol. Rapid Commun.* **2003**, *24*, 179.

[14] S. Kaita, M. Yamanaka, A.C. Horiuchi, Y. Wakatsuki, *Macromolecules* **2006**, *39*, 1359.

[15] G. Jeske, H. Lauke, H. Mauermann, P. N. Swepston, H. Schumann, T. J. Marks, *J. Am. Chem. Soc.* **1985**, *107*, 8091.

[16] (a) W.J. Evans, L.R. Chamberlain, T.A. Ulibarri, J.W. Ziller, *J. Am. Chem. Soc.* **1988**, *110*, 6423. (b) W.J. Evans, T.A. Ulibarri, J.W. Ziller, *J. Am. Chem. Soc.* **1990**, *112*, 2314.

[17] S. Kaita, N. Koga, Z. Hou, Y. Doi, Y. Wakatsuki, *Organometallics*, **2003**, *22*, 3077.

[18] R. Fukushima, O. Tardif, S. Kaita, Y. Wakatsuki, N. Koga, *Chem. Asian J.* **2021**, *16*, 1403.

[19] For reviews on the controlled coordinative chain transfer polymerization (CCTP) of ethylene, see: (a) R. Kempe, *Chem. Eur. J.* **2007**, *13*, 2764. (b) A. Valente, A. Mortreux, M. Visseaux, P. Zinck, *Chem. Rev.* **2013**, *113*, 3836. (c) D. J. Walsh, M.G. Hyatt, S. A. Miller, D. Guironnet, *ACS Catalysis* **2019**, *9*, 11153.

[20] M. Bochmann, S.J. Lancaster, *J. Organomet. Chem.* **1995**, *497*, 55.

[21] J. M. Camara, R.A. Petros, J.R. Norton, *J. Am. Chem. Soc.* **2011**, *133*, 5263.

[22] M. van Meurs, G.J.P Britovsek, V.C. Gibson, *J. Am. Chem. Soc.* **2005**, *127*, 9913.

[23] F. Wang, C. Zhang, Y. Hu, X. Jia, C. Bai, X. Zhang, *Polymer* **2012**, *53*, 6027.

[24] C. Boisson, V. Monteil, D. Ribour, R.F. Spitz, F. Barbotin, *Macromol. Chem. Phys.* **2003**, *204*, 1747.

[25] M.S.W. Chan, T.A. Ziegler, *Organometallics* **2000**, *19*, 5182.

[26] Z. Xu, K. Vanka, T. Ziegler, *Organometallics* **2004**, *23*, 1, 104.

[27] S.-Y. Yang, T. Ziegler, *Organometallics* **2006**, *25*, 887–900.

[28] C.R., Landis, K.A. Rosaaen, D.R. Sillars, *J. Am. Chem. Soc.* **2003**, *125*, 1710.

[29] M.-C. Chen, T.J. Marks, *J. Am. Chem. Soc.* **2001**, *123*, 11803.

[30] C.N. Rowley, T.K. Woo, *Organometallics* **2011**, *30*, 2071.

[31] A. Laine, B.B. Coussens, J.T. Hirvi, A. Berthoud, N. Friederichs, J.R. Severn, M. Linnolahti, *Organometallics* **2015**, *34*, 2415.

[32] R. Parveen, T.R. Cundari, J.M. Younker, G. Rodriguez, *Organometallics* **2020**, *39*, 2068.

[33] X. Wang, G. Zhou, B. Liu, Y. Luo, *Organometallics* **2018**, *37*, 882.

[34] K. Matsumoto, K.S. Sandhya, M. Takayanagi, N. Koga, M. Nagaoka, *Organometallics* **2016**, *35*, 4099.

[35] N.Misawa, Y.Suzuki, S. Saha, N. Koga, M. Nagaoka, *Organometallics* **2021**, *40*, 48.

[36] D. Mathis, E. P.A. Couzijn, P.Chen, *Organometallics* **2011**, *30*, 3834.

[37] L. Verrieux, J. Thuilliez, F. J. B. Dominique, C. Boisson, M. N. Poradowski, L. Perrin, *ACS Catal*. **2020**, *10*, 12359.

[38] L. Sian, A. Macchioni, C. Zuccaccia, *ACS Catal.* **2020**, *10*, 1591.

[39] Gaussian 09, Revision E.01, M. J. Frisch, G.W. Trucks, H. B. Schlegel, G.E. Scuseria, M. A. Robb, J. R. Cheeseman, G. Scalmani, V. Barone, B. Mennucci, G. A. Petersson, H. Nakatsuji, M. Caricato, X. Li, H.P. Hratchian, A. F. Izmaylov, J. Bloino, G. Zheng, J. L. Sonnenberg, M. Hada, M. Ehara, K. Toyota, R. Fukuda, J. Hasegawa, M. Ishida, T., Nakajima, Y. Honda, O. Kitao, H. Nakai, T. Vreven, J. A. Jr Montgomery, J. E. Peralta, F. Ogliaro, M. Bearpark, J. J. Heyd, E. Brothers, K. N. Kudin, V. N. Staroverov, T. Keith, R. Kobayashi, J. Normand, K. Raghavachari, A. Rendell, J. C. Burant, S. S. Iyengar, J. Tomasi, M. Cossi, N. Rega, J. M. Millam, M. Klene, J. E. Knox, J. B. Cross, V. Bakken, C. Adamo, J. Jaramillo, R. Gomperts, R. E. Stratmann, O. Yazyev, A. J. Austin, R. Cammi, C. Pomelli, J. W. Ochterski, R. L. Martin, K. Morokuma, V. G. Zakrzewski, G. A. Voth, P. Salvador, J. J. Dannenberg, S. Dapprich, A. D. Daniels, O. Farkas, J. B. Foresman, J. V. Ortiz, J. Cioslowski, D. J. Fox, Gaussian, Inc., Wallingford CT, **2013**.

[40] (a) Y. Zhao, D. G. Truhlar, *J. Chem. Theory Comput.* **2009**, *5*, 324. (b) Y. Zhao, D. G. Truhlar, *Acc. Chem. Res.* **2008**, *41*, 157.

[41] M. Dolg, H. Stoll, A. Savin, H. Preuss, *Theor. Chim. Acc.* **1989**, *75*, 173.

[42] T. H. Dunning Jr., P. J. Hay, in *Modern Theoretical Chemistry*, Vol. 3 (Eds.: H. F. Schaefer III), Plenum, New York, **1977**, pp. 1−28.

[43] M. M. Francl, W. J. Pietro, W. J. Hehre, J. S. Binkley, M. S. Gordon, D. J. DeFrees, J. A. Pople, *J. Chem. Phys.* **1982**, *77*, 3654.

[44] W. J. Stevens, H. Basch, M. Krauss, *J. Chem. Phys.* **1984**, *81*, 6026.

[45] V. Barone, M. Cossi, J. Tomasi, *J. Comput. Chem.* **1998**, *19*, 404.

[46] (a) S. Maeda, Y. Harabuchi, M. Takagi, K. Saita, K. Suzuki, T. Ichino, Y. Sumiya, K. Sugiyama, Y. Ono, *J. Comput. Chem.* **2018**, *39*, 233. (b) A. Banerjee, N. Adams, J. Simons, R. Shepard, *J. Phys. Chem.* **1985**, *89*, 52. (c) P. Culot, G. Dive, V. H. Nguyen, J. M. Ghuysen, *Theor. Chim. Acta*, **1992**, *82*, 189.

[47] S. Kozuch, S. Shaik, *Acc. Chem. Res.* **2011**, *44*, 101.

[48] E.D. Glendening, C.R. Landis, F. Weinhold, *J. Comput. Chem.* **2013**, *34*, 1429.

[49] Unpublished results.

[50] K. Ando, K. Morokuma, *Theor. Chem. Acc.* **2011**, *130*, 323

[51] S. Grimme, J. Antony, S. Ehrlich, H. Krieg, *J. Chem. Phys.* **2010**, *132*, 154104.

[52] R. F. Ribeiro, A. V. Marenich, C. J. Cramer, D. G. Truhlar, *J. Phys. Chem. B* **2011**, *115*, 14556.

[53] S. Grimme, *Chem. Eur. J.* **2012**, *18*, 9955.

Chapter 4

General Conclusion

In this thesis, I investigated the mechanism of ethylene and butadiene polymerization catalyzed by cationic gadolinium metallocene ([Cp*$_2$Gd][B(C_6F_5)$_4$]). [Cp*$_2$Gd][B(C_6F_5)$_4$]/Al(^{i}Bu)$_3$ system is a highly active and highly selective homogeneous "single-site" catalyst capable of synthesizing high *cis*-BR and high *cis*-IR as well as polyethylene. Therefore, we are searching for new coordination polymerization catalysts focusing on this catalyst system to create next generation synthetic rubbers, and are aiming to establish a catalyst design guideline based on the polymerization mechanism. However, the conventional polymerization mechanism cannot account for the polymerization activity of this catalyst system, since this reaction system has no initial Gd–alkyl bond, which is indispensable in the conventional mechanism. Therefore, I conducted computational study to elucidate the mechanism of this polymerization.

In Chapter 2, in order to elucidate the mechanism of this polymerization, I performed the DFT calculations on the polymerization of ethylene, the simplest monomer. First, I assumed that active species consisting of three components, [Cp*$_2$Gd]$^+$, [B(C_6F_5)$_4$]$^-$, and Al(^{i}Bu)$_3$, would be formed, and identified the most stable structure among them. The structure has no Gd-alkyl bond, and furthermore, it is thermodynamically infeasible to form a Gd-alkyl intermediate by transformation. Next, I showed that the counter anion is easily dissociated from Gd and the catalyst is activated in the process of coordination of the monomer to Gd. Then, I proposed a reaction mechanism in which the ethylene monomer coordinated by the Gd metallocene cation inserts into the Al-C bond of Al(^{i}Bu)$_3$ in propagation. Here, the interaction between the empty 5d orbitals of Gd and the π and π^* orbitals of ethylene decreases the activation energy of the insertion reaction.

In Chapter 3, I extended the mechanism of ethylene polymerization in Chapter 2 to butadiene polymerization and conducted a computational study on the specific 1,4-*cis* polymerization of butadiene with this catalytic system. First, in the initiation step, the butadiene monomer is inserted into the Al–C bond of $Al(^{i}Bu)_3$ via a four-centered transition state similar to ethylene polymerization. Then, the insertion product readily dissociated from $[Cp^*_2Gd]^+$, and isomerizes to produce four isomers. In the propagation, we found not only reaction pathways via the four-centered transition states, but also those via more stable eight-membered ring transition states. This mechanism of butadiene polymerization via the eight-membered ring transition state could explain the experimental results showing specific 1,4-*cis* selectivity. Based on the proposed mechanism, the specific 1,4-*cis* selectivity of this catalytic system is due to steric effects between the growing chain and the ^{i}Bu group of the $Al(^{i}Bu)_2$ unit, which is consistent with the experimental fact that the 1,4-*cis* selectivity is strongly influenced by the bulkiness of the alkylaluminum. In butadiene polymerization, the coordination of the Gd metallocene cation to the butadiene monomer lowers the activation energy of insertion into the Al–C bond, which is attributed to the interaction of the empty 5d orbital of Gd with the π and π* of butadiene.

In summary, I conducted a theoretical study on mechanism of ethylene and butadiene polymerization catalyzed by cationic gadolinium metallocene. As a result, I proposed a novel polymerization mechanism in which the metallocene Gd cation assists the direct insertion of the monomer into the Al–C bond of $Al(^{i}Bu)_3$, which is different from the conventional mechanism.

I expect that these findings on the polymerization mechanism will contribute to the precise control of polymerization reactions and catalyst design based on cationic Gd metallocene catalysts. For example, the computational model can be used to analyze the effects of the central metals and ligands, and the comparison of monomer species, which can be applied to catalyst design.

Furthermore, based on this reaction mechanism, it will be possible to analyze the copolymerization reaction using the quantum mechanics (QM) and the molecular dynamics (MD) methods. This will enable us to analyze the dissociation state of the counter anion and the coordination process of monomer species, which will contribute to further understanding of the polymerization reaction and catalyst design for this catalytic system.

The new polymerization mechanism will also lead to new developments for olefin and diene polymerization by metal complexes. Propagation by monomer insertion into the Al–C bond of alkylaluminum has not been found except in the Alfol process. The Alfol process requires high temperature and high pressure conditions, but in the present catalyst system, polymerization proceeds under mild reaction conditions because the cationic Gd metallocene coordinates to the monomer and assists the monomer insertion into Al–C bond of alkylaluminum.

I hope that my work in this thesis will contribute to further understanding of the polymerization with coordination polymerization catalysts and, eventually, help someone in the future to pave the way to the development of new and innovative polymerization reactions.

Acknowledgements

I would like to thank all who supported me in completing this thesis for their invaluable assistance and discussions. First, I would like to express my deepest gratitude to Prof. Nobuaki Koga for his kind and careful guidance and invaluable advice.

I'm grateful to Prof. Yasuo Wakatsuki for his kind advice and many helpful suggestions, and also thank Dr. Oliver Tardif for the many precise experiments for this thesis. I would also like to thank Prof. Masataka Nagaoka and Dr. Kentaro Matsumoto for their kind guidance and useful discussions during the dynamic behavior analysis collaboration related to this research. Furthermore, I thank my managers at Bridgestone co. for their understanding and cooperation in this work.

I would also like to express my sincere gratitude to Dr. Shojiro Kaita for his important advice, motivating and constantly supporting me in this work.

My sincere thanks go to my family and parents who continued to support and encourage me during my challenges.

Publication List

1. Rika Fukushima, Olivier Tardif, Shojiro Kaita, Yasuo Wakatsuki, and Nobuaki Koga, "Polymerization via Insertion of Ethylene into Al−C bond under Mild Conditions: Mechanistic Studies on the Promotion Exerted by a Catalytic Amount of Cationic Gadolinium Metallocene.", *Chemistry An Asian Journal* **2021**, *16*, 1403–1416.

   DOI: 10.1002/asia.202100193

   (Chapter 2)

2. Rika Fukushima, Olivier Tardif, Shojiro Kaita, Yasuo Wakatsuki, and Nobuaki Koga, "Non-π-Allyl Mechanism for the 1,4-*cis*-Butadiene Polymerization: Theoretical Study of Polymerization via Insertion of Butadiene into Al−C Bond with Cationic Gadolinium Metallocene.", *Chemistry An Asian Journal* accepted. *This paper has been selected to feature the front cover of the journal.

   DOI: 10.1002/asia.202200899

   (Chapter 3)